9151
NACA TN 2817

TECH LIBRARY KAFB, NM
0065898

NATIONAL ADVISORY COMMITTEE FOR AERONAUTICS

TECHNICAL NOTE 2817

A THEORETICAL AND EXPERIMENTAL INVESTIGATION OF THE EFFECTS OF YAW ON PRESSURES, FORCES, AND MOMENTS DURING SEAPLANE LANDINGS AND PLANING

By Robert F. Smiley

Langley Aeronautical Laboratory
Langley Field, Va.

Washington
November 1952

AFMDC
TECHNICAL LIBRARY
AFL 2811

TECH LIBRARY KAFB, NM
0065898

CONTENTS

NATIONAL ADVISORY COMMITTEE FOR AERONAUTICS

TECHNICAL NOTE 2817

A THEORETICAL AND EXPERIMENTAL INVESTIGATION OF THE EFFECTS OF YAW ON PRESSURES, FORCES, AND MOMENTS DURING SEAPLANE LANDINGS AND PLANING

By Robert F. Smiley

SUMMARY

A theoretical investigation was made of the hydrodynamic forces and moments experienced during yawed water landings and planing of seaplanes of arbitrary constant cross section. Equations are developed for the side force, the rolling moment, the yawing moment, the pressure distribution, and the peak pressure. For the special case of the non-chine-immersed straight-sided wedge, these equations are such that the time histories of the side force and rolling and yawing moments can be expressed as families of generalized curves.

Experimental measurements of the side force, the rolling and yawing moments, the pressure distribution, and the peak pressure, obtained during landing and planing tests made in the Langley impact basin with a float having an angle of dead rise of 22.5°, are presented and compared with the theoretical predictions. The landing tests covered yaw angles between 0° and 12° for trims of 3.2°, 6.3°, and 9.3° and the planing tests covered yaw angles of 6° and 9° for trims of 6.3° and 9.3°. In general, the experimental data appear to be in reasonable agreement with the corresponding theoretical predictions.

INTRODUCTION

In recent years much experimental and theoretical research has been directed toward the obtaining of information concerning the motions and hydrodynamic forces experienced during the landing or planing of seaplanes. For the case of the symmetrical landing or planing many theoretical and experimental data are now available (refs. 1 to 22). For the case of unsymmetrical landing or planing, however, very little experimental or analytical work has been done (refs. 23 to 25).

The purpose of this paper is to approach this problem of unsymmetrical loads by a theoretical and experimental study of the effects of yaw on

seaplane loads and motions. The analysis deals, in general, with the treatment of yaw forces on hulls of arbitrary constant cross section and deals, in particular, with the case of a wide straight-sided wedge.

A study is made of the pressure distribution, side force, and rolling moment occurring during the two-dimensional yawed impact of a symmetrical body on a smooth water surface. The problem of the oblique yawed impact and planing of a three-dimensional body of arbitrary constant cross section is then solved by the use of the results of the two-dimensional analysis. After a consideration of several constants needed for theoretical computations, experimental impact and planing data obtained from tests in the Langley impact basin, which are described in the appendix of this paper, are compared with the corresponding theoretical predictions.

SYMBOLS

Any consistent set of units may be used unless otherwise indicated. Bars over symbols indicate the average value of the quantities involved.

A	hydrodynamic aspect ratio, $\dfrac{(\text{Wetted length at keel})^2}{\text{Wetted area projected normal to keel}}$
a_ξ	perpendicular distance between keel and axis of rolling moments
a_ζ	distance between step and axis of yawing moments measured parallel to keel
B, B_1, B_2	side-force factors
b	beam of hull
c	wetted semiwidth of hull in any transverse section
E, E_1, E_2	rolling-moment factors
F_1, F_2	total hydrodynamic force on two sides of a wedge
F_ζ	hydrodynamic force normal to keel (parallel to ζ-axis)
F_η	hydrodynamic force perpendicular to seaplane plane of symmetry (parallel to η-axis)

$f(\beta)$ dead-rise function

G yawing-moment factor

g acceleration due to gravity, 32.2 ft/sec^2

H perpendicular distance between keel and plane of chines

h wetted height of hull in any transverse section

J empirical function of angle of dead rise

K constant for pressure calculations,

$$K \approx \frac{\pi}{2}\left(1 - \frac{3 \tan^2\beta \cos \beta}{1.7\pi^2} - \frac{\tan \beta \sin^2\beta}{3.3\pi}\right)$$

L longitudinal-wave-rise ratio

M_ξ hydrodynamic rolling moment about an axis parallel to ξ-axis and in $\xi\zeta$-plane; the moment is considered positive if it tends to decrease the angle of dead rise on side of hull having the largest impact force (advancing side of hull)

M_ζ hydrodynamic yawing moment about an axis parallel to ζ-axis and in $\zeta\xi$-plane; the moment is considered positive if it tends to reduce angle of yaw

n_1, n_2 two sides of a thick rectangular flat plate

n_{i_η} side-force load factor, $\frac{F_\eta}{W}$

n_{i_w} vertical load factor, $\frac{-\ddot{z}}{g}$

p instantaneous pressure

R transverse-wave-rise ratio

$S_{n_{ch}}$ wetted area of one side of seaplane projected normal to plane of symmetry of seaplane at chine immersion

$\Delta S_{n_{ch}}$ increase of wetted area of one side of seaplane projected normal to plane of symmetry of seaplane subsequent to chine immersion

S_1, S_2	wetted areas of two sides of seaplane projected normal to the X-axis
s	distance between a given flow plane and keel-water-surface intersection (parallel to ξ-axis)
t	time after water contact
V	velocity of hull relative to undisturbed water
V_ζ	velocity of hull normal to keel (parallel to ζ-axis)
$\dot{V}_\zeta$	acceleration of hull normal to keel (parallel to ζ-axis)
V_η	velocity of hull perpendicular to seaplane plane of symmetry (parallel to η-axis)
v	local fluid velocity relative to body at body surface
W	weight of hull
w	thickness of a rectangular flat plate
X,Y,Z	coordinate axes with respect to plane of seaplane landing; X-axis is in plane of seaplane motion and is parallel to water surface, Z-axis is in plane of seaplane motion and is perpendicular to water surface, and Y-axis is perpendicular to X- and Z-axes
X',Y',Z'	X-, Y-, Z-coordinate axes rotated about the Z-axis through yaw angle; X'-axis is in plane of symmetry of seaplane and is parallel to water surface, Z'-axis is in plane of symmetry of seaplane and is perpendicular to water surface, and Y'-axis is perpendicular to X'- and Z'-axes
$\dot{x}$	horizontal velocity of hull (parallel to X-axis)
$\ddot{x}$	horizontal acceleration of hull (parallel to X-axis)
z	vertical displacement of step (parallel to Z-axis)
$\dot{z}$	vertical velocity of hull (parallel to Z-axis)
$\ddot{z}$	vertical acceleration of hull (parallel to Z-axis)
α	constant for free-lateral-motion solution; $\frac{3B}{[f(\beta)]^2\varphi(A)}$
β	angle of dead rise, radians
β_1	average angle of dead rise, $\tan^{-1}\frac{2H}{b}$, radians
Γ	gamma function

γ	flight-path angle
ϵ	transverse slope of hull surface at any point
ζ	penetration of hull normal to keel (parallel to ζ-axis)
$\dot{\zeta}$	approximation for V_ζ, $\dot{x} \sin \tau + \dot{z} \cos \tau$
$\ddot{\zeta}$	approximation for $\dot{V}_\zeta$, $\ddot{x} \sin \tau + \ddot{z} \cos \tau$
η	absolute value of transverse distance from center of model (parallel to η-axis)
θ	effective angle of dead rise
λ	parameter used in equation (29)
ξ, η, ζ	coordinate axes with respect to seaplane; the ξ-axis is in plane of symmetry of seaplane and is parallel to keel, the η-axis is perpendicular to plane of symmetry of seaplane, and the ζ-axis is perpendicular to ξ- and η-axes
ξ	distance forward of step (parallel to ξ-axis)
ρ	mass density of water, 1.938 slugs/cu ft for tests
τ	trim
ϕ	velocity potential on surface of body
$\varphi(A)$	aspect-ratio correction
ψ	yaw angle

Subscripts:

a	restricted side motion
ch	at chine immersion
cp	center of pressure
f	free side motion
max	maximum
o	at water contact

p peak

u unyawed

l normal flow

2 transverse flow

Dimensionless variables:

κ approach parameter, $\frac{\sin \tau}{\sin \gamma_o} \cos (\tau + \gamma_o)$

C_l vertical-load-factor coefficient,

$$\frac{n i_w g}{\dot{z}_o^2} \left\{ \frac{6W \sin \tau \cos^2 \tau}{[f(\beta)]^2 \varphi(A) \pi \rho g} \right\}^{1/3}$$

C_d draft coefficient, $z \left\{ \frac{[f(\beta)]^2 \varphi(A) \pi \rho g}{6W \sin \tau \cos^2 \tau} \right\}^{1/3}$

C_t time coefficient, $t \dot{z}_o \left\{ \frac{[f(\beta)]^2 \varphi(A) \pi \rho g}{6W \sin \tau \cos^2 \tau} \right\}^{1/3}$

C_η or $C_{\eta f}$ side-force coefficient (C_η for restricted case, $C_{\eta f}$ for free case), $\dfrac{F_\eta}{\dfrac{B \pi \rho \dot{x}_o \dot{\zeta}_o \sin \psi}{2 \sqrt[3]{\tan \tau}} \left\{ \dfrac{6W}{[f(\beta)]^2 \varphi(A) \pi \rho g} \right\}^{2/3}}$

C_{m_ξ} rolling-moment coefficient for restricted case, $\dfrac{M_\xi}{\dfrac{\pi^2 BEW \dot{\zeta}_o \dot{x}_o \sin \psi}{4 [f(\beta)]^2 \varphi(A) g \sin^2 \beta}}$

δ_ξ rolling-moment parameter, $a_\xi \dfrac{12 \sin^2 \beta}{\pi^2 E} \left\{ \dfrac{[f(\beta)]^2 \varphi(A) \pi \rho g}{6W \tan \tau} \right\}^{1/3}$

C_{m_ζ} yawing-moment coefficient for restricted case, $\dfrac{M_\zeta}{\dfrac{BGW\dot{\zeta}_o\dot{x}_o \sin\psi}{[f(\beta)]^2\varphi(A)g \tan\tau}}$

δ_ζ yawing-moment parameter, $a_\zeta\dfrac{3}{\zeta G}\left\{\dfrac{[f(\beta)]^2\varphi(A)\pi g\rho \tan^2\tau}{6W}\right\}^{1/3}$

ANALYSIS OF TWO-DIMENSIONAL PROBLEM OF YAWED IMPACT

General analysis.- Before the specific problem of the yawed impact of a seaplane is discussed it is desirable to consider first the corresponding two-dimensional problem, namely, the oblique impact of a symmetrical body on a smooth water surface (fig. 1). For convenience, the body is assumed to be stationary and the fluid is assumed to be moving toward the body at a velocity V far from the body, the vertical and side components of this velocity being designated as V_ζ and V_η, respectively. Buoyant and viscous forces are neglected. The velocity potential for the flow and the corresponding fluid velocity at the body are designated as ϕ and v, respectively. As a first crude approximation this flow field can be considered to be the sum of the following two flows (see fig. 2): (1) the flow for the symmetrical vertical impact of the same body on a fluid moving at a velocity V_ζ at infinity, which will be designated by the subscript 1, and (2) the symmetrical horizontal flow about the corresponding vertically symmetrical completely submerged body at a velocity V_η which will be designated by the subscript 2. It should be noted that the application of this superimposition principle is not strictly correct because of the presence of the free surface in the basic problem. For lack of a better or simpler way to approach this problem, however, the principle is assumed to be approximately valid.

According to Bernoulli's equation the pressure (above atmospheric) on the body for the three problems represented in figures 1 and 2 is

$$p = \tfrac{1}{2}\rho(V^2 - v^2) - \rho\frac{\partial\phi}{\partial t} \tag{1}$$

$$p_1 = \tfrac{1}{2}\rho\left(V_\zeta^2 - v_1^2\right) - \rho\frac{\partial\phi_1}{\partial t} \tag{2}$$

$$p_2 = \frac{1}{2}\rho\left(V_\eta^2 - v_2^2\right) - \rho\frac{\partial \phi_2}{\partial t} \tag{3}$$

where equation (1) refers to the complete yawed flow of figure 1 and equations (2) and (3) refer to the vertical and horizontal components of the flow in figure 2, respectively. As the flow field of figure 1 is assumed to be the resultant of the flow fields in figure 2, then on the bottom of the body

$$\phi = \phi_1 + \phi_2 \tag{4}$$

$$v = v_1 \pm v_2 \tag{5}$$

The plus sign in equation (5) refers to the left side of the body and the minus sign refers to the right side (see arrows designating fluid flow directions in fig. 2). Substituting equations (4) and (5) and the relation $V^2 = V_\zeta^2 + V_\eta^2$ into equation (1) gives

$$p = \frac{1}{2}\rho\left[V_\zeta^2 + V_\eta^2 - \left(v_1 \pm v_2\right)^2\right] - \rho\frac{\partial \phi_1}{\partial t} - \rho\frac{\partial \phi_2}{\partial t}$$

$$= \frac{1}{2}\rho\left(V_\zeta^2 + V_\eta^2 - v_1^2 \pm 2v_1v_2 - v_2^2\right) - \rho\frac{\partial \phi_1}{\partial t} - \rho\frac{\partial \phi_2}{\partial t} \tag{6}$$

This analysis is now restricted to the determination of the first-order effects of the yaw; that is, the term in equation (6) which is proportional to V_η (that is, $\rho v_1 v_2$) is considered but terms proportional to V_η^2 $\left(\text{that is, } \frac{1}{2}\rho V_\eta^2,\ \frac{1}{2}\rho v_2^2, \text{ and } \rho\frac{\partial \phi_2}{\partial t}\right)$ are neglected. Then equation (6) reduces to the relation

$$p = \frac{1}{2}\rho\left(V_\zeta^2 - v_1^2\right) - \rho\frac{\partial \phi_1}{\partial t} \pm \rho v_1 v_2 \tag{7}$$

The difference in pressure between that for the yawed case and that for the unyawed case can be obtained by subtracting equation (2) from equation (7) and is

$$p - p_1 = \pm \rho v_1 v_2 \tag{8}$$

Equation (8) gives a first approximation for the pressure due to yaw on an arbitrarily shaped symmetric body. Because of the preceding simplifying assumption that a superimposition procedure is valid and because of the neglect of second-order terms proportional to the yaw velocity V_η, this equation should not necessarily be considered to be applicable to practical yaw conditions. Rather it is or should be considered as an equation which is probably approximately valid for infinitesimal yaw angles and which may be corrected later empirically to apply to the practical case.

According to equation (8) (see statement after eq. (5)) the unsymmetrical pressure or the pressure due to yaw is positive on one side of the body and negative on the other so that the net upward force due to yaw is zero. The vertical force on a yawed body at a vertical velocity V_ζ thus is to a first-order approximation the same as that on an unyawed body at the same vertical velocity V_ζ or

$$F_\zeta = F_{\zeta u} \tag{9}$$

The difference in pressure between the two sides of the body is from equation (8)

$$\Delta p = \rho v_1 v_2 - (-\rho v_1 v_2) = 2\rho v_1 v_2 \tag{10}$$

and the total side force per unit length dF_η/ds is equal to the average pressure difference $\overline{\Delta p}$ times the wetted height h or

$$\frac{dF_\eta}{ds} = \overline{\Delta p}h = 2\rho h\overline{v_1 v_2} \tag{11}$$

In order to evaluate the quantities v_1 and v_2, consider first the limiting case of a body of infinitesimal transverse slope ($\epsilon \to 0$). For this condition the body is substantially reduced to a flat plate (see fig. 3) so that the flow in the horizontal direction (fig. 3(b)) is substantially undisturbed or

$$v_2 = V_\eta \tag{12}$$

For a flat plate which is completely submerged the velocity distribution on the surface of the plate due solely to the vertical component of flow is (see, for example, ref. 1)

$$v_1 = V_\zeta \frac{\eta/c}{\sqrt{1 - \left(\frac{\eta}{c}\right)^2}} \tag{13}$$

According to Wagner (refs. 2 or 3) the flow on a non-chine-immersed body of infinitesimal slope is substantially the same as that for the completely submerged flat plate given by equation (13). (The velocity variation for the case where the chines are immersed and where the upper surface is not wetted is considered in a later section of this paper.) Substituting equations (12) and (13) into equation (8) gives the pressure due to yaw as

$$p - p_1 = \pm\rho V_\zeta V_\eta \frac{\eta/c}{\sqrt{1 - \left(\frac{\eta}{c}\right)^2}} \tag{14}$$

and the yaw or side force per unit length is then obtained from equations (11), (12), and (13) as

$$\frac{dF_\eta}{ds} = 2\rho V_\zeta V_\eta h \left[\frac{\eta/c}{\sqrt{1 - \left(\frac{\eta}{c}\right)^2}}\right]$$

$$= 2\rho V_\zeta V_\eta h \int_0^1 \frac{\eta/c}{\sqrt{1 - \left(\frac{\eta}{c}\right)^2}} \, d\left(\frac{\eta}{c}\right) \tag{15}$$

Evaluation of the integral in equation (15) gives

$$\frac{dF_\eta}{ds} = 2\rho V_\zeta V_\eta h \tag{16}$$

The relation between the wetted height h and the penetration of the body ζ (see fig. 1) has been obtained by Wagner for the unyawed case by using the flat-plate approximation. The resulting equations are given in references 2 and 3. For the special case of a straight-sided wedge Wagner obtained the relation

$$\frac{h}{\zeta} = \frac{\pi}{2} \tag{17}$$

These same relations are assumed to hold for the yawed case. Equations were also derived by Wagner for the symmetrical pressure distribution p_1. (See ref. 1, 2, or 3.) For the special case of a straight-sided wedge, the chines of which are not covered by water, Wagner's equations reduce to the relation

$$\frac{p_1}{\frac{1}{2}\rho V_\zeta^2} = \frac{\pi \cot \beta}{\sqrt{1 - \left(\frac{\eta}{c}\right)^2}} - \frac{1}{\left(\frac{c}{\eta}\right)^2 - 1} + \frac{2\dot{V}_\zeta c}{V_\zeta^2}\sqrt{1 - \left(\frac{\eta}{c}\right)^2} \tag{18}$$

First approximation for the straight-sided wedge.- A first approximation for the pressure distribution on a yawed straight-sided wedge is obtained by combining equations (14) and (18) as

$$\frac{p}{\frac{1}{2}\rho V_\zeta^2} = \frac{\pi \cot \beta}{\sqrt{1 - \left(\frac{\eta}{c}\right)^2}} - \frac{1}{\left(\frac{c}{\eta}\right)^2 - 1} + \frac{2\dot{V}_\zeta c}{V_\zeta^2}\sqrt{1 - \left(\frac{\eta}{c}\right)^2} \pm 2\frac{V_\eta}{V_\zeta}\frac{\eta/c}{\sqrt{1 - \left(\frac{\eta}{c}\right)^2}} \tag{19}$$

The wetted semiwidth c which is equal to $h \cot \beta$ for a straight-sided wedge (see fig. 4) is then given by equation (17) as

$$c = h \cot \beta = \zeta \frac{\pi}{2} \cot \beta \tag{20}$$

The side force per unit length is given by combining equations (16) and (17) as

$$\frac{dF_\eta}{ds} = \pi \rho V_\zeta V_\eta \zeta \tag{21}$$

The center of pressure of the side force η_{cp} is given by the relation

$$\eta_{cp} = \frac{\int_0^c \Delta p \, \eta \, d\eta}{\int_0^c \Delta p \, d\eta} \tag{22}$$

Substituting equations (10), (12), and (13) into equation (22) gives

$$\eta_{cp} = \frac{\int_0^c 2\rho V_\zeta V_\eta \frac{\eta/c}{\sqrt{1 - \left(\frac{\eta}{c}\right)^2}} \eta \, d\eta}{\int_0^c 2\rho V_\zeta V_\eta \frac{\eta/c}{\sqrt{1 - \left(\frac{\eta}{c}\right)^2}} d\eta} \tag{23}$$

or

$$\frac{\eta_{cp}}{c} = \frac{\int_0^1 \frac{\left(\frac{\eta}{c}\right)^2}{\sqrt{1 - \left(\frac{\eta}{c}\right)^2}} d\left(\frac{\eta}{c}\right)}{\int_0^1 \frac{\eta/c}{\sqrt{1 - \left(\frac{\eta}{c}\right)^2}} d\left(\frac{\eta}{c}\right)} \tag{24}$$

and integrating equation (24) gives

$$\frac{\eta_{cp}}{c} = \frac{\pi}{4} \tag{25}$$

The rolling moment per unit length about an axis at distance a_ξ above the keel (see fig. 4) is obtained as follows: The rolling moment due to the force on the right side of the wedge is equal to

$$F_{right}\left(a_\xi \sin \beta - \frac{\eta_{cp}}{\cos \beta}\right)$$

where F_{right} is the total force per unit length on the right side (which must be normal to the surface of the wedge) and where $a_\xi \sin \beta - \frac{\eta_{cp}}{\cos \beta}$ is the center-of-pressure distance (see fig. 4). Similarly, on the left side of the wedge the rolling moment is

$$-F_{left}\left(a_\xi \sin \beta - \frac{\eta_{cp}}{\cos \beta}\right)$$

and the total rolling moment per unit length is

$$\left(F_{right} - F_{left}\right)\left(a_\xi \sin \beta - \frac{\eta_{cp}}{\cos \beta}\right)$$

or

$$\left(F_{right} \sin \beta - F_{left} \sin \beta\right)\left(a_\xi - \frac{\eta_{cp}}{\sin \beta \cos \beta}\right)$$

The side force per unit length $\frac{dF_\eta}{ds}$ is, by definition, equal to $F_{right} \sin \beta - F_{left} \sin \beta$; therefore the rolling moment per unit length becomes

$$\frac{dM_\xi}{ds} = \frac{dF_\eta}{ds}\left(a_\xi - \frac{\eta_{cp}}{\sin \beta \cos \beta}\right) \tag{26}$$

and substitution of equations (20), (21), and (25) into equation (26) gives

$$\frac{dM_\xi}{ds} = \pi \rho V_\zeta V_\eta \zeta \left(a_\xi - \frac{\pi^2}{8 \sin^2 \beta} \zeta\right) \tag{27}$$

Second approximation for the straight-sided wedge.- This section is concerned with the development of a better approximation for the pressure distribution and yawing forces and moments on a straight-sided wedge than is given by equations (19), (21), (25), and (27) which were obtained for the limiting condition of a wedge of infinitely small slope ($\beta \rightarrow 0$). For this approximation the unyawed pressure p_1 is obtained from equation (18) in the same manner as for the first approximation so that the pressure distribution may be expressed by combining equations (8) and (18) as

$$\frac{p}{\frac{1}{2}\rho V_\zeta^2} = \frac{\pi \cot \beta}{\sqrt{1 - \left(\frac{\eta}{c}\right)^2}} - \frac{1}{\left(\frac{c}{\eta}\right)^2 - 1} + \frac{2V_\zeta c}{V_\zeta^2}\sqrt{1 - \left(\frac{\eta}{c}\right)^2} \pm 2 \frac{V_\eta}{V_\zeta} \frac{v_1}{V_\zeta} \frac{v_2}{V_\eta} \tag{28}$$

The best method of estimating the quantity v_1/V_ζ, which is the velocity distribution on the unyawed wedge, appeared to be the use of the detailed graphical solutions of Pierson for the constant-velocity impact of a straight-sided wedge on a smooth water surface. (See ref. 4.) The resulting curves for v_1/V_ζ, which can be obtained from figure 16 of reference 4, are shown in figure 5 of this paper. It is noted that these theoretical curves are easily interpolated. Also shown in this figure is the theoretical variation of v_1/V_ζ predicted by equation (13) for the first approximation.

In order to determine the quantity v_2/V_η, the solution is used for the symmetrical flow about a completely submerged straight-sided wedge. This problem has been solved by R. J. Monaghan (not generally available) and the method of solution is indicated in reference 5. The resulting equation for v_2/V_η is

$$\frac{v_2}{V_\eta} = \pm \left(\frac{\lambda^2}{1 - \lambda^2}\right)^{\beta/\pi} \tag{29}$$

where λ is defined by the relation

$$\frac{\eta}{c} = 1 - \frac{\sqrt{\pi}}{\Gamma\left(\frac{1}{2} + \frac{\beta}{\pi}\right)\Gamma\left(1 - \frac{\beta}{\pi}\right)} \int_0^\lambda \left(\frac{\lambda^2}{1 - \lambda^2}\right)^{\frac{1}{2} - \frac{\beta}{\pi}} d\lambda$$

and where Γ designates the gamma function. The variation of v_2/V_η with η/c as computed from this equation is shown in figure 6 for various angles of dead rise. Also shown is the variation predicted by equation (12) for the first approximation.

Curves of the product $v_1 v_2/V_\zeta V_\eta$ were obtained by multiplying together the corresponding values of v_1/V_ζ and v_2/V_η from figures 5 and 6 and are shown in figure 7 together with the prediction of the first approximation. These curves, which represent the pressure due to yaw (see eq. (8)), can be used with equation (28) to predict the pressure distribution on the yawed wedge.

The curves of figure 7 were graphically integrated to obtain the average value $\overline{v_1 v_2}$ and the results were substituted into equations (11)

and (17) to obtain the side force per unit length. The resulting equation for the side force is

$$\frac{dF_\eta}{ds} = B_1 \pi \rho V_\zeta V_\eta \zeta \tag{30}$$

where the quantity B_1, which represents the ratio between the side force for the second approximation and that for the first approximation, is shown in figure 8.

The center of pressure of the yaw force is found by graphical integration of the pressure according to equations (10) and (22) with the aid of the curves of figure 7. The resulting center-of-pressure locations are given by the relation

$$\frac{\eta_{cp}}{c} = \frac{\pi}{4} E_1 \tag{31}$$

where E_1, which represents the ratio between the center-of-pressure distance for the second approximation and that for the first approximation, is shown in figure 8.

The rolling moment per unit length according to equations (20), (26), (30), and (31) is

$$\frac{dM_\xi}{ds} = B_1 \pi \rho V_\zeta V_\eta \zeta \left(a_\xi - \frac{\pi^2 E_1}{8 \sin^2 \beta} \zeta \right) \tag{32}$$

Peak pressure on the straight-sided wedge.- According to Wagner (ref. 3) the peak pressure on a straight-sided unyawed wedge of small dead-rise angle is approximately equal to the dynamic pressure corresponding to the side velocity of the edge of the wetted semiwidth or

$$p_p = \frac{1}{2} \rho \left(\frac{dc}{dt} \right)^2$$

where

$$\frac{dc}{dt} = V_\zeta \frac{\pi}{2} \cot \beta$$

For the yawed case the side velocity of the edge of the wetted semiwidth is equal to the rate of expansion of the wetted width dc/dt plus or minus the side velocity of the body V_η so that the peak pressure for this case becomes approximately

$$p_p = \frac{1}{2}\rho\left(\frac{dc}{dt} \pm V_\eta\right)^2$$

and when dc/dt is assumed to be the same for both yawed and unyawed cases

$$p_p = \frac{1}{2}\rho\left(V_\zeta \frac{\pi}{2} \cot \beta \pm V_\eta\right)^2$$

$$= \frac{1}{2}\rho V_\zeta^2\left(\frac{\pi}{2} \cot \beta \pm \frac{V_\eta}{V_\zeta}\right)^2 \tag{33}$$

Effects of chine immersion for bodies of arbitrary shape.- In this section consideration is made of the effects of chine immersion on the side force and rolling moment during a yawed impact. According to equations (11) and (12) the side force is given approximately by the relation

$$\frac{dF_\eta}{ds} = 2\rho h V_\eta \overline{v_1}$$

or in a more convenient form

$$\frac{dF_\eta}{ds} = 2B_2\rho h V_\eta V_\zeta \tag{34}$$

where

$$B_2 = \frac{\overline{v_1}}{V_\zeta}$$

For the non-chine-immersed condition B_2 can be obtained as a first approximation by taking the average value of equation (13). For the chine-immersed case, however, equation (13) does not apply and some other means must be used to determine $\overline{v_1}$. This determination may be made approximately as follows: For deep immersions the fluid flow about

an impacting body is very similar to the steady, separated, free-streamline flow about the same body. (See fig. 9.) Solutions are available in reference 6 for the velocity during such free-streamline flow which indicate that B_2 is equal to approximately 0.3, 0.4, and 0.5 for dead-rise angles of 0°, 20°, and 40°, respectively.

The center of pressure (see eqs. 10, 12, and 22) according to the velocity relations of reference 6 is given by the relation $\eta_p = \frac{\pi}{4} E_2 c = \frac{\pi}{8} E_2 b$ where $E_2 \approx 0.8$ for dead-rise angles up to 40°. The rolling moment is obtained from this relation and equations (26) and (34) and becomes

$$\frac{dM_\xi}{ds} = 2B_2 \rho h V_\eta V_\zeta \left(a_\xi - \frac{\pi b E_2}{8 \sin \beta \cos \beta} \right) \tag{35}$$

ANALYSIS OF OBLIQUE YAWED SEAPLANE LANDINGS AND PLANING FOR RESTRICTED SIDE MOTION

General Analysis

The problem to be treated in this section is the fixed-trim, oblique, smooth-water landing of a seaplane of arbitrary constant hull cross section having a fixed angle of yaw. The angle of yaw ψ is defined as the angle between the landing plane (XZ-plane of fig. 10(a)) and the plane of symmetry of the seaplane (X'Z'-plane of fig. 10(b)). The motion of the seaplane is assumed to be restricted to the XZ-plane; that is, there is assumed to be no side motion in the Y-direction. In an actual seaplane landing the seaplane is, of course, not restricted to motion in the XZ-plane but is free to accelerate perpendicular to the plane of landing (in the Y-direction) as a result of the side force. However, the restricted case corresponds to the model testing conditions for the experimental data of this paper and it happens that the equations for the unrestricted-side-motion condition can be conveniently expressed in terms of those for the restricted case; therefore, it is expedient to consider the restricted case first. The unrestricted or free case is considered separately in a subsequent section.

Consider the motion of the seaplane at a given instant of time (see fig. 10(a)). The yawed float moves forward (in the X-direction) at a velocity $\dot{x}$, vertically down (in the Z-direction) at a velocity $\dot{z}$, and to the side (in the Y-direction) with zero velocity. If this motion is viewed perpendicular to the plane of symmetry of the seaplane (see fig. 10(b)), it appears that an unyawed seaplane is moving forward (in the X'-direction) with a velocity $\dot{x} \cos \psi$, down (in the Z'-direction)

at a velocity $\dot{z}$, and sidewise (in the Y'-direction) at a velocity V_η where

$$V_\eta = \dot{x} \sin \psi \tag{36}$$

In the theoretical treatment of the landing of unyawed seaplanes (refs. 7 to 11), it is generally assumed that the flow processes in a given transverse plane, stationary in space and oriented normal to the keel (see aa' and bb' in fig. 10(b)), can be considered to be similar to those in the corresponding two-dimensional problem. In the present case the velocity of penetration into this plane (aa' or bb') or the velocity normal to the keel V_ζ is seen from figure 10(b) to be equal to

$$V_\zeta = \dot{z} \cos \tau + \dot{x} \sin \tau \cos \psi \tag{37}$$

and can be satisfactorily approximated by the simpler relation

$$V_\zeta \approx \dot{z} \cos \tau + \dot{x} \sin \tau = \dot{\zeta} \tag{38}$$

for most practical angles of yaw since the cosine of the yaw angle is usually close to unity. The side velocity (parallel to the Y'-axis) is given by equation (36).

Equations (36) and (38) used together with the equations of the previous section on the two-dimensional problem provide a first approximation for the side forces in terms of the instantaneous velocities $\dot{x}$ and $\dot{z}$ and the normal displacement ζ. In order to determine these quantities as a function of time, the motion of a yawed seaplane in the XZ-plane is assumed to be the same as that for the unyawed seaplane; that is, the time histories of the draft, vertical velocity, horizontal velocity, vertical acceleration, and vertical hydrodynamic force are assumed to be the same for the yawed and unyawed cases. (A subsequent section of this paper shows that this assumption is substantiated by experimental data for a float having an angle of dead rise of 22.5° for yaw angles at least up to 12°. It is also noted that this assumption is consistent with eq. (9).) Procedures for computing the vertical motions for the unyawed case are given in references 7 to 12. References 8 and 12 consider the seaplane of arbitrary constant cross section, references 11 and 12 consider the V-bottom seaplane with considerable chine immersion, and references 7, 9, and 10 deal particularly with the V-bottom seaplane having little or no chine immersion.

The Wide V-Bottom Seaplane

The special problem of the yawed impact of a wide, constant-dead-rise V-bottom surface, the chines of which do not penetrate the water surface, is now considered in detail. In addition to the assumptions of the preceding sections the weight of the seaplane is assumed to be counterbalanced by an equal constant wing-lift force throughout any landing. The motions of the unyawed seaplane for this case are discussed in detail in reference 9 and equations and dimensionless plots for these motions are presented therein.

Side force.- When equations (30), (36), and (38) are combined, the side force per unit length of float is obtained as

$$\frac{dF_\eta}{ds} = B_1 \pi \rho \ddot{\zeta} \dot{x} \zeta \sin \psi \tag{39}$$

The relation between ζ and s (see fig. 10(c)) is given by the relation

$$\zeta = s \tan \tau \tag{40}$$

Combining equations (39) and (40) and integrating the result gives the total side force as

$$F_\eta = \int_0^{z/\sin \tau} B_1 \pi \rho \ddot{\zeta} \dot{x} s \sin \psi \tan \tau \, ds$$

$$= \frac{B_1 \pi \rho \ddot{\zeta} \dot{x} z^2 \sin \psi}{2 \sin \tau \cos \tau} \tag{41}$$

Since equation (41) is based upon many inexact assumptions, it is unlikely to be always in good agreement with the experimental data. Consequently, equation (41) is modified empirically here by the substitution of some empirical quantity B for B_1 into equation (41) so that

$$F_\eta = \frac{B \pi \rho \ddot{\zeta} \dot{x} z^2 \sin \psi}{2 \sin \tau \cos \tau} \tag{42}$$

The empirical quantity B is probably substantially a function of dead rise alone and of the same order of magnitude as B_1.

In order to convert the side force into a dimensionless variable similar to those used in reference 9, equation (42) may first be rewritten in the form

$$\frac{F_\eta}{\dfrac{B\pi\rho\dot{x}_o\dot{\zeta}_o \sin\psi}{2\sqrt[3]{\tan\tau}}\left\{\dfrac{6W}{[f(\beta)]^2\varphi(A)\pi\rho g}\right\}^{2/3}} = \frac{\dot{x}}{\dot{x}_o}\frac{\dot{\zeta}}{\dot{\zeta}_o}z^2\left\{\frac{[f(\beta)]^2\varphi(A)\pi\rho g}{6W \sin\tau \cos^2\tau}\right\}^{2/3} \tag{43}$$

In the terminology of reference 9 the term $z^2\left\{\dfrac{[f(\beta)]^2\varphi(A)\pi\rho g}{6W \sin\tau \cos^2\tau}\right\}^{2/3}$ is the square of the dimensionless draft coefficient C_d. The term on the left of the equation is defined here as the dimensionless side-force coefficient C_η

$$C_\eta = \frac{F_\eta}{\dfrac{B\pi\rho\dot{x}_o\dot{\zeta}_o \sin\psi}{2\sqrt[3]{\tan\tau}}\left\{\dfrac{6W}{[f(\beta)]^2\varphi(A)\rho\pi g}\right\}^{2/3}} \tag{44}$$

so that equation (43) can be rewritten as

$$C_\eta = \frac{\dot{x}}{\dot{x}_o}\frac{\dot{\zeta}}{\dot{\zeta}_o}C_d^2 \tag{45}$$

According to the analysis of reference 9 the time histories of $\dot{\zeta}/\dot{\zeta}_o$ and C_d are functions only of the approach parameter κ where $\kappa = \dfrac{\sin\tau}{\sin\gamma_o}\cos(\gamma_o + \tau)$. The time history of $\dot{x}/\dot{x}_o$, although easily computed, is not a function of κ alone. However, during many impacts the change in horizontal velocity is small; therefore, it appears desirable, in the interest of simplicity, to ignore this variation and approximate equation (45) by the simpler relation

$$C_\eta = \frac{\dot{\zeta}}{\dot{\zeta}_o}C_d^2 \tag{46}$$

so that the time history of the side-force coefficient becomes a function of κ alone. (This approximation leads to a conservative estimate of the side force.) Theoretical time histories of C_η (according to eq. (46)) for various values of κ have been computed from the solutions of reference 9 and are shown in figure 11. The maximum values of C_η are plotted against κ in figure 12. This latter theoretical curve can be approximated within about 3 percent by the following empirical equation:

$$C_{\eta_{max}} = \frac{10}{19 + 29\kappa + \kappa^2} \qquad (0 < \kappa < 10)$$

The time to reach maximum side force is shown in figure 13 together with the times to reach maximum vertical load and maximum draft.

Rolling moment.- The rolling moment can be obtained by substituting equations (36), (38), and (40) into equation (32) and integrating the result over the float bottom. Also B is substituted for B_1. The resulting equation for the rolling moment is

$$M_\xi = B\pi\rho\dot{\zeta}\dot{x}\sin\psi\int_0^{z/\sin\tau} s\tan\tau\left(a_\xi - \frac{\pi^2 E_1\tan\tau}{8\sin^2\beta}s\right)ds$$

$$= \frac{B\pi\rho\dot{\zeta}\dot{x}\sin\psi}{\sin\tau\cos\tau}\left(\frac{a_\xi z^2}{2} - \frac{\pi^2 E_1 z^3}{24\sin^2\beta\cos\tau}\right)$$

$$= \frac{B\pi\rho\dot{\zeta}\dot{x}z^2\sin\psi}{2\sin\tau\cos\tau}a_\xi\left(1 - \frac{\pi^2 E_1 z}{12a_\xi\sin^2\beta\cos\tau}\right) \qquad (47)$$

and substituting equations (42) and (44) into equation (47) gives

$$M_\xi = F_\eta a_\xi\left(1 - \frac{\pi^2 E_1 z}{12a_\xi\sin^2\beta\cos\tau}\right)$$

$$= C_\eta\frac{a_\xi B\pi\rho\dot{\zeta}_o\dot{x}_o\sin\psi}{2\sqrt[3]{\tan\tau}}\left\{\frac{6W}{\left[f(\beta)\right]^2\varphi(A)\pi\rho g}\right\}^{2/3}\left(1 - \frac{\pi^2 E_1 z}{12a_\xi\sin^2\beta\cos\tau}\right)$$

The quantity E_1 which represents the ratio between the center-of-pressure distance for the second approximation and that for the first approximation for the two-dimensional case is now replaced by the quantity E which represents the actual center of pressure. This quantity E is probably substantially a function of dead rise alone and is probably somewhat similar to E_1. With this substitution and also by replacing z by $\left\{\frac{6W \sin \tau \cos^2\tau}{[f(\beta)]^2\varphi(A)\pi\rho g}\right\}^{1/3} C_d$ according to the definition of C_d in reference 9 the preceding equation becomes

$$M_\xi = C_\eta \frac{a_\xi B\pi\rho\dot{\zeta}_o\dot{x}_o \sin\psi}{2\sqrt[3]{\tan\tau}} \left\{\frac{6W}{[f(\beta)]^2\varphi(A)\pi\rho g}\right\}^{2/3} \left(1 - \frac{\pi^2 E C_d}{12 a_\xi \sin^2\beta \cos\tau} \left\{\frac{6W \sin\tau\cos^2\tau}{[f(\beta)]^2\varphi(A)\pi\rho g}\right\}^{1/3}\right)$$

or

$$M_\xi = \frac{\pi^2 BEW\dot{\zeta}_o\dot{x}_o \sin\psi}{4[f(\beta)]^2\varphi(A) g \sin^2\beta} C_\eta(\delta_\xi - C_d) \tag{48}$$

where

$$\delta_\xi = a_\xi \frac{12 \sin^2\beta}{\pi^2 E} \left\{\frac{[f(\beta)]^2\varphi(A)\pi\rho g}{6W \tan\tau}\right\}^{1/3} \tag{49}$$

The rolling-moment dimensionless coefficient is now defined as

$$C_{m_\xi} = \frac{M_\xi}{\frac{\pi^2 BEW\dot{\zeta}_o\dot{x}_o \sin\psi}{4[f(\beta)]^2\varphi(A) g \sin^2\beta}} \tag{50}$$

which from equation (48) is equal to

$$C_{m_\xi} = C_\eta\left(\delta_\xi - C_d\right) = \delta_\xi C_\eta - C_\eta C_d \tag{51}$$

Since the time histories of both C_η and C_d are functions of κ only but δ_ξ is not a function of κ, equation (51) shows that the time history of the rolling moment is different for each combination of κ and δ_ξ so that a single family of generalized curves like figure 11 cannot be given for the rolling-moment time history. For any specific case, however, the curve of C_{m_ξ} can be obtained by combining the pertinent C_η curve of figure 11 (multiplied by δ_ξ) with the corresponding $C_\eta C_d$ curve of figure 14 (which figure was obtained by combining the C_η curves of fig. 11 with the C_d curves of fig. 6 of ref. 9). The variation of the maximum rolling-moment coefficient with κ is shown in figure 15 for several values of δ_ξ.

Yawing moment.- The hydrodynamic yawing moment about an axis perpendicular to the keel at a distance a_ζ forward of the step (see fig. 10(c)) is given by the relation

$$M_\zeta = \int_0^{z/\sin\tau} \frac{dF_\eta}{ds}\left(a_\zeta - \frac{z}{\sin\tau} + s\right)ds \tag{52}$$

Substitution of equations (39), (40), and (42) into equation (52), substitution of B for B_1, and integration of the result yields the following equation for the yawing moment:

$$M_\zeta = B\pi\rho\dot{x}\dot{\zeta}\sin\psi\tan\tau\int_0^{z/\sin\tau} s\left(a_\zeta - \frac{z}{\sin\tau} + s\right)ds$$

$$= \frac{B\pi\rho\dot{x}\dot{\zeta}z^2\sin\psi}{2\sin\tau\cos\tau}\left(a_\zeta - \frac{z}{\sin\tau} + \frac{2z}{3\sin\tau}\right)$$

$$= F_\eta a_\zeta\left(1 - \frac{z}{3a_\zeta\sin\tau}\right) \tag{53}$$

In order to allow for the inaccuracies in the assumptions leading to equation (53), this equation is modified here by the insertion of an empirical constant G so that equation (53) becomes

$$M_\zeta = F_\eta a_\zeta \left(1 - \frac{Gz}{3a_\zeta \sin \tau}\right) \tag{54}$$

Substitution of equation (44) and the relation between z and C_d into equation (54) gives the relation

$$M_\zeta = \frac{BGW\dot{x}_o\dot{\zeta}_o \sin \psi}{[f(\beta)]^2\varphi(A)g \tan \tau} C_\eta \left[\frac{3a_\zeta}{G}\left\{\frac{[f(\beta)]^2\varphi(A)\pi\rho g \tan^2\tau}{6W}\right\}^{1/3} - C_d\right] \tag{55}$$

When the dimensionless yawing-moment coefficient C_{m_ζ} is defined as

$$C_{m_\zeta} = \frac{M_\zeta}{\dfrac{BGW\dot{x}_o\dot{\zeta}_o \sin \psi}{[f(\beta)]^2\varphi(A)g \tan \tau}} \tag{56}$$

and δ_ζ as

$$\delta_\zeta = a_\zeta \frac{3}{G}\left\{\frac{[f(\beta)]^2\varphi(A)\pi\rho g \tan^2\tau}{6W}\right\}^{1/3} \tag{57}$$

equation (55) can be written in the form

$$C_{m_\zeta} = C_\eta(\delta_\zeta - C_d) = \delta_\zeta C_\eta - C_\eta C_d \tag{58}$$

Since equations (51) and (58) for the rolling and yawing moments have been expressed in identical form, the time histories of the yawing moments can be computed from the generalized curves of figures 11 and 14 in the same manner as for the rolling moments. The maximum yawing moments can be obtained from figure 15 in a like manner.

Pressure distribution.- In order to make equations (19) and (28) applicable to the three-dimensional problem, V_ζ and V_η in these

equations are replaced by the values given by equations (36) and (38), the term containing the acceleration is corrected by an aspect-ratio correction (see ref. 13), and the angle of dead rise β is replaced by a more general quantity θ, called the effective angle of dead rise (see ref. 14). Equations (19) and (28), respectively, become

$$\frac{p}{\frac{1}{2}\rho\dot{\zeta}^2} = \frac{\pi \cot \theta}{\sqrt{1 - \left(\frac{\eta}{c}\right)^2}} - \frac{1}{\left(\frac{c}{\eta}\right)^2 - 1} + \frac{2\ddot{\zeta}c\varphi(A)}{\dot{\zeta}^2}\sqrt{1 - \left(\frac{\eta}{c}\right)^2} \pm 2\frac{\dot{x}\sin\psi}{\dot{\zeta}}\frac{\frac{\eta}{c}}{\sqrt{1 - \left(\frac{\eta}{c}\right)^2}} \tag{59}$$

for the first approximation and

$$\frac{p}{\frac{1}{2}\rho\dot{\zeta}^2} = \frac{\pi \cot \theta}{\sqrt{1 - \left(\frac{\eta}{c}\right)^2}} - \frac{1}{\left(\frac{c}{\eta}\right)^2 - 1} + \frac{2\ddot{\zeta}c\varphi(A)}{\dot{\zeta}^2}\sqrt{1 - \left(\frac{\eta}{c}\right)^2} \pm 2\frac{\dot{x}\sin\psi}{\dot{\zeta}}\frac{V_1}{V_\zeta}\frac{V_2}{V_\eta} \tag{60}$$

for the second approximation where

$$\varphi(A) = \sqrt{\frac{1}{1 + \frac{1}{A^2}}}\left(1 - \frac{0.425}{A + \frac{1}{A}}\right) \qquad (0 < A < \infty) \tag{61}$$

$$\varphi(A) = 1 - \frac{1}{2A} \qquad (A > 1.5) \tag{62}$$

and

$$A = \frac{(\text{Wetted length at keel})^2}{\text{Wetted area projected normal to keel}} \tag{63}$$

Reasons for the substitution of θ for β, which substitution was introduced by Pierson and Leshnover for the unyawed case in reference 14, are discussed in references 14 and 15. Several rather similar equations have been proposed for θ in these papers and are as follows:

$$\left.\begin{aligned} \pi \cot \theta_1 &= 2\sqrt{\frac{K^2 - 2K \sin^2\beta - K^2\sin^2\beta \tan^2\tau}{\sin^2\beta + K^2\tan^2\tau}} && \left(\pi \cot \theta_1 \geqq 2\right) \\ \pi \cot \theta_1 &= \frac{(K - \sin^2\beta)^2}{\sin^2\beta + K^2\tan^2\tau} + \cos^2\beta && \left(\pi \cot \theta_1 \leqq 2\right) \end{aligned}\right\} \quad (64)$$

$$\left.\begin{aligned} \pi \cot \theta_2 &= 2\sqrt{\frac{1 - \frac{4}{\pi^2}\tan^2\beta}{\tan^2\tau + \frac{4}{\pi^2}\tan^2\beta}} && \left(\pi \cot \theta_2 \geqq 2\right) \\ \pi \cot \theta_2 &= \frac{1}{\sin^2\tau + \frac{4}{\pi^2}\tan^2\beta \cos^2\tau} && \left(\pi \cot \theta_2 \leqq 2\right) \end{aligned}\right\} \quad (65)$$

$$\left.\begin{aligned} \pi \cot \theta_3 &= 2\sqrt{\frac{1 - J^2}{\tan^2\tau + J^2}} && \left(\pi \cot \theta_3 \geqq 2\right) \\ \pi \cot \theta_3 &= \frac{1}{\sin^2\tau + J^2\cos^2\tau} && \left(\pi \cot \theta_3 \leqq 2\right) \end{aligned}\right\} \quad (66)$$

where

$$\left.\begin{aligned} J &= \frac{2}{\pi}\tan\beta && (\beta \to 0) \\ J &= 0.293 && (\beta = 22.5^\circ) \\ J &= \frac{2}{\pi}\tan\beta && (\beta = 30^\circ) \end{aligned}\right\} \quad (67)$$

and

$$K \approx \frac{\pi}{2}\left(1 - \frac{3\tan^2\beta\cos\beta}{1.7\pi^2} - \frac{\tan\beta\sin^2\beta}{3.3\pi}\right)$$

The relative merits of these equations for θ are discussed in reference 15. Equation (66) appeared to give the best agreement with experimental data for the unyawed case for an angle of dead rise of 22.5° (ref. 15) and is therefore used subsequently for comparisons of theoretical and experimental pressure distributions.

Peak pressure.- In order to convert equation (33) for the peak pressure to the three-dimensional case, the terms V_η and V_ζ are replaced by $\dot{x} \sin \psi$ and $\dot{\zeta}$, respectively (see eqs. (36) and (38)); the following equation results:

$$\frac{p_p}{\frac{1}{2}\rho\dot{\zeta}^2} = \left(\frac{\pi}{2} \cot \beta \pm \frac{\dot{x} \sin \psi}{\dot{\zeta}}\right)^2 \tag{68}$$

Reference 16 shows that, for the unyawed case, equation (68) does not adequately take into account the effect of trim on the peak pressure. In order to take this effect into account, equation (68) which, for the unyawed case, reduces to the relation

$$\frac{p_p}{\frac{1}{2}\rho\dot{\zeta}^2} = \left(\frac{\pi}{2} \cot \beta\right)^2 \qquad (\psi = 0) \tag{69}$$

was empirically modified in reference 16 to obtain the following equation for the peak pressure at any finite angle of trim between 0° and 90°:

$$\frac{p_p}{\frac{1}{2}\rho\dot{\zeta}^2} = \frac{1}{\sin^2\tau + \frac{\cos^2\tau}{\left(\frac{\pi}{2} \cot \beta\right)^2}} \qquad (\psi = 0) \tag{70}$$

(See eq. (3) of ref. 16.) The corresponding modification of equation (68) is

$$\frac{p_p}{\frac{1}{2}\rho\dot{\zeta}^2} = \frac{1}{\sin^2\tau + \frac{\cos^2\tau}{\left(\frac{\pi}{2} \cot \beta \pm \frac{\dot{x} \sin \psi}{\dot{\zeta}}\right)^2}} \tag{71}$$

(Compare with eqs. (69) and (70).) Reference 15 shows that equation (70) was overconservative for the unyawed case for an angle of dead rise of 22.5°. This difficulty was remedied by replacing the quantity $\frac{\pi}{2}\cot\beta$ by an empirical function $\frac{1}{J}$ where J is given by equations (67). Application of this same substitution to equation (71) gives the following final equation for the peak pressure on a yawed wedge:

$$\frac{p_p}{\frac{1}{2}\rho\dot{\zeta}^2} = \frac{1}{\sin^2\tau + \frac{\cos^2\tau}{\left(\frac{1}{J} \pm \frac{\dot{x}\sin\psi}{\dot{\zeta}}\right)^2}} \tag{72}$$

Steady planing.- For the special case of steady planing ($\dot{z} = 0$, $\dot{\zeta} = V\sin\tau$, $\dot{x} = V$) the equations of the preceding sections for the side force and the rolling and yawing moments reduce to the following relations:

$$F_\eta = \frac{B\pi\rho V^2 z^2 \sin\psi}{2\cos\tau} \tag{73}$$

$$M_\xi = \frac{B\pi\rho V^2 z^2 \sin\psi}{2\cos\tau}\left(a_\xi - \frac{E\pi^2 z}{12\sin^2\beta\cos\tau}\right) \tag{74}$$

$$M_\zeta = \frac{B\pi\rho V^2 z^2 \sin\psi}{2\cos\tau}\left(a_\zeta - \frac{Gz}{3\sin\tau}\right) \tag{75}$$

(See eqs. (42), (47), and (54), with E substituted for E_1 in eq. (47).) The ratio between the side force and the normal force is also of some interest. According to reference 9 the normal force in planing is

$$F_\zeta = \frac{\pi\left[f(\beta)\right]^2\varphi(A)\rho V^2 z^2\tan\tau}{2} \tag{76}$$

so that when equation (73) is divided by equation (76) this ratio becomes

$$\frac{F_\eta}{F_\zeta} = \frac{B \sin \psi}{\left[f(\beta)\right]^2 \varphi(A) \sin \tau} \tag{77}$$

The Yawed Seaplane After Chine Immersion

Occurrence of chine immersion.- Chine immersion is considered to occur when the wave generated by the motion of the seaplane meets the chine-step intersection. From an examination of figure 10(d) it is seen that this immersion occurs when

$$z = z_{ch} = \frac{H \cos \tau}{RL} \tag{78}$$

where R and L are wave-rise ratios illustrated in figure 10(d). For the special case of the straight-sided wedge $H = \frac{b}{2} \tan \beta$ and equation (78) becomes

$$z_{ch} = \frac{b \tan \beta \cos \tau}{2RL} \tag{79}$$

In the previous sections of this paper, the ratio R for the straight-sided wedge has been considered to be equal to $\pi/2$ (see eq. (17)) and the ratio L has been considered equal to unity so that equation (79) becomes

$$z_{ch} = \frac{b \tan \beta \cos \tau}{\pi} \tag{80}$$

Actually, according to experimental and theoretical information given in references 4, 5, 15, 17, and 18, the ratio R is either equal to or somewhat less than $\pi/2$. The ratio L is either equal to or somewhat greater than unity. Thus the two effects tend to compensate each other so that equation (80) may give a reasonable prediction of the draft at chine immersion.

For cases of seaplanes which differ slightly from straight-sided V-shapes it is suggested that equation (80) be modified as follows:

$$z_{ch} = \frac{b \tan \beta_1 \cos \tau}{\pi} \tag{81}$$

where β_1 is the average angle of dead rise as indicated in figure 10(b) and is defined by the relation

$$\tan \beta_1 = \frac{2H}{b} \tag{82}$$

Side force.- The side force after chine immersion on a seaplane of arbitrary constant cross section is obtained by integrating equation (30) over the non-chine-immersed length of the seaplane (see eq. (17)), by integrating equation (34) over the chine-immersed length of the seaplane, and by substituting equations (36) and (38) into the resulting equation to obtain

$$F_\eta = 2B\rho V_\zeta V_\eta \int_0^{z_{ch}/\sin \tau} h \, ds + 2B_2 \rho V_\zeta V_\eta \int_{z_{ch}/\sin \tau}^{z/\sin \tau} h \, ds$$

$$= 2\rho V_\zeta V_\eta \left(BS_{n_{ch}} + B_2 \Delta S_{n_{ch}}\right)$$

$$= 2\rho \dot{x}_\zeta^{\cdot\cdot} \sin \psi \left(BS_{n_{ch}} + B_2 \Delta S_{n_{ch}}\right) \tag{83}$$

(The constant B_1 has been replaced by B in the first term of this equation to make this equation consistent with the analysis of the preceding sections for the non-chine-immersed case at the instant of chine immersion.) The term $S_{n_{ch}}$ is the wetted area of one side of the seaplane projected normal to the plane of symmetry of the seaplane at the time of chine immersion and $\Delta S_{n_{ch}}$ is the increase in wetted area subsequent to chine immersion. These wetted areas include only the areas of the seaplane which lie below the plane of the chines. Usually the flow separates from the hull at the chines so that there is no wetted area above the chines. Cases where there may be such wetted areas, however, are considered in a subsequent section of this paper.

The wetted areas needed for equation (83) can be obtained from an observation of figure 10(b) as

$$S_{n_{ch}} = \frac{1}{2} H \frac{2H}{\pi \tan \tau}$$

$$= \frac{b^2 \tan^2 \beta_1}{4\pi \tan \tau}$$

and

$$\Delta S_{n_{ch}} = H\left(\frac{z}{\sin \tau} - \frac{2H}{\pi \tan \tau}\right)$$

$$= \frac{b \tan \beta_1}{2}\left(\frac{z}{\sin \tau} - \frac{b \tan \beta_1}{\pi \tan \tau}\right)$$

so that equation (83) becomes

$$F_\eta = \frac{\rho b^2 \ddot{x} \zeta \tan \beta_1 \sin \psi}{\sin \tau}\left[\frac{B \tan \beta_1 \cos \tau}{2\pi} + B_2\left(\frac{z}{b} - \frac{\tan \beta_1 \cos \tau}{\pi}\right)\right] \quad (84)$$

Rolling moment.- The rolling moment after chine immersion of a seaplane of arbitrary constant cross section, which depends on the characteristics of the individual hull shape concerned, is not considered in this paper. The rolling moment of a straight-sided wedge, however, can be easily obtained by integrating the rolling moment per unit length along the hull. For non-chine-immersed sections this quantity is given by equation (32); for chine-immersed sections, by equation (35). The resulting equation for the rolling moment is

$$M_\xi = \frac{\rho \zeta \ddot{x} b^3 \tan \beta \sin \psi}{2 \sin \tau}\left[\frac{B \tan \beta \cos \tau}{\pi}\left(\frac{a_\xi}{b} - \frac{\pi E}{12 \sin \beta \cos \beta}\right) + \right.$$

$$\left. 2B_2\left(\frac{a_\xi}{b} - \frac{\pi E_2}{8 \sin \beta \cos \beta}\right)\left(\frac{z}{b} - \frac{\tan \beta \cos \tau}{\pi}\right)\right] \quad (85)$$

(The constants B_1 and E_1 have been replaced by B and E in order to make this equation consistent with the analysis for the non-chine-immersed case at the instant of chine immersion.)

Yawing moment.- The yawing moment after chine immersion for a seaplane of arbitrary constant cross section can be obtained similarly from integration of equation (52) as

$$M_\zeta = \frac{\rho \ddot{x} \zeta b^3 \tan \beta_1 \sin \psi}{\sin \tau} \left\{ \frac{B \tan \beta_1 \cos \tau}{2\pi} \left[\frac{a_\zeta}{b} - \frac{G}{\sin \tau} \left(\frac{z}{b} - \frac{2 \tan \beta_1 \cos \tau}{3\pi} \right) \right] + B_2 \left(\frac{z}{b} - \frac{\tan \beta_1 \cos \tau}{\pi} \right) \left[\frac{a_\zeta}{b} - \frac{G}{2 \sin \tau} \left(\frac{z}{b} - \frac{\tan \beta_1 \cos \tau}{\pi} \right) \right] \right\} \tag{86}$$

Further Refinements of the Chine-Immersion Theory

The preceding development for the forces and moments on chine-immersed yawed bodies took into account only those forces acting on the parts of the bodies below the chines. On actual seaplanes, however, there are often substantially vertical walls extending above the chines which may also experience yawing forces and moments. In order to obtain a rough estimate of the order of magnitude of these forces, consider the problem of the steady planing of a rectangular flat plate of finite thickness w (fig. 16). For this case the theory of the preceding parts of this paper gives no information regarding the unsymmetrical forces and moments. In figure 16(b) the motion of the plate is broken up into two components, one parallel to the plane of symmetry of the plate ($\dot{x} \cos \psi$) and one perpendicular to this plane ($\dot{x} \sin \psi$). Thus the side n_1 of the plate recedes from the water (is not wetted) and therefore has no water pressure on it. The side n_2, on the other hand, may or may not be wetted. If it is wetted, it penetrates the water at the side velocity $V_\eta = \dot{x} \sin \psi$ and therefore has a water pressure on it. The side motion of this side n_2 somewhat resembles the motion of a two-dimensional flat plate of beam w with separated flow behind the plate, for which case (see ref. 6 or 19) the average pressure per unit area is

$$\overline{p} = 0.44 \rho V_\eta^2 \tag{87}$$

Strictly speaking, equation (87) should give correct results only for an infinitely large ratio of wetted length to plate thickness (two-dimensional flow) and for zero beam (such that there is no interference between the flow below the hull and on the sides). If the ratio of wetted length to plate thickness is small, equation (87) for zero beam

may considerably underestimate the actual pressure and, if the beam is increased, the flow under the float will tend to separate at the sides and thus reduce the side pressure. Thus the two effects tend partly to compensate each other. With these reservations in mind, it is suggested that, in lieu of a more satisfactory procedure, a pressure equal to the value given by equation (87) be considered to act on one side of any parts of a seaplane above the chines which are submerged below the water surface and which are believed to be wetted by the water and that the yawing forces and moments on these submerged parts be obtained by integrating this pressure over the wetted areas concerned. Although the resulting yawing forces and moments are hardly precisely correct, even for the case of the long rectangular flat plate, they are probably reasonable as a first approximation.

Another Theory for the Side Force on Chine-Immersed or Non-Chine-Immersed Straight-Sided Wedges

The preceding sections of this paper have presented an analysis of the yawing forces based primarily upon the concept of two-dimensional flow in transverse planes. The applicability of the equations resulting from that analysis, however, has not yet been established for all practical conditions; therefore, it is desirable to consider also other possible methods for computing the yawing forces. For the special case of the side force only, such a method, which happens to be simpler in form than that of the preceding sections, is as follows. Consider the case of a planing wedge (fig. 17). When this wedge is viewed in a plane perpendicular to the direction of motion, it is seen that the projected area of one side of the wetted surface (S_1 in fig. 17) is larger than the projected area of the other side S_2, the corresponding total wetted areas corresponding to S_1 and S_2 being assumed to be equal. If the total force (normal to the plating) on each side of the float (F_1 and F_2) is considered to be divided approximately proportionally to this projected area difference $\left(\text{that is } \frac{F_1}{F_2} = \frac{S_1}{S_2}\right)$ the side force is equal to the difference between the horizontal components of these forces or

$$F_\eta = (F_1 - F_2) \sin \beta = \left(F_1 - \frac{F_1 S_2}{S_1}\right) \sin \beta = \frac{F_1}{S_1}\left(S_1 - S_2\right) \sin \beta \qquad (88)$$

and the force normal to the keel is equal to the sum of the normal (to the keel) components of these forces or

$$F_\zeta = (F_1 + F_2) \cos \beta = \left(F_1 + \frac{F_1 S_2}{S_1}\right) \cos \beta = \frac{F_1}{S_1} (S_1 + S_2) \cos \beta \qquad (89)$$

When equations (88) and (89) are combined, the side force can be rewritten as

$$\frac{F_\eta}{F_\zeta} = \frac{S_1 - S_2}{S_1 + S_2} \tan \beta \qquad (90)$$

By a consideration of the geometry of the float it can be shown that the ratio $\frac{S_1 - S_2}{S_1 + S_2}$ is given by the relation

$$\frac{S_1 - S_2}{S_1 + S_2} = \frac{\tan \psi \tan \beta}{\sin \tau} \qquad (91)$$

which is valid for both chine-immersed and non-chine-immersed wedges. Equation (90) therefore can be written as

$$\frac{F_\eta}{F_\zeta} = \frac{\tan \psi \tan^2 \beta}{\sin \tau} \qquad (92)$$

Substituting the relations $V_\eta = \dot{x} \sin \psi$ (see eq. (36)) and $V_\zeta = \dot{x} \sin \tau \cos \psi$ (see eq. (37)) and rearranging equation (92) yields the following relation:

$$\frac{F_\eta}{F_\zeta} \cot \beta = \frac{V_\eta}{V_\zeta} \tan \beta \qquad (93)$$

The significance of the right-hand side of equation (93) is indicated in figure 18 which shows transverse cross sections of a non-chine-immersed wedge for values of $\frac{V_\eta}{V_\zeta} \tan \beta$ less than and greater than unity. For $\frac{V_\eta}{V_\zeta} \tan \beta$ larger than unity, only one side of the float is wetted by water; therefore, for these cases the ratio between the side and normal forces is equal to the tangent of the angle of dead rise (since the total force is substantially normal to the plating) or

$$\frac{F_\eta}{F_\zeta} \cot \beta = 1 \qquad \left(\frac{V_\eta}{V_\zeta} \tan \beta \geqq 1\right) \tag{94}$$

For values of $\frac{V_\eta}{V_\zeta} \tan \beta$ less than unity, the data of figure 19 show that experimental planing data for a wedge having an angle of dead rise of 22.5° give higher values of $\frac{F_\eta}{F_\zeta} \cot \beta$ than are predicted by equation (93). (See the appendix for a description of these tests.) This result suggests that a more adequate equation for the side force could be written in the form

$$\frac{F_\eta}{F_\zeta} \cot \beta = f\left(\frac{V_\eta}{V_\zeta} \tan \beta\right) \tag{95}$$

where the functional relation is to be determined empirically. Since this relation must satisfy equation (94), it is probable that the relation will not vary much with the angle of dead rise. The following simple equation is proposed for this relation (see fig. 19)

$$\frac{F_\eta}{F_\zeta} \cot \beta = \sin\left(\frac{\pi}{2} \frac{V_\eta}{V_\zeta} \tan \beta\right) \qquad \left(\frac{V_\eta}{V_\zeta} \tan \beta \leqq 1\right) \tag{96}$$

Equations (94) and (96), which were obtained for the planing case, may be considered to apply also approximately for the impact condition. This application is shown in figure 19 where experimental impact data for a wedge having an angle of dead rise of 22.5° (see appendix) for various trims are shown to be approximately in agreement with the variation of $\frac{F_\eta}{F_\zeta} \cot \beta$ with $\frac{V_\eta}{V_\zeta} \tan \beta$ given by the planing data and equation (96). Although it is realized that the actual variation probably changes with dead rise, trim, flight path, and other variables, it is believed that equation (96) will give reasonable results, at least for rough calculations, for arbitrary yawed landing conditions.

It is noted that for $\frac{V_\eta}{V_\zeta} \tan \beta$ near to and greater than unity the experimental impact data give values of $\frac{F_\eta}{F_\zeta} \cot \beta$ greater than unity.

This result indicates that there is a negative pressure on the low-pressure side of the float. Although such an effect would not exist for the planing case (the water would not wet one side of the float for $\frac{V_\eta}{V_\zeta} \tan \beta > 1$) during these particular yawed impacts, during earlier stages of the impacts (before the time represented by the test points shown) the quantity $\frac{V_\eta}{V_\zeta} \tan \beta$ was small enough to permit wetting of both sides of the float. The suction results from the tendency of the water to separate from the low-pressure side as the quantity $\frac{V_\eta}{V_\zeta} \tan \beta$ increases above unity.

ANALYSIS OF OBLIQUE YAWED SEAPLANE LANDINGS FOR FREE SIDE MOTION

Basic considerations.- In the preceding sections of this paper it has been assumed that the motion of the seaplane during landing is restricted to the plane of its landing (XZ-plane of fig. 10(a)) or that there is no side motion (in the Y-direction). Since in an actual landing a seaplane is free to accelerate to the side as a result of the side force, it is desirable to determine the relations between the yawing forces in such a free yawed landing and those in the previously discussed restricted yawed landing. As for the restricted-landing analysis, it is assumed that the vertical motions and forces are unaffected by the angle of yaw and that the change in horizontal velocity during an impact is small.

Consider the motion of the seaplane in a horizontal direction normal to the keel. The force in this direction, which is the side force F_{η_f}, must (according to Newton's second law) equal the mass of the seaplane $\frac{W}{g}$ times the rate of change of the side velocity $\frac{dV_{\eta_f}}{dt}$ or

$$F_{\eta_f} = - \frac{W}{g} \frac{dV_{\eta_f}}{dt} \tag{97}$$

(the negative sign indicates that F_{η_f} and V_{η_f} have been defined as positive in opposite directions). The side force for the general case of a body of constant arbitrary hull cross section, whether restricted

in side motion or not, is given by equation (83) as

$$F_\eta = 2\rho V_\zeta V_\eta \left(BSn_{ch} + B_2 \Delta Sn_{ch}\right)$$

For the restricted case of the previous sections V_η was considered to be substantially constant as a consequence of the assumption of no side motion and of the assumption $\dot{x} = \dot{x}_o$; thus V_{η_a} was equal to its initial value or

$$V_{\eta_a} = V_{\eta_o} \tag{98}$$

and equation (83) for the restricted case becomes

$$F_{\eta_a} = 2\rho V_\zeta V_{\eta_o} \left(BSn_{ch} + B_2 \Delta Sn_{ch}\right) \tag{99}$$

For the free case V_η is a variable (having, of course, the same initial value V_{η_o} as for the restricted case) and F_η is given by equation (83) as

$$F_{\eta_f} = 2\rho V_\zeta V_{\eta_f} \left(BSn_{ch} + B_2 \Delta Sn_{ch}\right) \tag{100}$$

When equations (99) and (100) are combined, the relation between the side forces for the free and restricted cases becomes

$$\frac{F_{\eta_f}}{F_{\eta_a}} = \frac{V_{\eta_f}}{V_{\eta_o}} \tag{101}$$

(It should be noted that the variables V_ζ, Sn_{ch}, and ΔSn_{ch} in eqs. (99) and (100), which depend only on the vertical and horizontal motions, have been considered identical for the two cases of free and restricted landings.) A combination of equations (97) and (101) and a rearrangement gives the following relation (see eq. (36)):

$$\frac{dV_{\eta_f}}{V_{\eta_f}} = -\frac{gF_{\eta_a}}{WV_{\eta_o}}\,dt = -\frac{gF_{\eta_a}}{W\dot{x}_o \sin \psi}\,dt \tag{102}$$

which, when integrated, becomes

$$\frac{V_{\eta_f}}{V_{\eta_o}} = e^{-\int_0^t \frac{gF_{\eta_a}}{W\dot{x}_o \sin \psi}\,dt} \tag{103}$$

When equations (103) and (101) are combined, the ratio between the side force for the free and restricted cases is

$$\frac{F_{\eta_f}}{F_{\eta_a}} = e^{-\int_0^t \frac{gF_{\eta_a}}{W\dot{x}_o \sin \psi}\,dt} \tag{104}$$

The same ratio is similarly applicable to the rolling and yawing moments, that is,

$$\frac{F_{\eta_f}}{F_{\eta_a}} = \frac{M_{\zeta_f}}{M_{\zeta_a}} = \frac{M_{\xi_f}}{M_{\xi_a}} = e^{-\int_0^t \frac{gF_{\eta_a}}{W\dot{x}_o \sin \psi}\,dt} \tag{105}$$

Equation (105) gives all the relations necessary for converting the equations of the previous sections for the restricted landing to those of the more realistic free landing.

The wide non-chine-immersed wedge.- For the special case of the wide non-chine-immersed straight-sided wedge, equation (105) can (after much trigonometrical manipulation) be expressed in the following form:

$$\frac{F_{\eta_f}}{F_{\eta_a}} = \frac{M_{\zeta_f}}{M_{\zeta_a}} = \frac{M_{\xi_f}}{M_{\xi_a}} = e^{-\alpha(1+\kappa)\int_0^{C_t} C_\eta\,dC_t} \tag{106}$$

where

$$\alpha = \frac{3B}{\left[f(\beta)\right]^2 \varphi(A)} \tag{107}$$

(see definitions of C_η, C_t, and κ) and where C_η is given by figure 11. (It should be noted that the quantity α is primarily a function of the seaplane dead rise alone except for the quantity $\varphi(A)$ which is usually near unity.) The integral $(1 + \kappa) \int_0^{C_t} C_\eta \, dC_t$ (obtained from graphical integration of the curves in fig. 11) is shown in figure 20, for various values of κ, as a function of C_t. The reduction of maximum side force due to the change from restricted to free motion (obtained from fig. 20 and eq. (106)) is shown in figure 21 as a function of κ for various values of α. The maximum side-force coefficient for the free case, as defined by the relation

$$C_{\eta_f} = \frac{F_{\eta_f}}{\dfrac{B\pi\rho\dot{x}_o\dot{\zeta}_o \sin\psi}{2\sqrt[3]{\tan\tau}} \left\{ \dfrac{6W}{\left[f(\beta)\right]^2 \varphi(A) \pi\rho g} \right\}^{2/3}} \tag{108}$$

(same definition as for the restricted case), is given in figure 22 as a function of κ for various values of α.

CONSTANTS FOR THEORETICAL SOLUTIONS

Dead-rise–aspect-ratio function.- In order to make theoretical solutions for the unsymmetrical forces and moments for the wide straight-sided wedge it is first necessary to solve the symmetrical problem according to the methods of reference 9. This solution involves the use of the quantity $\sqrt[3]{\left[f(\beta)\right]^2 \varphi(A)}$ which is related to the maximum vertical force (during a landing with wing lift equal to seaplane weight) in reference 9 by the relation

$$\sqrt[3]{[f(\beta)]^2\varphi(A)} = \frac{n_{i_{w_{max}}}g}{C_{l_{max}}\dot{z}_o^2}\sqrt[3]{\frac{6W \sin\tau \cos^2\tau}{\pi\rho g}} \tag{109}$$

where $C_{l_{max}}$ is given by the solid curve in figure 23. This quantity $\sqrt[3]{[f(\beta)]^2\varphi(A)}$ was determined for an angle of dead rise of 22.5° from equation (109) by using experimental maximum-load data from table I of this paper and from table II of reference 15. The resulting values for all these impacts for which the maximum load occurred prior to chine immersion are shown in figure 24. The solid faired curve drawn through these test points was used for all computations in this paper.

For angles of dead rise other than 22.5° it is suggested that the dead-rise–aspect-ratio function be computed from the relation

$$[f(\beta)]^2\varphi(A) = \left(\frac{\pi}{2\beta} - 1\right)^2\varphi(A) \tag{110}$$

where $\varphi(A)$ is given by equations (61) and (62) and where

$$A = \frac{2 \tan\beta}{\pi \tan\tau} \tag{111}$$

according to equations (17) and (63). Equation (110) gives the dead-rise function proposed by Wagner in reference 2 modified by an aspect-ratio correction. From a consideration of the experimental and theoretical information in references 4, 5, 7, 9, 10, 15, and 20 and in this paper it appears that equation (110) is reasonably satisfactory for angles of dead rise from 30° to 50°. For angles of dead rise smaller than 30° the experimental evidence in references 7, 15, and 20 and in this paper indicates that the actual dead-rise–aspect-ratio function is somewhat smaller than the value given by equation (110) (see, for example, the dashed line in fig. 24). The experimental evidence in these various references, however, is not completely consistent or conclusive; therefore, no attempt is made in this paper to define more accurately the dead-rise function.

Yawing coefficients.- The following values of the quantities B, E, and G were empirically chosen from the experimental data in this paper and were used for all computations in this paper for $\beta = 22.5°$:

$$B = 1.2; \quad E = 0.7; \quad G = 1.2 \tag{112}$$

When it is necessary to determine the quantity B for other angles of dead rise, it is noted that the value of B given by equations (112) is substantially equal to the value given by the second two-dimensional approximation B_1 shown in figure 8. Consequently, it is recommended that this curve for B_1 be used for B for computations for other angles of dead rise.

It is noted that the value of E given in equations (112) is smaller than the corresponding value of E_1 (see fig. 8). Purely arbitrarily it is suggested that the faired curve drawn through $E = 0.7$ at $\beta = 22.5$ be used to compute E for other angles of dead rise.

It is suggested that the value of G given by equations (112) be used for all angles of dead rise.

COMPARISONS BETWEEN THEORY AND EXPERIMENT FOR THE NON-CHINE-IMMERSED WEDGE

Experimental motions and forces as obtained from a yawed landing and planing investigation at the Langley impact basin (see appendix) are compared with the theoretical predictions of this paper in figures 23 and 25 to 37. In all cases the theoretical relations used are those derived in the section of this paper entitled "The Wide V-bottom Seaplane."

Landing Investigation

Vertical loads and motions.- Experimental time histories and maximum values of the draft, vertical velocity, and vertical acceleration (or vertical hydrodynamic load) for landings with yaw angles between 0° and 12°, shown in figures 23 and 25 to 28, appear to be substantially independent of the yaw angle and are in reasonable agreement with the predictions of the theory of reference 9.

Side load.- Comparisons of theoretical and experimental side loads shown in figures 29 and 30 indicate that the experimental side loads are in reasonable agreement with the theoretical values for yaw angles at least up to 12°.

Rolling and yawing moments.- Comparisons of theoretical and experimental maximum rolling moments, rolling-moment time histories, and

yawing-moment time histories, shown in figures 31, 32, and 33, respectively, indicate that these quantities are in reasonable agreement.

Times to maximum vertical load, maximum side load, and maximum draft.- In figure 34 comparisons are shown between the experimental and theoretical times to maximum vertical load, maximum side load, and maximum draft. The experimental and theoretical times are seen to be in reasonable agreement.

Pressure distribution.- Theoretical pressure distributions, as computed from the two approximations of equations (59) and (60), are shown in figure 35 together with the corresponding experimental pressure distributions for several trims and yaw angles. Fair agreement is seen to exist, the second approximation theory (eq. (60)) giving somewhat better results than the first approximation theory (eq. (59)).

Peak pressures.- Experimental and theoretical peak pressures are compared in figure 36 for several yawed impacts. Fair agreement is seen to exist.

Planing Investigation

Experimental yawing forces and moments during planing are compared with the corresponding theoretical forces and moments (computed from eqs. (73) to (75) and (77)) in figure 37. It is seen that the experimental side loads, rolling and yawing moments, and ratios of side to normal load are in reasonable agreement with the corresponding theoretical quantities.

CONCLUDING REMARKS

An approximate theory has been developed for predicting the unsymmetrical forces and moments during the yawed impact or planing of seaplanes. From comparisons of the results of theoretical calculations with experimental side force, rolling and yawing moment, and pressure data presented in this paper for a non-chine-immersed straight-sided wedge having an angle of dead rise of 22.5° and yaw angles up to 12°, the proposed theory appears to give reasonable results for the cases tested. Although it is probable that the proposed theory is also at least qualitatively applicable to other angles of dead rise and to the

chine-immersed case, the extent of quantitative agreement for such conditions remains to be determined by future experiments.

Langley Aeronautical Laboratory,
National Advisory Committee for Aeronautics,
Langley Field, Va., June 21, 1952.

APPENDIX

EXPERIMENTAL INVESTIGATION

Description of Tests and Instruments

A series of smooth-water yawed and unyawed landing and planing tests was made at the Langley impact basin (ref. 21) with a prismatic V-bottom float having an angle of dead rise of 22.5°. Details of this model are shown in figure 38.

Landing tests.- Thirty-six landings were made with the float loaded to a weight of 1177 pounds which corresponded to a beam-loading coefficient of 0.48. These landings covered yaw angles between 0° and 12° and initial flight-path angles between approximately 3° and 9°. During each landing a compressed-air engine (described in ref. 21) exerted a vertical lift force on the model equal to its weight so that the model simulated a seaplane with wing lift equal to the weight of the seaplane. Otherwise the model was free to move in the vertical direction. The model was attached to a towing carriage weighing approximately 5400 pounds. Because of this large additional carriage inertia, the model did not slow down very much (horizontally) during any landing.

Time histories of the following quantities were measured during each landing: vertical draft, vertical velocity, vertical acceleration (vertical force), horizontal velocity, side force, rolling moment, yawing moment, and pressure distribution. The instruments used for measuring horizontal velocity and initial vertical velocity are described in reference 21. The instruments used for measuring time histories of the vertical motions and of the pressure distribution are described in reference 15. The locations of the pressure gages used in this investigation are shown in table II and figure 39. The hydrodynamic forces due to yaw were measured as follows: A six-component strain-gage-type dynamometer measured the side force, rolling moment, and yawing moment at a position above the float. These moments and forces differ from the corresponding hydrodynamic quantities because of inertia forces and moments resulting from structural oscillations of the float beneath the dynamometer. The inertia force due to side oscillations, which occurred at a frequency of approximately 3.5 cycles per second, was measured by a side accelerometer mounted on the float. The effects of another structural oscillation, which occurred at a frequency of approximately 13 cycles per second and which can be seen in figure 33, were not taken into account.

Planing tests.- Four planing runs were made in the Langley impact basin according to the procedure outlined in reference 22. During these

runs, measurements of the pressure distribution, the side load, the rolling moment, the yawing moment, the total force normal to the keel, and the horizontal velocity were recorded. The instruments used were the same as for the landing tests except that the normal force was measured by the previously mentioned dynamometer for the planing runs. The draft corresponding to each planing run was obtained by observing the wetted length, as given by observation of the experimental pressure distributions, and multiplying it by the sine of the trim. If the water rises up in front of the float, this quantity (wetted length times the sine of the trim) may be greater than the actual draft; however, this rise is probably small for the conditions tested.

Precision of Measurements

The instrumentation used in these tests gives measurements that are estimated to be accurate usually within the following limits:

Horizontal velocity, ft/sec	±0.5
Vertical velocity at water contact, ft/sec	±0.2
Vertical velocity after water contact, ft/sec	±0.5
Vertical acceleration, percent	±5
Pressure, lb/sq in.	±2 ±0.1p
Time, sec	±0.005
Draft for landings, ft	±0.03
Side force, lb	±50
Rolling moment, ft-lb	±100
Yawing moment, ft-lb	±200

In order to evaluate properly the experimental data from most instruments, the dynamic response characteristics of the instruments and the corresponding recording galvanometers had to be taken into account. Analysis of this dynamic response for the experimental conditions of these tests showed that the response characteristics of the instrument-galvanometer circuits were of such a nature that the magnitudes of the recorded motions and forces should be reasonably accurate but that the circuits had small time lags. All the data presented in this paper have been corrected for these time lags.

Experimental Results

Landing tests.- The initial vertical, horizontal, and resultant velocities, flight-path angles, trims, and yaw angles for all landings are presented in table I together with the measured over-all loads and motions. Time histories of these quantities for several landings are shown in figures 26 to 28, 30, 32, and 33. The values of the maximum pressures recorded on each pressure gage are presented for all runs

in table III and the corresponding times of maximum pressure are presented in table IV. Time histories of the vertical velocity are presented in table V. In table VI instantaneous pressure distributions from several landings together with the corresponding measurements of time, draft, vertical velocity, and vertical load factor are given. The corresponding horizontal velocities are substantially the same as the initial values given in table I since the change in horizontal velocity during any impact was small.

Planing tests.- The experimental over-all loads and pressure-distribution measurements obtained during the four planing runs are presented in table VII together with the planing conditions of trim, yaw, draft, and horizontal velocity.

REFERENCES

1. Pierson, John D.: On the Pressure Distribution for a Wedge Penetrating a Fluid Surface. Preprint No. 167, S.M.F. Fund Paper, Inst. Aero. Sci. (Rep. No. 336, Project No. NR 062-012, Office of Naval Res., Exp. Towing Tank, Stevens Inst. Tech.), June 1948.

2. Wagner, Herbert: Über Stoss- und Gleitvorgänge an der Oberfläche von Flüssigkeiten. Z.f.a.M.M., Bd. 12, Heft 4, Aug. 1932, pp. 193-215.

3. Wagner, Herbert: Landing of Seaplanes. NACA TM 622, 1931.

4. Pierson, John D.: The Penetration of a Fluid Surface by a Wedge. S.M.F. Fund Paper No. FF-3, Inst. Aero. Sci. (Rep. No. 381, Project No. NR062-012, Office Naval Res., Exp. Towing Tank, Stevens Inst. Tech.), July 1950.

5. Bisplinghoff, R. L., and Doherty, C. S.: A Two-Dimensional Study of the Impact of Wedges on a Water Surface. Contract No. NOa(s)-9921, Dept. Aero. Eng., M.I.T., Mar. 20, 1950.

6. Korvin-Kroukovsky, B. V., and Chabrow, Faye R.: The Discontinuous Fluid Flow Past an Immersed Wedge. Preprint No. 169, S.M.F. Fund Paper, Inst. Aero. Sci. (Rep. No. 334, Project No. NR 062-012, Office of Naval Res., Exp. Towing Tank, Stevens Inst. Tech.), Oct. 1948.

7. Mayo, Wilbur L.: Analysis and Modification of Theory for Impact of Seaplanes on Water. NACA Rep. 810, 1945. (Supersedes NACA TN 1008.)

8. Milwitzky, Benjamin: A Theoretical Investigation of Hydrodynamic Impact Loads on Scalloped-Bottom Seaplanes and Comparisons with Experiment. NACA Rep. 867, 1947. (Supersedes NACA TN 1363.)

9. Milwitzky, Benjamin: A Generalized Theoretical and Experimental Investigation of the Motions and Hydrodynamic Loads Experienced by V-Bottom Seaplanes During Step-Landing Impacts. NACA TN 1516, 1948.

10. Milwitzky, Benjamin: A Generalized Theoretical Investigation of the Hydrodynamic Pitching Moments Experienced by V-Bottom Seaplanes During Step-Landing Impacts and Comparisons with Experiment. NACA TN 1630, 1948.

11. Schnitzer, Emanuel: Theory and Procedure for Determining Loads and Motions in Chine-Immersed Hydrodynamic Impact of Prismatic Bodies. NACA TN 2813, 1952.

12. Smiley, Robert F.: The Application of Planing Characteristics to the Calculation of the Water-Landing Loads and Motions of Seaplanes of Arbitrary Constant Cross Section. NACA TN 2814, 1952.

13. Smiley, Robert F.: A Semiempirical Procedure for Computing the Water-Pressure Distribution on Flat and V-Bottom Prismatic Surfaces During Impact or Planing. NACA TN 2583, 1951.

14. Pierson, John D., and Leshnover, Samuel: A Study of the Flow, Pressures, and Loads Pertaining to Prismatic Vee-Planing Surfaces. S.M.F. Fund Paper No. FF-2, Inst. Aero. Sci. (Rep. No. 382, Project No. NR 062-012, Office of Naval Res., Exp. Towing Tank, Stevens Inst. Tech.), May 1950.

15. Smiley, Robert F.: Water-Pressure Distributions During Landing of a Prismatic Model Having an Angle of Dead Rise of $22\frac{1}{2}^\circ$ and Beam-Loading Coefficients of 0.48 and 0.97. NACA TN 2816, 1952.

16. Smiley, Robert F.: A Study of Water Pressure Distributions During Landings With Special Reference to a Prismatic Model Having a Heavy Beam Loading and a 30° Angle of Dead Rise. NACA TN 2111, 1950.

17. Korvin-Kroukovsky, B. V., Savitsky, Daniel, and Lehman, William F.: Wetted Area and Center of Pressure of Planing Surfaces. Preprint No. 244, S.M.F. Fund Paper, Inst. Aero. Sci. (Rep. No. 360, Project No. NR062-012, Office Naval Res., Exp. Towing Tank, Stevens Inst. Tech., Aug. 1949.)

18. Steiner, Margaret F.: Comparison of Over-All Impact Loads Obtained During Seaplane Landing Tests With Loads Predicted by Hydrodynamic Theory. NACA TN 1781, 1949.

19. Lamb, Horace: Hydrodynamics. Sixth ed., Cambridge Univ. Press, 1932, p. 102.

20. Steiner, Margaret F.: Analysis of Planing Data for Use in Predicting Hydrodynamic Impact Loads. NACA TN 1694, 1948.

21. Batterson, Sidney A.: The NACA Impact Basin and Water Landing Tests of a Float Model at Various Velocities and Weights. NACA Rep. 795, 1944. (Supersedes NACA ACR L4H15.)

22. Smiley, Robert F.: An Experimental Study of Water-Pressure Distributions During Landings and Planing of a Heavily Loaded Rectangular Flat-Plate Model. NACA TN 2453, 1951.

23. Gott, J. P.: Note on the Directional Stability of Seaplanes on the Water. R. & M. No. 1776, British A.R.C., 1937.

24. Locke, F. W. S., Jr.: Some Yawing Tests of a $\frac{1}{30}$-Scale Model of the Hull of the XPB2M-1 Flying Boat. NACA ARR 3G06, 1943.

25. Locke, F. W. S., Jr.: An Empirical Study of Low Aspect Ratio Lifting Surfaces With Particular Regard to Planing Craft. Jour. Aero. Sci., vol. 16, no. 3, Mar. 1949, pp. 184-188.

TABLE I

INITIAL LANDING CONDITIONS AND OVER-ALL LOADS AND MOTIONS

[$\beta = 22.5^\circ$]

Run	τ (deg)	Ψ (deg)	At contact				At $M_{t_{max}}$		At $n_{i_{w_{max}}}$		At $n_{i_{\eta_{max}}}$				At z_{max}		Time, t, at exit (sec)
			V_o (fps)	$\dot{z}_o$ (fps)	$\dot{x}_o$ (fps)	γ_o (deg)	t (sec)	M_t (lb-ft)	t (sec)	n_{i_w}	t (sec)	n_{i_η}	n_{i_w}	$\dot{z}$ (fps)	t (sec)	z (ft)	
1	3.2	0	71.9	4.1	71.8	3.27	----	----	0.095	1.17	----	----	----	---	0.168	0.40	0.468
2	3.2	6	71.6	4.1	71.5	3.28	0.12	580	.095	1.09	0.12	0.30	0.96	1.5	.187	.43	.467
3	3.2	-9	71.9	4.1	71.8	3.27	.10	880	.090	1.21	.10	.50	1.19	2.0	.179	.41	.462
4	3.2	9	71.6	4.2	71.5	3.36	.13	900	.102	1.16	.13	.47	1.02	1.0	.166	.41	.457
5	3.2	12	71.6	4.2	71.5	3.36	.11	1130	.100	1.27	.12	.64	1.18	1.2	.157	.40	----
6	3.2	0	71.6	5.0	71.4	4.01	----	----	.078	1.59	----	----	----	---	.160	.45	.459
7	3.2	3	71.8	5.0	71.6	4.00	----	----	.070	1.58	.11	.18	1.24	1.4	.160	.44	.447
8	3.2	6	73.8	5.1	73.6	3.96	.09	640	.063	1.59	.10	.42	1.43	2.0	.157	.46	.430
9	3.2	6	59.1	4.1	59.0	3.97	.13	440	.100	.96	.14	.25	.84	1.3	.203	.48	No exit
10	3.2	-6	58.5	4.1	58.4	4.01	.15	430	.080	1.09	.15	.26	.81	.8	.188	.43	-------
11	3.2	9	58.6	4.0	58.5	3.91	.12	650	.106	.92	.12	.38	.92	1.9	.205	.47	No exit
12	6.3	3	49.9	6.4	49.5	7.37	----	----	.080	1.98	.12	.12	1.48	1.5	.160	.58	.464
13	6.3	0	50.6	7.6	50.0	8.64	----	----	.070	2.31	----	----	----	---	.189	.68	.457
14	6.3	3	48.9	7.6	48.3	8.94	----	----	.076	2.27	.14	.13	1.02	.7	.163	.66	.466
15	6.3	6	49.0	7.6	48.4	8.91	----	----	.071	2.25	.08	.28	2.21	4.3	.185	.70	.460
16	9.3	0	66.9	3.8	66.8	3.26	----	----	.107	1.35	----	----	----	---	.142	.35	.316
17	9.3	3	66.8	3.8	66.7	3.26	.11	170	.108	1.20	.11	.10	1.19	1.7	.159	.39	.318
18	9.3	6	66.6	3.6	66.5	3.10	.12	370	.126	1.05	.13	.16	1.03	1.4	.187	.48	.335
19	9.3	-9	67.0	3.6	66.9	3.08	.13	600	.118	1.15	.13	.28	1.04	1.0	.160	.38	.332
20	9.3	-12	67.2	3.3	67.1	2.82	.14	720	.115	1.11	.13	.38	1.07	.9	.160	.35	.333
21	9.3	12	71.8	4.1	71.7	3.28	.12	860	.106	1.49	.13	.42	1.26	.5	.140	.38	.286
22	9.3	0	56.4	4.1	56.3	4.17	----	----	.112	1.21	----	----	----	---	.171	.46	.373
23	9.3	3	69.5	4.6	69.4	3.79	----	----	.099	1.69	.10	.12	1.69	2.0	.145	.42	.299
24	9.3	6	56.6	4.0	56.5	4.05	----	----	.112	1.29	.14	.23	1.16	.8	.162	.43	.366
25	9.3	-6	58.1	4.2	57.9	4.15	----	----	.110	1.31	.12	.23	1.30	1.5	.162	.44	.351
26	9.3	6	57.9	4.2	57.8	4.16	----	----	.110	1.36	.14	.24	1.16	.7	.160	.44	.355
27	9.3	9	67.3	4.3	67.2	3.66	.13	620	.112	1.47	.13	.32	1.32	.6	.145	.40	.314
28	9.3	9	56.7	4.1	56.6	4.14	----	----	.120	1.24	.13	.28	1.22	1.2	.162	.43	.372
29	9.3	0	89.6	7.4	89.3	4.74	----	----	.078	3.58	----	----	----	---	.102	.48	-------
30	9.3	0	91.0	7.8	90.7	4.92	----	----	.069	3.83	----	----	----	---	.095	.47	.208
31	9.3	3	79.9	6.2	79.7	4.45	----	----	.082	2.81	.11	.19	2.36	-.4	.105	.41	.239
32	9.3	3	80.5	6.3	80.3	4.49	----	----	.080	2.84	.08	.20	2.84	2.2	.106	.43	.237
33	9.3	3	47.5	3.9	47.3	4.71	----	----	.124	1.00	.15	.08	.95	1.1	.187	.47	.429
34	9.3	3	49.6	4.1	49.4	4.76	----	----	.116	1.20	.13	.11	1.13	1.5	.177	.46	.413
35	9.3	9	46.2	4.1	46.0	5.09	----	----	.132	1.15	.15	.26	1.09	1.0	.182	.49	.442
36	9.3	12	36.3	4.0	36.1	6.32	----	----	-----	----	----	----	----	---	-----	----	.655

NACA

TABLE II

PRESSURE-GAGE POSITIONS

[See fig. 39]

Gage	ξ (ft)	η (ft)
1	0.23	0.47
2	.23	.77
3	.23	1.08
4	.23	1.39
5	.73	.47
6	.73	.77
7	.73	1.08
8	.73	1.39
9	1.02	.62
10	1.07	.47
11	1.07	.77
12	1.07	1.08
13	1.07	1.39
14	1.17	.62
15	1.48	.47
16	1.48	.77
17	1.48	1.08
18	1.82	.32
19	1.82	.47

Gage	ξ (ft)	η (ft)
20	1.82	0.62
21	1.82	.77
22	1.82	.93
23	1.82	1.08
24	1.82	1.24
25	2.23	.47
26	2.23	.77
27	2.57	.47
28	2.57	.77
29	.73	-.47
30	.73	-.62
31	.73	-.77
32	.73	-.93
33	1.07	-.32
34	1.07	-.93
35	1.48	-.32
36	1.48	-.47
37	1.48	-.77

TABLE III

INITIAL LANDING CONDITIONS AND MAXIMUM BOTTOM PRESSURES

[$\beta = 22.5^\circ$]

Run	τ (deg)	ψ (deg)	V_o (fps)	$\dot{z}_o$ (fps)	$\dot{x}_o$ (fps)	γ_o (deg)	Maximum pressure (lb/sq in.) at gage number -																	
							1	2	3	4	5	6	7	8	9	10	11	12	13	14	15	16	17	18	19
1	3.2	0	71.9	4.1	71.8	3.27	5.4	5.4	2.7	1.6	3.5	4.4	3.3	1.2	4.4	4.4	5.4	3.7	1.3	5.3	2.3	4.1	---	----	4.3
2	3.2	6	71.6	4.1	71.5	3.28	8.3	9.0	4.4	----	----	6.4	6.4	---	6.3	6.6	11.3	5.8	.8	7.8	7.0	6.9	4.8	9.1	5.7
3	3.2	-9	71.9	4.1	71.8	3.27	----	----	.7	----	----	----	1.2	---	2.5	1.4	2.5	1.5	---	.9	1.8	.7	---	1.9	1.9
4	3.2	9	71.6	4.2	71.5	3.36	9.8	10.3	5.0	3.3	10.3	----	8.4	---	8.5	8.0	10.2	7.6	---	9.7	8.0	7.6	---	11.8	6.2
5	3.2	12	71.6	4.2	71.5	3.36	11.1	10.0	5.0	4.6	----	6.4	8.9	---	8.3	9.6	10.3	8.6	---	9.9	10.5	7.8	---	11.0	7.5
6	3.2	0	71.6	5.0	71.4	4.01	6.0	7.1	2.6	2.3	----	4.7	4.2	2.1	5.2	5.4	6.3	4.6	---	5.4	5.2	5.0	---	7.7	4.8
7	3.2	3	71.8	5.0	71.6	4.00	8.3	7.4	----	2.8	4.6	7.4	6.8	4.1	9.2	7.5	7.3	5.6	2.3	7.7	8.7	7.3	---	9.4	8.0
8	3.2	6	73.8	5.1	73.6	3.96	10.9	11.6	6.3	3.5	----	8.0	9.7	4.5	10.0	9.2	6.4	7.8	2.9	11.0	8.5	9.0	---	15.6	7.0
9	3.2	6	59.1	4.1	59.0	3.97	5.4	3.0	2.3	3.3	3.6	4.1	4.4	2.0	5.7	4.6	5.8	5.1	---	5.5	4.8	4.3	---	7.6	4.8
10	3.2	-6	58.5	4.1	58.4	4.01	2.6	2.6	-.9	----	3.1	----	1.2	.9	2.7	2.3	2.5	---	---	1.7	1.8	1.6	---	3.4	----
11	3.2	9	58.6	4.0	58.5	3.91	6.8	5.9	2.6	2.9	4.6	3.3	5.4	1.8	7.7	5.5	6.5	6.1	.6	6.6	5.3	5.2	---	8.3	4.2
12	6.3	3	49.9	6.4	49.5	7.37	7.5	8.6	4.0	4.5	----	5.0	7.5	---	7.1	8.5	7.3	8.2	4.7	8.3	8.2	5.9	6.6	9.8	6.6
13	6.3	0	50.6	7.6	50.0	8.64	8.9	9.0	4.5	----	9.7	6.6	7.2	---	7.9	9.8	8.9	7.0	5.0	10.4	9.8	6.9	---	11.6	6.5
14	6.3	3	48.9	7.6	48.3	8.94	6.9	8.5	3.7	4.2	----	----	7.5	---	7.1	9.3	8.4	8.4	5.5	8.7	9.1	7.3	---	10.0	5.7
15	6.3	6	49.0	7.6	48.4	8.91	9.1	10.9	5.2	6.4	10.5	7.5	9.4	---	9.3	10.7	10.1	9.4	7.1	11.3	10.7	9.0	7.6	12.7	7.6
16	9.3	0	66.9	3.8	66.8	3.26	13.8	14.5	8.3	1.6	----	5.8	2.3	---	9.6	----	3.6	.9	1.6	11.7	2.1	1.7	0	----	0
17	9.3	3	66.8	3.8	66.7	3.26	12.2	11.4	3.2	1.9	7.3	9.6	0	---	9.0	9.5	0	1.4	.8	3.5	1.1	.7	0	.8	0
18	9.3	6	66.6	3.6	66.5	3.10	12.0	11.3	3.6	2.0	11.6	5.9	1.9	---	10.0	9.7	2.5	1.9	1.2	3.1	2.2	2.4	---	1.2	0
19	9.3	-9	67.0	3.6	66.9	3.08	4.6	4.6	2.3	2.0	3.3	----	2.1	---	1.5	3.1	2.7	1.9	0	2.2	2.7	1.7	0	0	0
20	9.3	-12	67.2	3.3	67.1	2.82	3.5	2.9	2.8	1.9	2.3	1.8	2.3	---	2.1	1.8	2.3	1.2	0	2.2	2.4	0	0	.5	0
21	9.3	12	71.8	4.1	71.7	3.28	16.5	17.0	7.7	1.7	----	0	.8	---	14.7	16.4	4.9	2.0	.7	15.2	13.5	1.4	---	----	0
22	9.3	0	56.4	4.1	56.3	4.17	5.9	7.1	2.5	2.4	----	----	3.5	---	7.4	6.7	5.3	1.7	-.8	6.1	6.3	1.5	---	7.2	----
23	9.3	3	69.5	4.6	69.4	3.79	13.6	13.7	5.3	2.1	----	8.9	1.4	---	12.8	12.8	2.4	1.8	1.1	11.7	5.0	1.8	---	15.8	----
24	9.3	6	56.6	4.0	56.5	4.05	11.3	12.4	7.0	3.0	5.8	----	8.9	---	10.6	----	----	---	---	12.3	----	----	---	12.9	6.1
25	9.3	-6	58.1	4.2	57.9	4.15	7.4	7.8	4.6	1.5	5.1	7.0	5.1	2.4	7.1	----	----	---	.4	7.5	----	----	---	8.1	4.0
26	9.3	6	57.9	4.2	57.8	4.16	11.7	12.1	7.8	3.9	----	----	21.0	---	10.7	----	----	---	---	13.2	----	4.4	---	13.5	7.1
27	9.3	9	67.3	4.3	67.2	3.66	16.6	17.1	7.5	2.0	10.6	----	2.5	---	15.4	13.0	12.2	2.4	---	15.5	10.3	2.1	---	6.4	----
28	9.3	9	56.7	4.1	56.6	4.14	----	----	----	----	----	----	----	---	----	----	----	----	---	----	----	----	---	----	----
29	9.3	0	89.6	7.4	89.3	4.74	20.3	19.3	13.7	8.3	----	14.8	14.5	3.2	22.2	----	20.1	---	---	18.3	18.8	4.0	---	14.5	0
30	9.3	0	91.0	7.8	90.7	4.92	21.4	23.5	10.2	11.1	----	12.0	16.2	---	18.5	21.1	18.8	4.6	---	20.2	17.3	10.5	---	16.5	16.0
31	9.3	3	79.9	6.2	79.7	4.45	17.7	19.3	9.9	6.1	----	12.7	14.3	1.9	16.1	18.1	15.7	2.9	0	17.0	----	1.9	---	19.0	12.4
32	9.3	3	80.5	6.3	80.3	4.49	20.8	21.2	13.7	8.3	----	16.3	19.9	0	20.9	----	----	---	0	25.0	----	8.5	---	21.0	14.3
33	9.3	3	47.5	3.9	47.3	4.71	7.0	7.2	3.5	2.5	----	5.1	5.7	---	----	6.9	7.1	---	---	7.5	5.8	4.0	---	8.7	----
34	9.3	3	49.6	4.1	49.4	4.76	9.1	9.5	4.9	3.4	----	3.2	7.2	0	7.9	----	----	---	0	8.5	----	4.8	---	9.7	5.2
35	9.3	9	46.2	4.1	46.0	5.09	----	----	----	----	----	----	----	---	----	----	----	---	---	----	----	----	---	----	----
36	9.3	12	36.3	4.0	36.1	6.32	6.0	6.2	2.3	4.0	4.7	----	6.2	---	7.1	-2.5	----	---	1.7	7.7	----	4.8	---	9.0	4.3

TABLE III - Concluded

INITIAL LANDING CONDITIONS AND MAXIMUM BOTTOM PRESSURES - Concluded

[$\beta = 22.5°$]

Run	τ (deg)	ψ (deg)	V_o (fps)	$\dot{z}_o$ (fps)	$\dot{x}_o$ (fps)	γ_o (deg)	Maximum pressure (lb/sq in.) at gage number -																
							20	21	22	23	24	25	26	27	28	29	30	31	32	33	34	35	36	37
1	3.2	0	71.9	4.1	71.8	3.27	4.7	5.8	3.6	0.8	0.7	4.3	---	3.0	1.2	5.8	7.0	----	5.0	6.4	----	4.0	6.0	1.3
2	3.2	6	71.6	4.1	71.5	3.28	9.8	8.7	4.6	2.1	1.0	6.6	---	3.0	2.9	2.7	1.6	1.4	2.4	3.1	----	1.9	3.3	1.5
3	3.2	-9	71.9	4.1	71.8	3.27	1.2	2.5	1.1	.5	.2	1.6	---	.9	1.5	10.1	7.7	7.8	9.4	11.6	----	8.2	10.9	5.2
4	3.2	9	71.6	4.2	71.5	3.36	8.3	9.9	6.7	4.7	1.1	7.6	---	3.5	----	2.2	1.2	.7	1.7	2.3	----	2.1	2.0	1.2
5	3.2	12	71.6	4.2	71.5	3.36	10.0	11.3	7.9	----	.8	9.2	---	3.7	4.4	1.5	-1.8	-.9	1.9	1.7	----	----	1.3	----
6	3.2	0	71.6	5.0	71.4	4.01	4.6	6.7	4.3	3.3	1.2	4.6	---	2.4	2.2	6.2	4.5	----	5.4	6.9	----	5.1	6.7	2.1
7	3.2	3	71.8	5.0	71.6	4.00	9.8	9.5	6.4	4.8	1.5	7.4	---	3.3	----	----	4.9	----	9.3	----	4.8	5.7	6.5	----
8	3.2	6	73.8	5.1	73.6	3.96	7.7	10.8	8.0	6.9	3.2	8.7	---	3.7	----	4.5	2.9	2.1	4.1	5.2	----	3.0	5.2	----
9	3.2	6	59.1	4.1	59.0	3.97	6.8	6.2	3.2	3.9	.2	5.0	---	1.8	1.6	1.9	1.2	1.3	1.6	2.1	----	1.8	3.2	1.1
10	3.2	-6	58.5	4.1	58.4	4.01	----	3.1	---	----	----	2.5	---	1.1	-2.1	6.0	4.6	2.1	5.1	6.7	----	4.9	----	4.2
11	3.2	9	58.6	4.0	58.5	3.91	6.0	7.5	4.1	5.1	----	5.8	---	2.8	----	1.5	.4	1.1	1.1	1.5	----	.8	2.0	.8
12	6.3	3	49.9	6.4	49.5	7.37	8.1	9.0	5.7	----	3.3	7.8	5.3	3.8	4.1	6.7	4.6	4.6	5.0	7.5	----	5.0	6.5	3.8
13	6.3	0	50.6	7.6	50.0	8.64	8.1	9.5	5.8	----	4.5	8.4	5.5	4.0	4.2	9.3	5.9	5.8	6.5	10.3	----	7.0	8.8	----
14	6.3	3	48.9	7.6	48.3	8.94	8.1	9.0	6.6	----	4.4	9.1	6.3	4.3	3.9	8.1	5.3	5.3	5.9	8.8	----	7.0	7.2	4.1
15	6.3	6	49.0	7.6	48.4	8.91	9.5	12.4	8.8	----	6.2	11.2	8.0	5.9	5.6	6.9	4.7	4.0	5.5	6.8	----	5.9	6.6	3.8
16	9.3	0	66.9	3.8	66.8	3.26	0	0	0	0	0	14.6	---	0	0	13.4	9.8	7.6	3.7	14.0	----	9.3	4.5	1.1
17	9.3	3	66.8	3.8	66.7	3.26	0	0	0	0	0	0	0	0	0	10.1	6.9	4.4	.9	11.5	----	6.8	1.0	0
18	9.3	6	66.6	3.6	66.5	3.10	0	0	0	0	0	0	0	0	0	7.1	3.3	3.8	1.1	8.3	----	4.5	1.0	.5
19	9.3	-9	67.0	3.6	66.9	3.08	0	0	0	0	0	0	0	0	0	14.9	----	9.6	1.1	17.1	----	10.1	1.3	1.4
20	9.3	-12	67.2	3.3	67.1	2.82	0	0	0	0	0	0	0	0	0	18.1	10.7	12.2	1.1	19.1	----	11.9	1.3	1.4
21	9.3	12	71.8	4.1	71.7	3.28	0	0	0	0	0	0	0	0	0	5.1	2.9	2.3	1.9	6.4	----	3.4	3.7	0
22	9.3	0	56.4	4.1	56.3	4.17	----	----	1.2	----	1.0	----	---	---	----	8.0	4.6	5.0	5.7	9.2	----	5.9	7.3	----
23	9.3	3	69.5	4.6	69.4	3.79	----	----	---	1.0	1.0	----	---	---	----	12.4	8.0	----	7.2	13.1	----	8.4	10.0	----
24	9.3	6	56.6	4.0	56.5	4.05	----	----	---	----	----	----	---	---	----	----	----	----	----	----	----	----	----	----
25	9.3	-6	58.1	4.2	57.9	4.15	----	----	---	----	----	----	---	---	----	----	11.2	9.9	----	----	3.4	6.3	5.9	----
26	9.3	6	57.9	4.2	57.8	4.16	----	.3	---	.7	.7	.5	---	---	----	----	6.4	5.4	----	----	7.6	12.4	13.7	1.1
27	9.3	9	67.3	4.3	67.2	3.66	----	----	---	----	1.0	----	---	---	----	6.5	4.1	3.7	4.2	8.2	4.6	7.3	7.6	1.8
28	9.3	9	56.7	4.1	56.6	4.14	----	----	---	----	----	----	---	---	----	----	----	----	----	----	----	4.6	6.7	.9
29	9.3	0	89.6	7.4	89.3	4.74	----	----	---	----	----	----	---	---	----	21.4	17.6	17.5	19.3	31.5	----	20.5	23.2	2.0
30	9.3	0	91.0	7.8	90.7	4.92	1.1	1.9	---	----	-.5	.8	---	---	----	22.9	6.9	14.7	16.5	22.8	----	17.1	16.6	12.4
31	9.3	3	79.9	6.2	79.7	4.45	0	1.2	1.4	----	.7	0	.8	0	0	17.0	9.8	9.4	11.5	16.6	----	12.2	12.2	----
32	9.3	3	80.5	6.3	80.3	4.49	----	1.3	.5	1.0	1.4	1.1	---	---	----	----	----	----	----	----	10.6	14.6	9.8	4.7
33	9.3	3	47.5	3.9	47.3	4.71	----	----	---	----	----	----	---	---	----	6.5	4.6	1.9	4.4	6.9	----	----	6.4	2.6
34	9.3	3	49.6	4.1	49.4	4.76	3.7	.6	0	0	.3	0	---	0	0	----	5.1	4.6	----	----	3.9	5.8	7.2	4.2
35	9.3	9	46.2	4.1	46.0	5.09	----	----	---	----	----	----	---	---	----	----	----	----	----	----	2.9	3.6	5.9	----
36	9.3	12	36.3	4.0	36.1	6.32	6.2	5.7	1.9	-1.2	-1.9	5.7	---	1.3	----	----	1.4	----	----	----	2.5	2.3	1.2	2.5

TABLE IV

TIMES OF MAXIMUM BOTTOM PRESSURES

$[\beta = 22.5^\circ]$

Run	Time of maximum pressure (sec) on gage number -																		
	1	2	3	4	5	6	7	8	9	10	11	12	13	14	15	16	17	18	19
1	0.033	0.057	0.090	0.100	0.040	0.065	0.099	0.110	0.057	0.048	0.078	0.117	0.150	0.060	0.058	0.081	———	———	0.059
2	———	———	———	———	———	———	———	———	———	———	.078	.116	———	———	.058	———	———	———	———
3	———	———	.091	———	.040	———	.101	———	.056	.048	.078	———	———	.059	.058	.080	.089	.047	.059
4	.034	.058	.089	.150	.040	.066	.101	———	.056	.048	.076	.113	———	.060	.058	.081	.130	.048	.060
5	.031	.055	.083	.145	.037	.062	.091	———	.053	.046	.075	.106	———	.056	.055	.077	.117	.044	.056
6	.028	.048	.073	.112	.035	.054	.081	.137	.047	.041	.065	.093	———	.050	.048	.067	.099	.040	.050
7	.025	.043	.065	.105	.029	.049	.073	.115	.044	.037	.058	.084	.140	.046	.045	.060	.088	.036	.045
8	.026	.045	.068	.101	.033	.052	.075	.118	.044	.039	.060	.088	.137	.047	.046	.063	.093	.037	.047
9	.035	.060	.091	.137	.043	.068	.101	.185	.060	.052	.079	.123	———	.063	.059	.084	.125	.051	.062
10	.033	.057	.155	———	.040	———	.096	.144	.054	.049	.075	———	———	.059	.057	.079	.124	.046	———
11	.037	.063	.095	.139	.044	.070	.104	.179	.061	.053	.081	.117	.087	.065	.061	.086	.129	.052	.064
12	.021	.036	.054	.072	.028	.045	.063	.083	.043	.039	.059	.077	.097	.046	.052	.061	.081	.045	.052
13	.016	.028	.044	.060	.023	.035	.049	.068	.033	.033	.047	.063	.078	.035	.040	.050	.067	.035	.042
14	.018	.032	.048	.066	.024	———	.055	.074	.037	.034	.052	.068	.084	.041	.045	.053	.072	.039	.044
15	.018	.032	.048	.062	.025	.039	.053	.071	.036	.034	.050	.065	.079	.040	.044	.053	.069	.039	.045
16	.043	.074	.128	.083	———	.104	.081	.102	.107	———	.072	.110	.165	.133	.137	.163	———	———	———
17	.041	.070	.134	.122	.063	.111	———	———	.113	.090	———	.143	.106	.134	.113	.133	———	.133	———
18	.050	.084	.045	.095	.077	.136	.116	.105	.140	.106	.115	.165	.156	.147	.130	.160	———	.204	———
19	.045	.078	.110	.135	.072	———	.130	.141	.135	.101	.123	.188	———	.144	.148	.160	———	———	———
20	.051	.084	.169	.142	.077	.117	.133	.172	.143	.109	.130	.185	———	.122	.204	———	———	.202	———
21	.042	.068	.108	.068	.061	———	.060	.072	.094	.079	.127	.129	.098	.108	.118	.112	———	———	———
22	.042	.068	.104	.099	.063	———	.149	———	.092	.084	.123	.156	.109	.102	.112	.149	———	.118	———
23	.037	.059	.093	.066	.053	.082	.080	.080	.082	.073	.129	.129	.095	.095	.107	.110	———	.125	———
24	.040	.064	.097	.147	.057	———	.132	———	.087	———	———	———	———	.096	———	———	———	.107	.127
25	.038	.061	.094	.137	.057	.086	.129	.107	.083	———	———	———	.110	.094	———	———	———	.107	.129
26	———	———	———	———	———	———	———	———	———	———	———	———	———	———	———	———	———	———	———
27	.039	.064	.099	.105	.062	———	.066	.082	.089	.080	.132	.127	———	.104	.117	.124	———	.132	———
28	———	———	———	———	———	———	———	———	———	———	———	———	———	———	———	———	———	———	———
29	.023	.037	.060	.094	———	.050	.075	.065	.050	———	.070	———	———	.056	.065	.093	———	.063	———
30	.019	.030	.048	.076	.029	.043	.068	———	.043	.040	.062	.093	———	.048	.057	.081	.093	.054	.068
31	.023	.040	.063	.098	.037	.056	.087	.058	.056	.051	.077	.095	———	.063	.070	.078	———	.070	.090
32	.023	.039	.060	.090	.036	.054	.082	———	.053	———	———	———	———	.060	———	.099	———	.068	.082
33	.043	.067	.099	.151	.061	.091	.129	.175	———	.080	.116	———	———	.099	.107	.159	———	.109	———
34	.037	.062	.090	.127	.057	.081	.117	———	.081	———	———	———	———	.092	———	.137	———	.100	.117
35	———	———	———	———	———	———	———	———	———	———	———	———	———	———	———	———	———	———	———
36	.040	.063	.094	.125	.058	———	.114	.160	.083	———	———	———	.200	.090	———	.125	.174	.098	.112

NACA

TABLE IV - Concluded

TIMES OF MAXIMUM BOTTOM PRESSURES - Concluded

[$\beta = 22.5^\circ$]

Run	Time of maximum pressure (sec) on gage number -																	
	20	21	22	23	24	25	26	27	28	29	30	31	32	33	34	35	36	37
1	0.074	0.090	0.116	0.125	0.126	0.067	———	0.076	0.107	0.045	0.055	———	0.083	0.038	———	0.044	0.056	0.081
2	———	———	———	———	———	———	———	———	———	.045	———	0.071	.086	.039	———	.043	.056	———
3	.075	.094	.129	.094	.094	.067	———	.074	.143	.043	.053	.069	.081	.037	———	.043	.054	.079
4	.075	.093	.115	.155	.098	.068	———	.076	———	.045	.057	.071	.086	.037	———	.112	.055	.084
5	.071	.085	.104	.145	.093	.064	———	.070	.098	.048	.165	.111	.086	.041	———	———	.053	———
6	.062	.076	.092	.114	.127	.057	———	.064	———	.037	.047	———	.069	.033	———	.038	.047	.065
7	.055	.066	.080	.100	.135	.053	———	.059	———	———	.045	———	.065	.028	0.069	.034	.044	———
8	.058	.071	.083	.105	.140	.053	———	.059	.079	.036	.045	.056	.068	.031	———	.037	.045	———
9	.077	.093	.113	.150	.092	.070	———	.079	———	.048	.059	.073	.088	.040	———	.046	.058	.087
10	———	.089	———	———	———	.067	———	.074	———	.045	.055	.067	.081	.038	———	.044	———	.079
11	.079	.094	.114	.149	———	.073	———	.080	.109	.049	.062	.076	.090	.040	———	.047	.059	.089
12	.062	.070	.081	.094	.113	.062	0.078	.071	.089	.036	.040	.053	.061	.035	———	.043	.050	.064
13	.050	.058	.067	.078	.090	.051	.065	.059	.071	.030	.035	.044	.051	.028	———	.034	.041	.054
14	.053	.062	.071	.082	.094	.054	.068	.061	.076	.031	.036	.046	.053	.030	———	.036	.043	.055
15	.053	.060	.068	.078	.090	.054	.065	.060	.073	.031	.036	.046	.052	.030	———	.036	.043	.056
16	———	———	———	———	———	.092	———	———	———	.070	.088	.107	.138	.074	———	.102	.137	.178
17	———	———	———	———	———	———	———	———	———	.071	.083	.108	.158	.073	———	.104	.138	———
18	———	———	———	———	———	———	———	———	———	.080	.100	.135	.010	.085	———	.130	.135	.128
19	———	———	———	———	———	———	———	———	———	.080	.095	.128	.088	.083	———	.126	.123	.175
20	———	———	———	———	———	———	———	———	———	.084	.100	.136	.078	.088	———	.132	.125	.182
21	———	———	.163	———	———	———	———	———	———	.061	.075	.093	.124	.064	———	.087	.114	———
22	———	———	.139	.141	.149	———	———	———	———	.068	.083	.096	.116	.071	———	.092	.111	———
23	———	———	.170	.130	.190	———	———	———	———	.058	.070	———	.108	.060	———	.182	.104	———
24	———	———	———	———	———	———	———	———	———	———	.077	.090	———	.066	.135	.086	.102	———
25	———	———	———	———	———	———	———	———	———	———	.074	.087	———	.064	.132	.083	.097	.052
26	———	———	———	———	———	———	———	———	———	———	———	.085	———	.061	.124	.081	.094	———
27	———	———	———	———	.214	———	———	———	———	.063	.076	.093	.124	.067	———	.090	.112	.151
28	———	———	———	———	———	———	———	———	———	———	———	———	———	———	———	———	———	———
29	———	———	———	———	———	———	———	———	———	.038	.046	.055	.066	.040	———	.052	.063	.096
30	.087	.065	———	———	.108	.093	———	———	———	.035	.039	.052	.059	.036	———	.047	.055	.088
31	———	.084	.149	.102	.168	———	.128	———	———	.044	.050	.063	.074	.045	———	.058	.069	———
32	———	.079	.099	.095	.104	.105	———	———	———	———	.049	———	———	.042	.084	.054	.064	.101
33	———	———	———	———	———	———	———	———	———	.067	.079	.095	.110	.070	———	———	.105	.153
34	.152	.115	———	.138	.142	———	———	———	———	———	.072	.087	———	———	.123	.082	.095	.134
35	———	———	———	———	———	———	———	———	———	———	———	———	———	.065	.122	.085	.097	———
36	.130	.152	.193	.120	.160	.144	———	.200	———	———	.075	———	———	.065	.116	.082	.096	.130

NACA

TABLE V

VERTICAL-VELOCITY TIME HISTORIES

[$\beta = 22.5^{\circ}$]

Run	$\dot{z}$ (fps) at time -																				
	0.00 sec	0.01 sec	0.02 sec	0.03 sec	0.04 sec	0.05 sec	0.06 sec	0.07 sec	0.08 sec	0.09 sec	0.10 sec	0.11 sec	0.12 sec	0.13 sec	0.14 sec	0.15 sec	0.16 sec	0.17 sec	0.18 sec	0.19 sec	0.20 sec
1	4.1	4.1	4.1	4.0	3.9	3.7	3.4	3.1	2.7	2.4	2.0	1.6	1.3	1.0	0.7	0.4	0.2	0	-0.2	-0.4	----
2	4.1	4.1	4.1	4.0	3.9	3.7	3.5	3.2	2.8	2.5	2.1	1.8	1.5	1.2	.9	.7	.5	.3	.1	0	-0.2
3	4.1	4.1	4.1	4.0	3.9	3.7	3.4	3.1	2.7	2.3	2.0	1.6	1.3	1.0	.7	.5	.3	.1	0	-.1	----
4	4.2	4.2	4.2	4.1	4.0	3.8	3.5	3.2	2.8	2.5	2.1	1.7	1.4	1.0	.7	.4	.1	-.1	-.3	-.5	-.7
5	4.2	4.2	4.2	4.1	4.0	3.8	3.5	3.2	2.8	2.4	2.0	1.6	1.2	.9	.5	.2	-.1	-.3	-.5	----	----
6	5.0	5.0	4.9	4.8	4.6	4.3	3.9	3.4	2.9	2.4	2.0	1.5	1.2	.8	.5	.2	0	-.2	----	----	----
7	5.0	5.0	5.0	4.9	4.6	4.3	3.8	3.3	2.8	2.3	1.9	1.4	1.1	.8	.5	.2	0	---	----	----	----
8	5.1	5.1	5.1	5.0	4.8	4.5	4.0	3.5	3.0	2.5	2.0	1.6	1.2	.8	.5	---	---	---	----	----	----
9	4.1	4.1	4.1	4.0	3.9	3.8	3.6	3.4	3.1	2.8	2.5	2.2	1.9	1.6	1.3	1.1	.8	.6	.4	.2	----
10	4.1	4.1	4.0	4.0	3.9	3.7	3.5	3.2	2.9	2.5	2.2	1.9	1.6	1.3	1.0	.8	.5	.3	.2	----	----
11	4.0	4.0	4.0	3.9	3.8	3.7	3.5	3.3	3.1	2.8	2.5	2.2	1.9	1.6	1.3	1.1	.9	.6	.4	.3	.1
12	6.4	6.4	6.3	6.2	5.9	5.5	5.0	4.4	3.8	3.2	2.6	2.0	1.5	1.1	.7	.3	---	---	----	----	----
13	7.6	7.5	7.4	7.1	6.7	6.1	5.5	4.7	4.0	3.3	2.7	2.2	1.8	1.4	1.1	.8	.6	.4	.2	0	----
14	7.6	7.5	7.4	7.2	6.9	6.4	5.7	5.0	4.3	3.6	2.9	2.3	1.7	1.1	.7	.4	---	---	----	----	----
15	7.6	7.6	7.5	7.2	6.9	6.4	5.7	5.0	4.3	3.6	2.9	2.4	1.9	1.5	1.1	.8	.5	.3	.1	-.1	----
16	3.8	3.8	3.7	3.7	3.5	3.4	3.1	2.8	2.5	2.1	1.7	1.3	.9	.5	.1	---	---	---	----	----	----
17	3.8	3.8	3.8	3.7	3.6	3.5	3.3	3.1	2.8	2.5	2.1	1.7	1.4	1.0	.7	---	---	---	----	----	----
18	3.6	3.6	3.6	3.6	3.6	3.5	3.3	3.2	2.9	2.7	2.4	2.1	1.8	1.4	1.1	.8	.6	.3	.1	-.1	----
19	3.6	3.6	3.6	3.5	3.5	3.3	3.2	3.0	2.7	2.4	2.1	1.8	1.4	1.0	.7	---	---	---	----	----	----
20	3.3	3.3	3.3	3.3	3.2	3.1	3.0	2.8	2.5	2.3	2.0	1.6	1.3	.9	.6	.3	0	---	----	----	----
21	4.1	4.1	4.1	4.0	3.9	3.7	3.4	3.1	2.7	2.3	1.8	1.3	.9	.5	0	---	---	---	----	----	----
22	4.1	4.1	4.1	4.1	4.0	3.9	3.7	3.5	3.2	2.9	2.6	2.2	1.9	1.5	1.1	.8	---	---	----	----	----
23	4.6	4.6	4.6	4.5	4.3	4.1	3.8	3.4	3.0	2.5	2.0	1.4	1.0	.5	.2	---	---	---	----	----	----
24	4.0	4.0	4.0	4.0	3.9	3.8	3.6	3.4	3.1	2.8	2.4	2.0	1.6	1.2	.8	.4	.1	-.2	-.5	----	----
25	4.2	4.2	4.2	4.2	4.1	3.9	3.7	3.5	3.1	2.8	2.4	2.0	1.5	1.1	.7	.4	.1	-.2	-.5	----	----
26	4.2	4.2	4.2	4.2	4.1	4.0	3.8	3.5	3.2	2.8	2.4	1.9	1.5	1.1	.7	.3	0	-.3	-.6	----	----
27	4.3	4.3	4.2	4.2	4.0	3.8	3.6	3.2	2.9	2.4	2.0	1.5	1.0	.6	.2	-.2	---	---	----	----	----
28	4.1	4.1	4.1	4.0	3.9	3.8	3.6	3.4	3.1	2.7	2.4	2.0	1.6	1.2	.8	.4	.1	-.2	-.5	-.7	-.9
29	7.4	7.3	7.2	6.8	6.2	5.4	4.4	3.3	2.2	1.1	.2	-.6	-1.2	---	---	---	---	---	----	----	----
30	7.8	7.7	7.5	7.0	6.3	5.3	4.1	2.9	1.6	.5	-.5	-1.4	----	---	---	---	---	---	----	----	----
31	6.2	6.1	5.9	5.6	5.2	4.6	3.9	3.1	2.2	1.3	.4	-.4	----	---	---	---	---	---	----	----	----
32	6.3	6.3	6.1	5.9	5.4	4.7	4.0	3.1	2.2	1.3	.5	-.3	-.9	---	---	---	---	---	----	----	----
33	3.9	3.9	3.9	3.9	3.8	3.7	3.6	3.4	3.2	2.9	2.6	2.3	2.0	1.7	1.4	1.1	.8	.5	.2	-.1	----
34	4.1	4.1	4.1	4.1	4.0	3.9	3.7	3.5	3.2	2.9	2.6	2.2	1.8	1.5	1.1	.8	.5	.2	-.1	----	----
35	4.1	4.1	4.1	4.1	4.0	3.9	3.7	3.6	3.3	3.0	2.7	2.4	2.1	1.7	1.3	1.0	.6	.3	0	----	----
36	4.0	---	---	---	---	---	---	---	---	---	---	---	---	---	---	---	---	---	----	----	----

TABLE VI

INSTANTANEOUS PRESSURE DISTRIBUTIONS

[β = 22.5°]

Run	τ (deg)	ψ (deg)	t (sec)	z (ft)	$\dot{z}$ (fps)	n_{i_w}	Pressure (lb/sq in.) at gage number -														
							1	2	3	4	5	6	7	8	9	10	11	12	13	14	15
1	3.2	0	0.116	0.37	1.4	1.06	1.8	3.2	1.9	1.2	1.5	1.6	2.6	0.6	1.3	1.2	3.5	3.5	0.8	0.6	1.0
3	3.2	-9	.129	.38	1.0	.84	.5	1.6	0	0	0	0	.5	.3	----	0	1.8	1.8	0	-1.4	.5
4	3.2	9	.115	.38	1.5	1.11	1.6	3.0	2.7	1.1	2.0	---	6.5	0	2.8	1.3	4.1	7.9	0	1.1	1.5
5	3.2	12	.104	.36	1.9	1.27	.9	2.6	2.5	2.0	---	2.1	6.2	0	2.9	1.8	4.1	---	0	1.4	1.9
6	3.2	0	.092	.38	2.3	1.41	1.3	2.2	1.7	---	---	.9	3.3	0	1.5	1.1	3.0	4.4	----	.6	1.1
7	3.2	3	.080	.35	2.8	1.55	2.1	3.9	1.4	2.1	3.1	3.4	5.5	0	3.5	3.4	4.1	0	1.4	1.4	2.5
8	3.2	6	.083	.37	2.8	1.52	2.9	5.2	4.9	1.6	---	3.6	8.4	.9	3.3	3.0	4.8	4.6	.8	3.0	2.9
9	3.2	6	.113	.39	2.1	.93	.5	.8	.5	1.2	.8	---	3.5	-.6	2.2	0	2.5	5.3	-.2	0	.9
10	3.2	-6	.113	.38	1.8	.93	0	0	-.5	0	0	-.6	.5	0	1.2	-.7	1.0	1.7	0	-1.4	0
11	3.2	9	.114	.39	2.1	.92	.3	.6	1.9	1.2	0	.9	4.2	-1.2	2.4	0	3.1	4.4	-.4	.6	.4
12	6.3	3	.078	.44	3.9	1.97	0	0	0	4.0	---	1.1	3.5	----	2.4	.7	3.1	7.8	-.4	1.4	2.1
13	6.3	0	.065	.44	5.1	2.28	0	.6	.9	---	1.2	1.0	3.4	----	2.5	2.4	3.4	7.0	0	2.8	2.1
14	6.3	3	.068	.46	5.2	2.24	.4	1.6	1.1	4.2	---	0	4.3	----	3.3	2.2	4.6	8.4	0	1.8	2.8
15	6.3	6	.065	.45	5.4	2.20	1.2	1.0	1.4	4.7	2.6	2.1	5.5	----	2.9	2.6	5.4	9.4	0	3.3	3.4
22	9.3	0	.123	.42	1.8	1.15	.4	.6	.9	1.4	---	0	0	----	3.7	2.2	5.9	1.3	-.4	3.3	5.2
23	9.3	3	.129	.42	.6	1.26	1.3	3.1	3.2	2.4	---	3.9	-1.5	----	7.2	4.0	6.3	1.3	-1.1	7.3	4.3
24	9.3	6	.127	.41	1.3	1.24	2.3	3.2	4.0	1.2	7.6	---	8.4	0	5.1	0	0	0	0	6.7	0
25	9.3	-6	.129	.42	1.2	1.24	2.2	3.8	3.0	1.8	2.3	4.0	5.3	----	3.2	0	0	0	.4	3.6	0
27	9.3	9	.132	.40	.5	1.29	1.8	3.8	5.0	2.0	2.5	---	-1.4	----	9.6	4.1	12.5	1.9	-.8	11.3	9.2
31	9.3	3	.087	.40	1.5	2.80	3.2	4.9	5.2	5.2	---	6.6	14.3	----	8.3	6.4	13.4	2.0	0	9.2	10.3
32	9.3	3	.082	.40	2.1	2.84	5.5	7.0	8.0	5.1	---	8.3	19.7	----	10.1	0	0	0	.6	13.0	0
34	9.3	3	.117	.41	2.0	1.20	1.5	2.6	2.3	1.0	---	1.6	7.5	0	----	0	0	0	0	4.4	0

TABLE VI - Concluded

INSTANTANEOUS PRESSURE DISTRIBUTIONS - Concluded

[$\beta = 22.5^{\circ}$]

Run	Pressure (lb/sq in.) at gage number -																					
	16	17	18	19	20	21	22	23	24	25	26	27	28	29	30	31	32	33	34	35	36	37
1	1.3	---	----	2.4	2.3	4.2	3.8	0	0.5	1.9	0	1.5	0.5	1.9	2.2	---	2.7	2.0	---	1.3	1.6	0.4
3	-.7	0	1.1	1.4	.8	1.9	.6	.5	0	1.1	0	---	-1.0	1.4	1.2	1.7	4.2	2.1	---	1.1	2.1	1.0
4	2.6	---	3.8	3.3	3.6	6.2	6.5	.5	.8	3.4	0	1.5	2.7	0	-.9	-.4	.9	1.0	---	-2.1	.3	.6
5	2.5	---	1.2	2.5	4.4	7.3	7.6	---	.7	3.7	---	1.5	3.6	0	-.9	-.9	0	.5	---	0	0	0
6	1.3	---	3.5	2.9	2.7	4.8	4.3	0	.5	2.4	0	1.1	.7	1.4	.7	.7	2.7	2.0	---	1.0	1.6	---
7	2.0	---	3.8	2.7	---	5.7	---	0	1.0	4.1	0	2.0	0	0	2.1	0	---	---	3.1	0	1.0	---
8	4.4	---	----	4.5	4.1	7.5	7.5	.7	1.8	3.8	0	2.1	----	1.9	---	.6	2.7	1.8	---	1.4	1.4	---
9	.9	---	2.2	1.9	2.9	4.3	3.4	0	0	1.8	0	.9	1.2	0	1.4	-.7	.5	1.3	---	0	.7	1.1
10	-.2	0	1.2	1.4	0	1.6	.7	0	0	1.1	0	.5	1.2	.5	0	.8	2.0	1.3	---	.8	.8	1.3
11	1.5	0	2.2	1.4	2.5	4.7	2.7	0	0	2.4	0	.9	----	-.7	2.0	-.9	0	1.0	---	.8	0	.8
12	2.8	3.9	2.5	3.3	3.9	6.4	3.9	---	.5	3.8	4.9	1.9	-.4	.9	-.4	1.1	2.5	2.9	---	.8	2.0	2.6
13	2.5	---	3.5	4.9	4.4	7.3	4.4	0	1.3	4.3	5.5	3.1	-.8	1.7	1.3	1.6	3.4	2.5	---	1.8	2.8	1.9
14	3.3	---	3.2	3.2	4.2	7.8	3.7	---	1.0	4.8	6.3	2.7	-.8	1.3	.4	1.4	2.7	2.7	---	1.3	2.4	2.8
15	4.1	3.2	3.5	4.2	5.5	9.9	3.8	---	1.3	5.6	4.9	4.5	-.8	1.3	0	1.1	2.8	2.4	---	1.4	1.7	2.7
22	-1.5	0	6.7	0	0	0	0	---	0	0	0	0	0	1.5	1.1	2.5	5.3	3.6	---	2.3	5.3	---
23	----	0	----	0	0	0	-.7	-.5	0	0	0	---	0	1.5	.7	2.0	6.1	4.2	---	2.7	7.1	---
24	-.6	---	8.9	3.3	0	0	0	0	0	0	0	0	0	0	.9	---	---	---	---	2.0	2.5	0
25	0	---	5.9	4.0	0	---	0	0	0	0	0	0	0	0	4.9	4.7	0	---	---	5.0	7.8	.3
27	-2.3	---	6.3	0	0	0	-.7	---	0	0	0	0	0	.4	-.2	1.1	3.3	4.1	---	1.7	4.9	.3
31	-1.5	---	11.3	12.4	---	1.5	---	---	---	---	0	---	13.4	4.3	2.2	4.6	8.7	6.4	---	5.9	7.7	---
32	0	---	15.4	13.8	0	1.3	0	0	0	---	---	0	0	0	3.8	---	0	.7	---	6.7	6.5	0
34	1.1	---	6.3	4.8	0	.6	0	0	0	0	0	---	0	0	1.3	2.3	---	0	---	2.3	4.1	.3

TABLE VII

PLANING DATA

[$\beta = 22.5^\circ$]

Run	τ (deg)	ψ (deg)	z (ft)	$\dot{x}$ (fps)	F_ζ (lb)	F_η (lb)	M_ξ (lb-ft)	M_ζ (lb-ft)	Pressure (lb/sq/in.) at gage number - 1	2	3	4	5	6	7
37	6.3	6	0.46	41.8	777	165	172	187	1.2	0.9	0.8	1.2	----	1.4	2.3
38	6.3	6	.47	60.8	----	----	----	----	.8	1.0	1.6	-2.3	----	-.7	9.8
39	6.3	9	.47	60.2	1560	468	568	520	1.6	1.9	2.6	2.7	----	2.4	11.4
40	9.3	6	.47	53.8	1900	278	294	406	.8	.6	2.0	----	----	3.2	----

Run	Pressure (lb/sq in.) at gage number - 8	9	10	11	12	13	14	15	16	17	18	19	20	21	22
37	----	0.9	0.9	1.7	1.2	0.4	0	1.5	1.8	----	1.7	----	2.1	2.1	1.5
38	----	-.5	1.8	2.8	5.4	0	1.8	2.2	2.9	----	3.5	1.7	3.3	6.8	3.2
39	----	2.0	1.9	4.3	7.1	1.1	2.8	2.7	5.0	----	4.0	2.5	4.1	8.0	.7
40	----	3.0	2.7	5.4	6.5	0	4.0	3.9	7.3	----	5.8	4.1	7.1	1.2	.5

Run	Pressure (lb/sq in.) at gage number 23	24	25	26	27	28	29	30	31	32	33	34	35	36	37
37	0.3	0.5	2.4	----	----	----	0.6	0	-0.4	0.9	0	----	0	0	0
38	1.2	1.0	3.9	0.8	1.8	-1.6	----	0.4	----	1.3	0.7	----	0	0	1.1
39	----	.9	4.8	0	2.9	0	.8	.2	.4	.8	----	----	.8	1.2	.1
40	0	.8	.3	0	0	0	.8	1.1	.7	1.9	----	----	.9	1.6	2.3

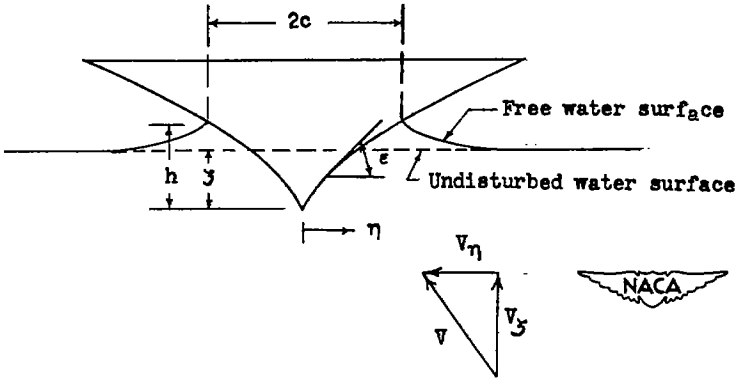

Figure 1.- The oblique impact of a symmetrical body. Two-dimensional problem.

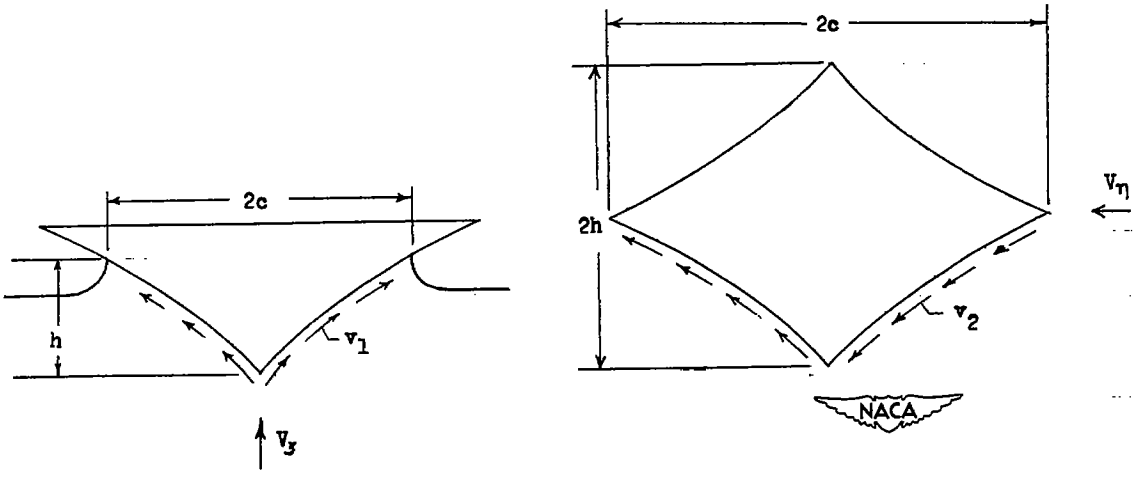

(a) Vertical component. (b) Horizontal component.

Figure 2.- Resolution of the oblique impact into two component flows. Two-dimensional problem.

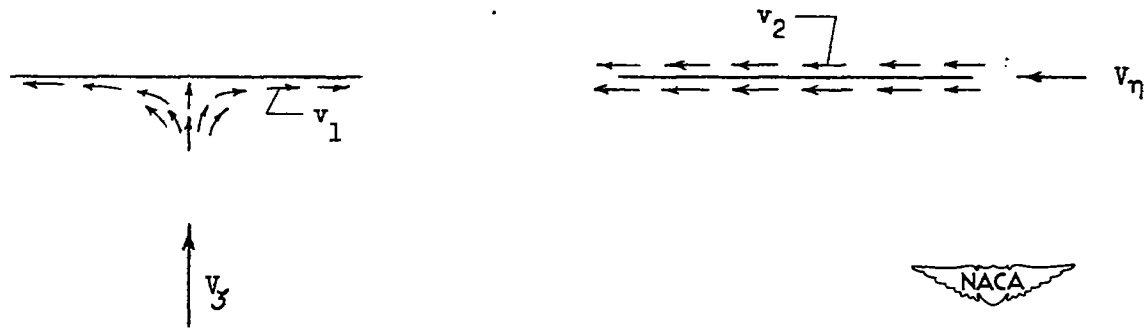

(a) Vertical component. (b) Horizontal component.

Figure 3.- Resolution of the oblique impact into two component flows at very small body slopes. Two-dimensional problem.

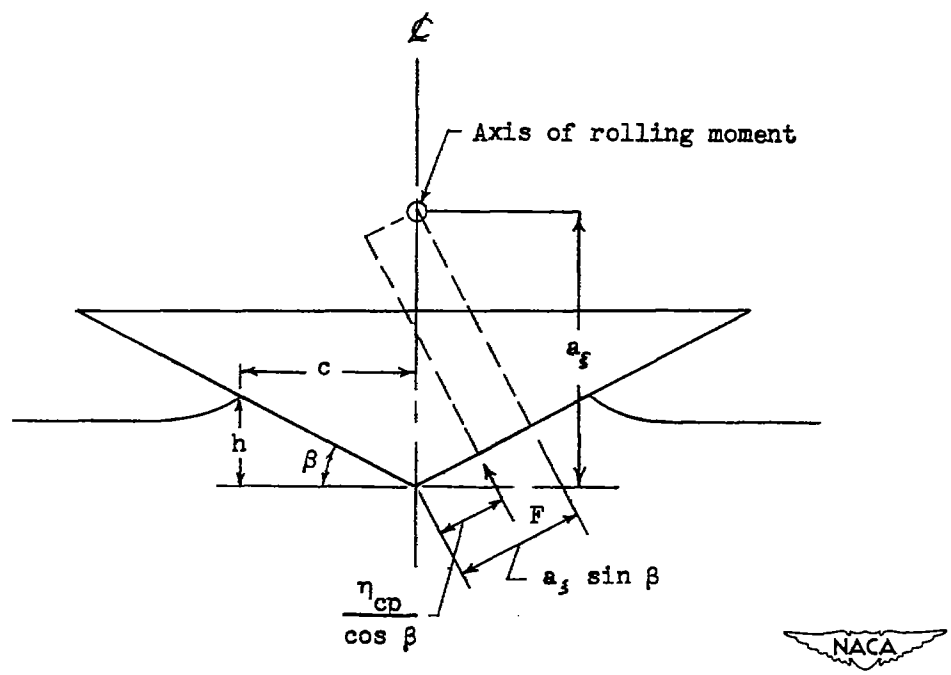

Figure 4.- Geometric relations for a straight-sided wedge.

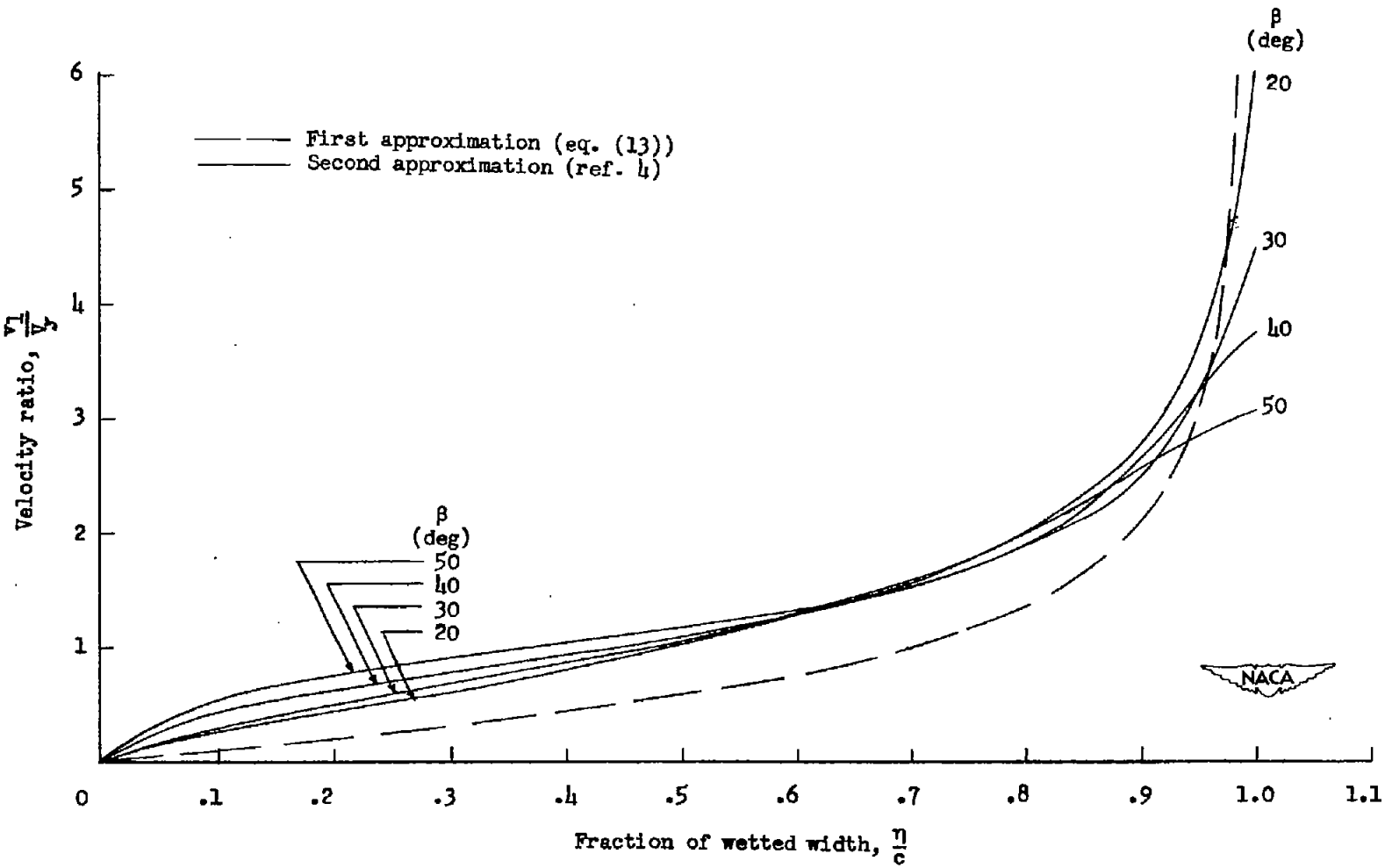

Figure 5.- Variation of the velocity ratio v_1/V_ζ on the side of a straight-sided two-dimensional wedge.

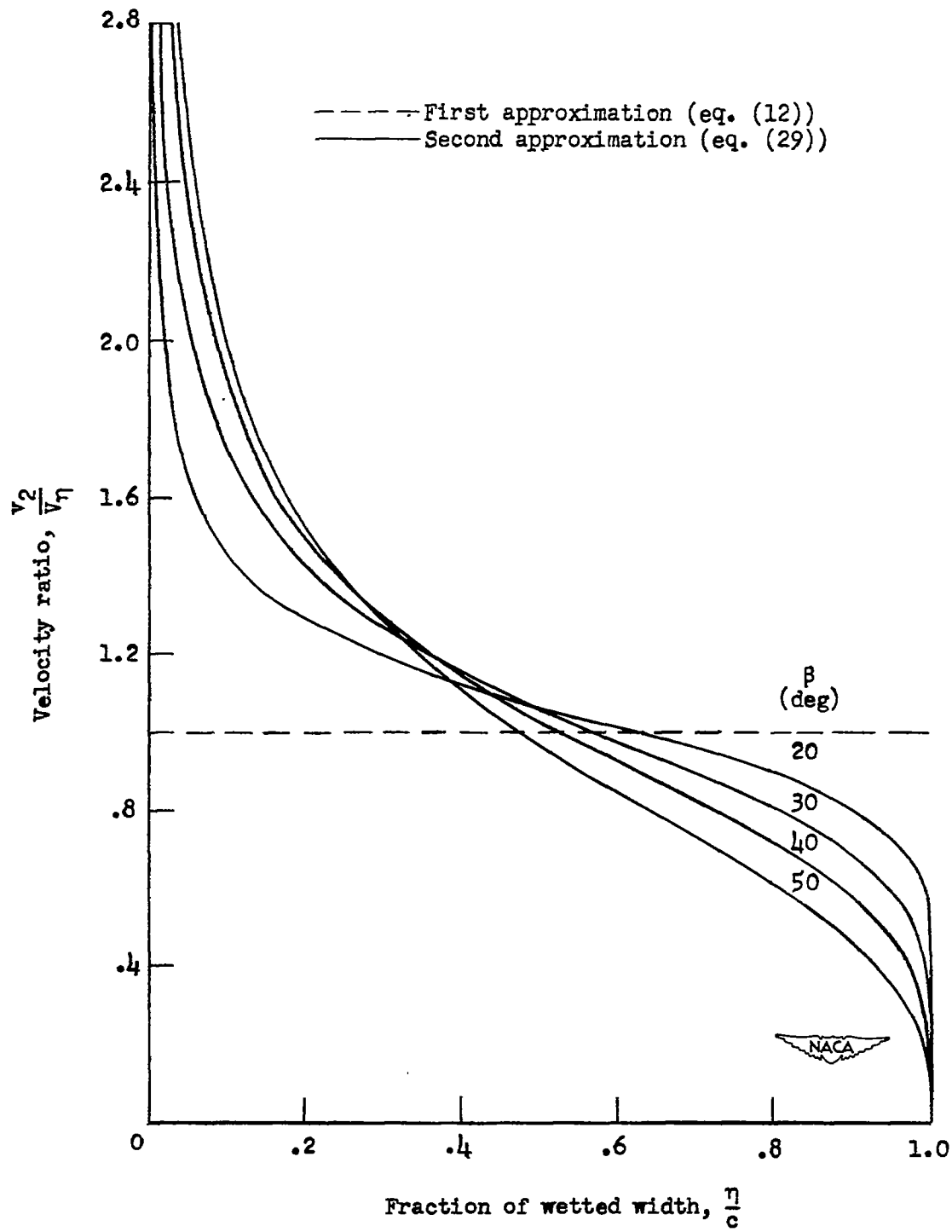

Figure 6.- Variation of the velocity ratio v_2/V_η on the side of a straight-sided two-dimensional wedge.

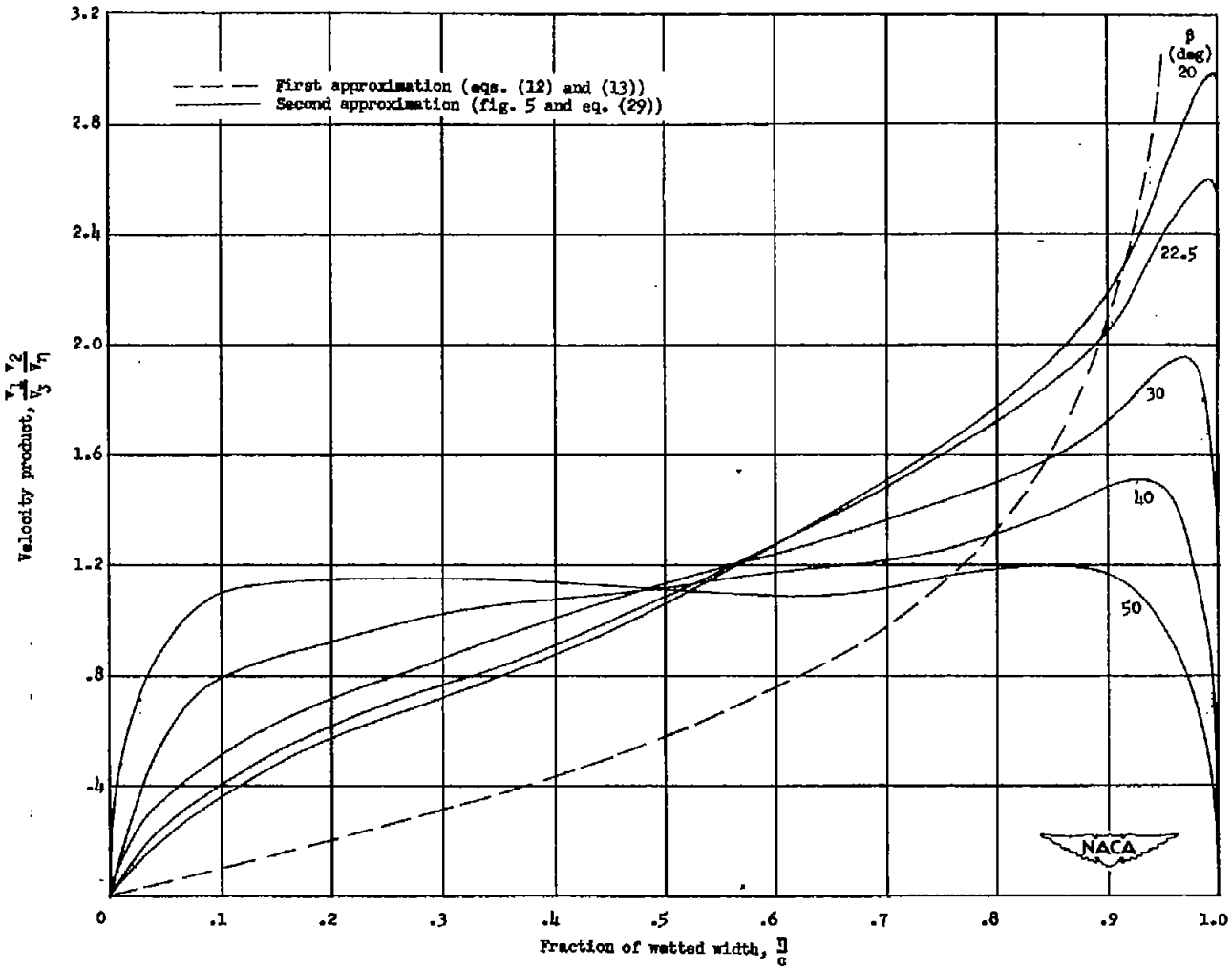

Figure 7.- Variation of the velocity product $\frac{v_1}{V_\zeta}\frac{v_2}{V_\eta}$ on the side of a straight-sided two-dimensional wedge.

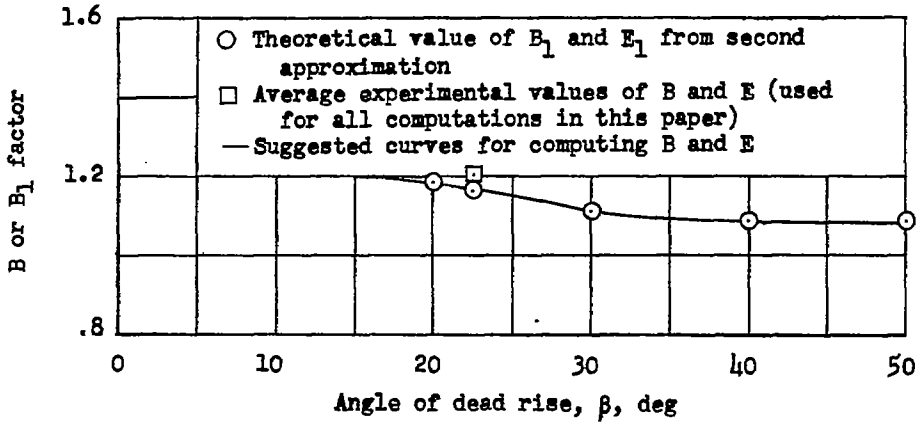

(a) B or B_1 factor.

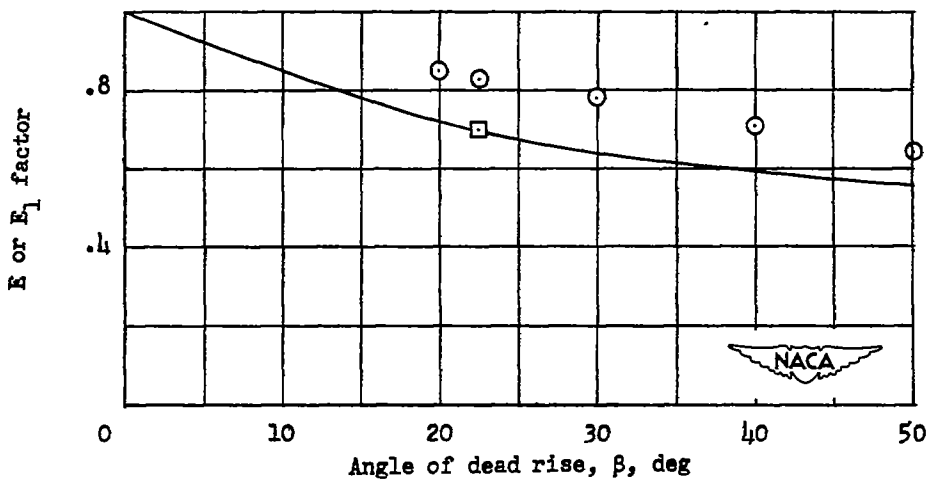

(b) E or E_1 factor.

Figure 8.- Yawing factors.

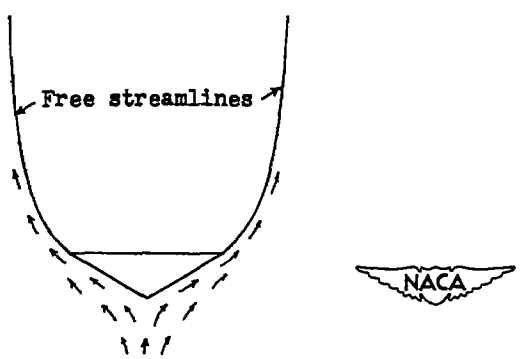

Figure 9.- The two-dimensional separated flow about a submerged wedge. Transverse section of wedge.

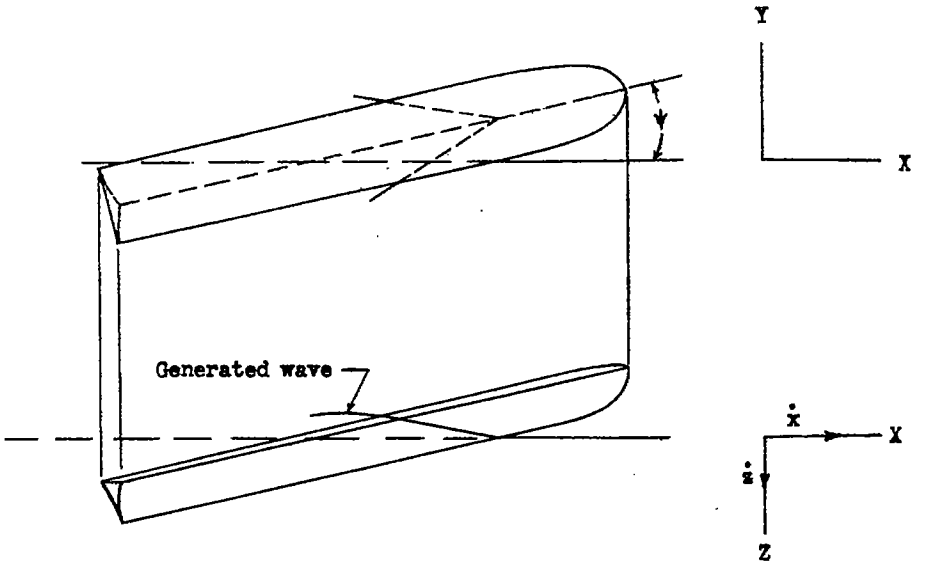

(a) Yawed landing of a seaplane viewed perpendicular to plane of landing.

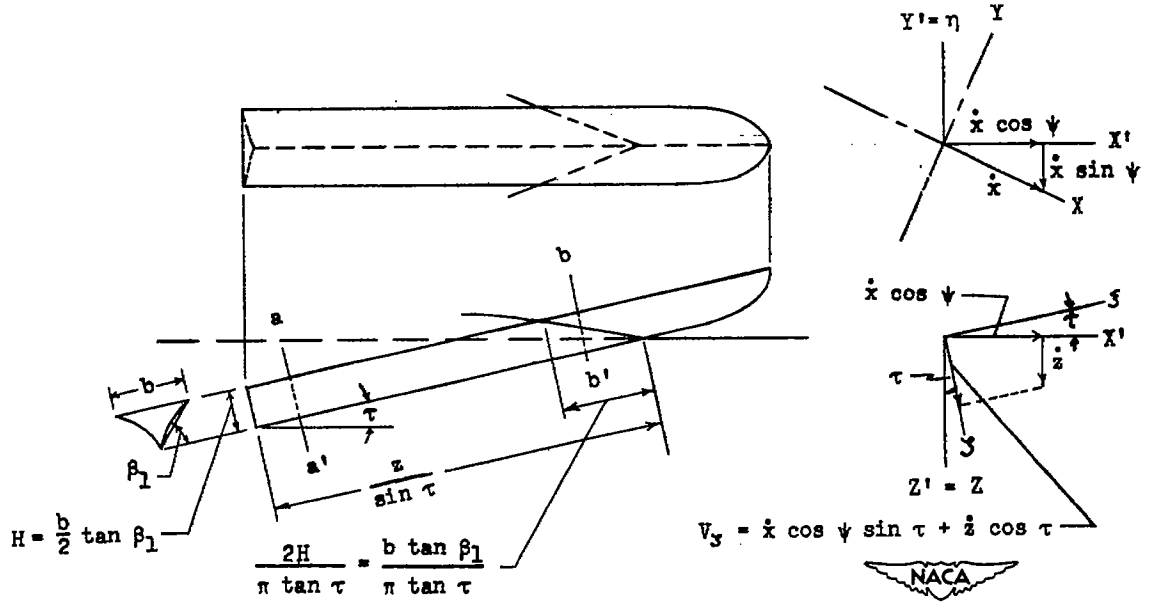

(b) Yawed landing of a seaplane viewed perpendicular to plane of seaplane symmetry (fig. 10(a) rotated through the angle ψ about the Z- or Z'-axis).

Figure 10.- Geometrical relations during a yawed seaplane landing.

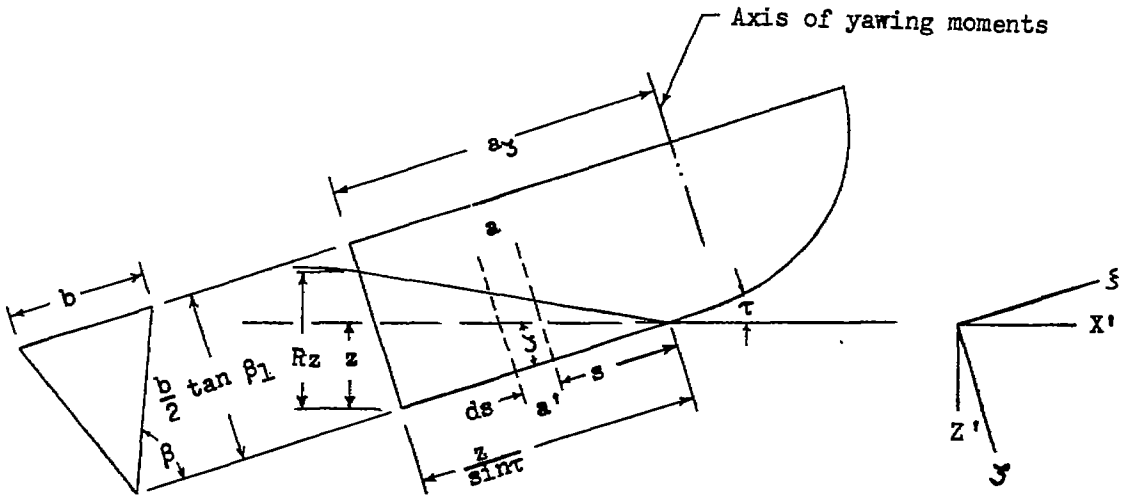

(c) Yawed landing of a non-chine-immersed seaplane without longitudinal water pile-up, viewed perpendicular to seaplane plane of symmetry.

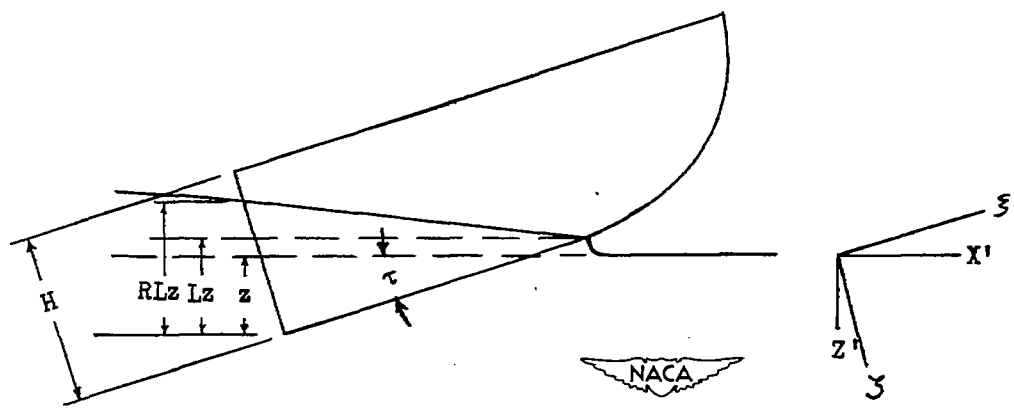

(d) Yawed landing of a non-chine-immersed seaplane with longitudinal water pile-up, viewed perpendicular to seaplane plane of symmetry.

Figure 10.- Concluded.

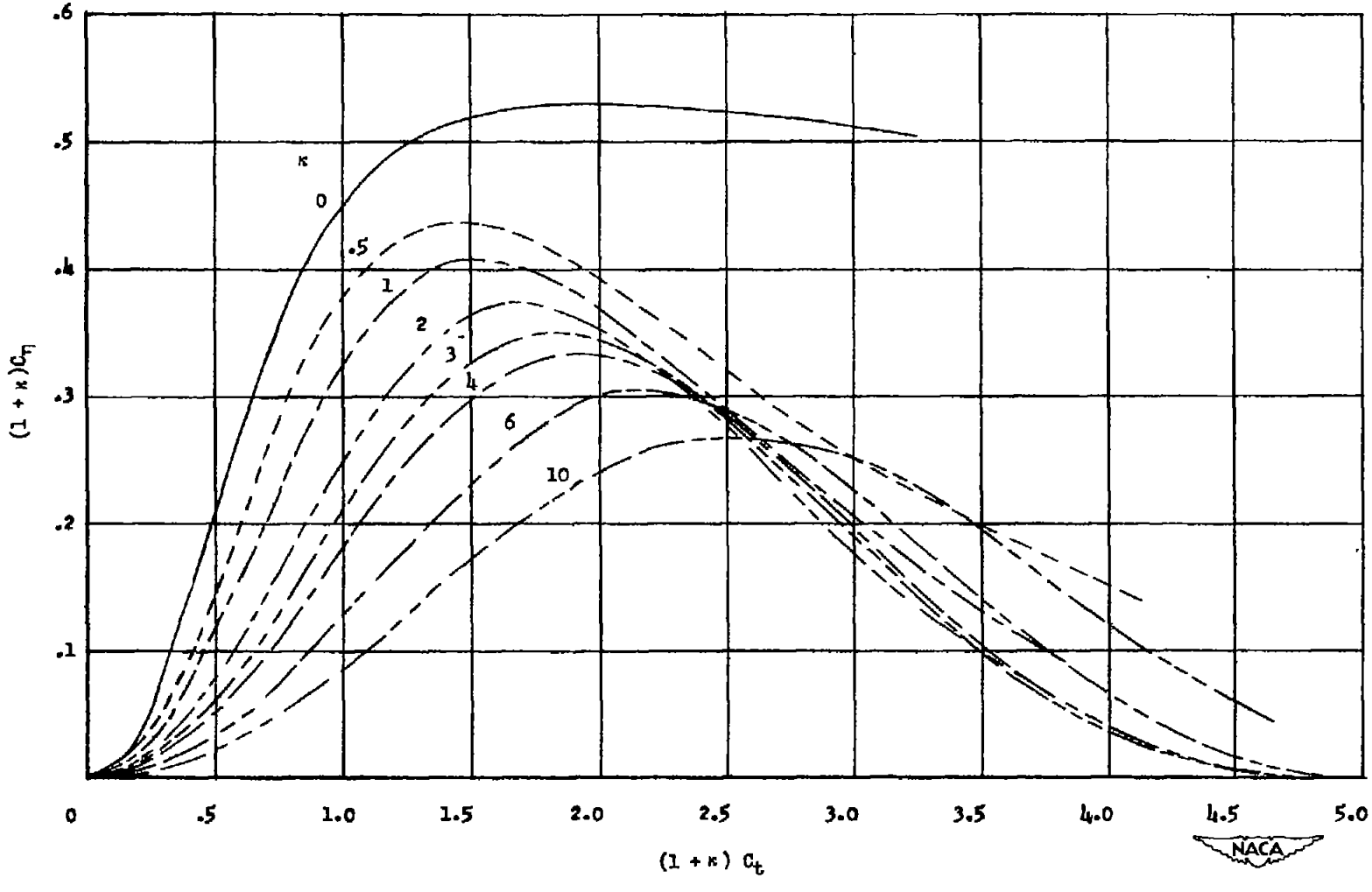

Figure 11.- Theoretical time histories of the side-force coefficient for a non-chine-immersed wedge. (Ordinates and abscissas have been multiplied by the factor $1+\kappa$ to facilitate interpolation.)

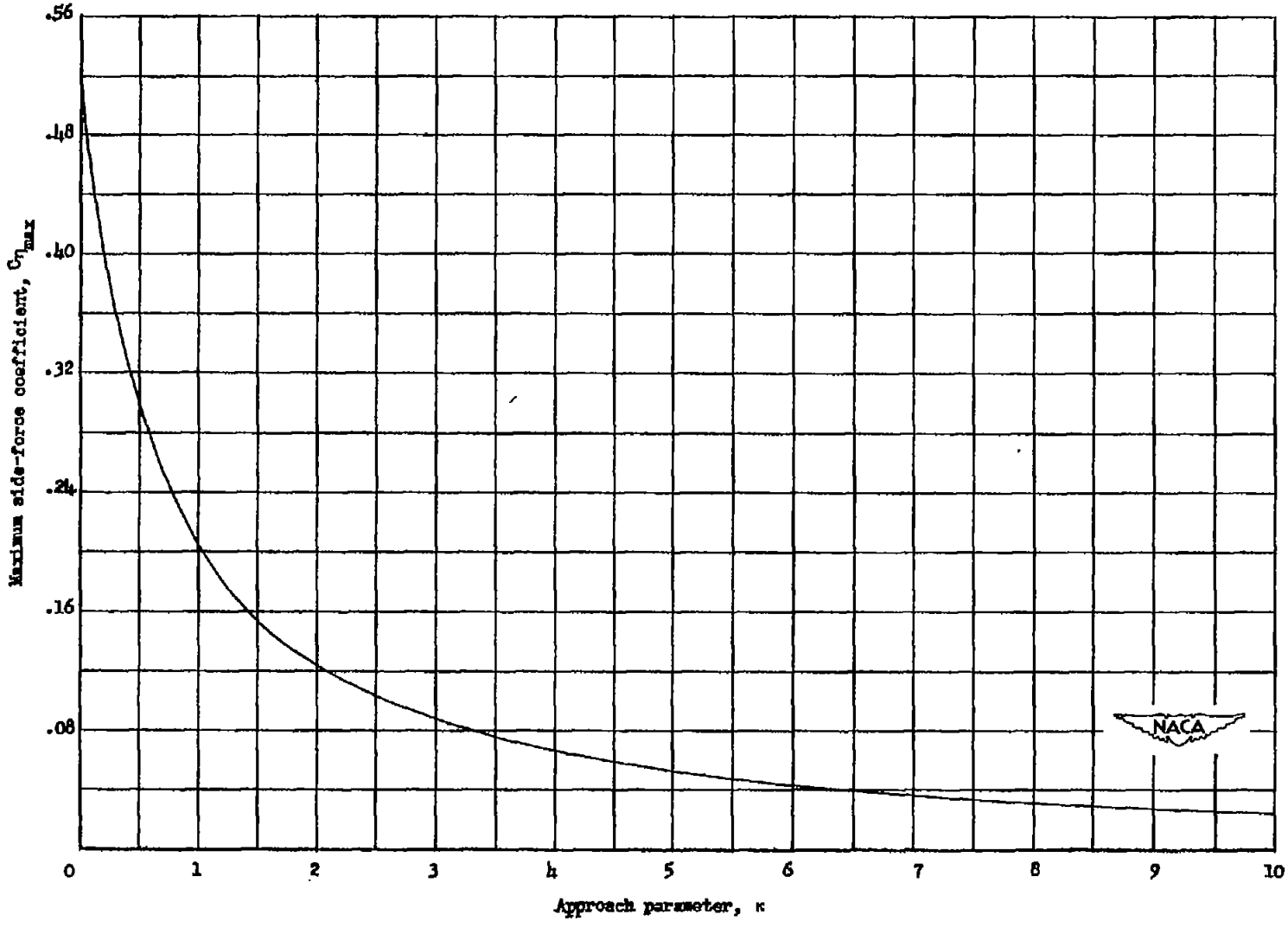

Figure 12.- Theoretical variation of the maximum side-force coefficient with the approach parameter for a non-chine-immersed wedge.

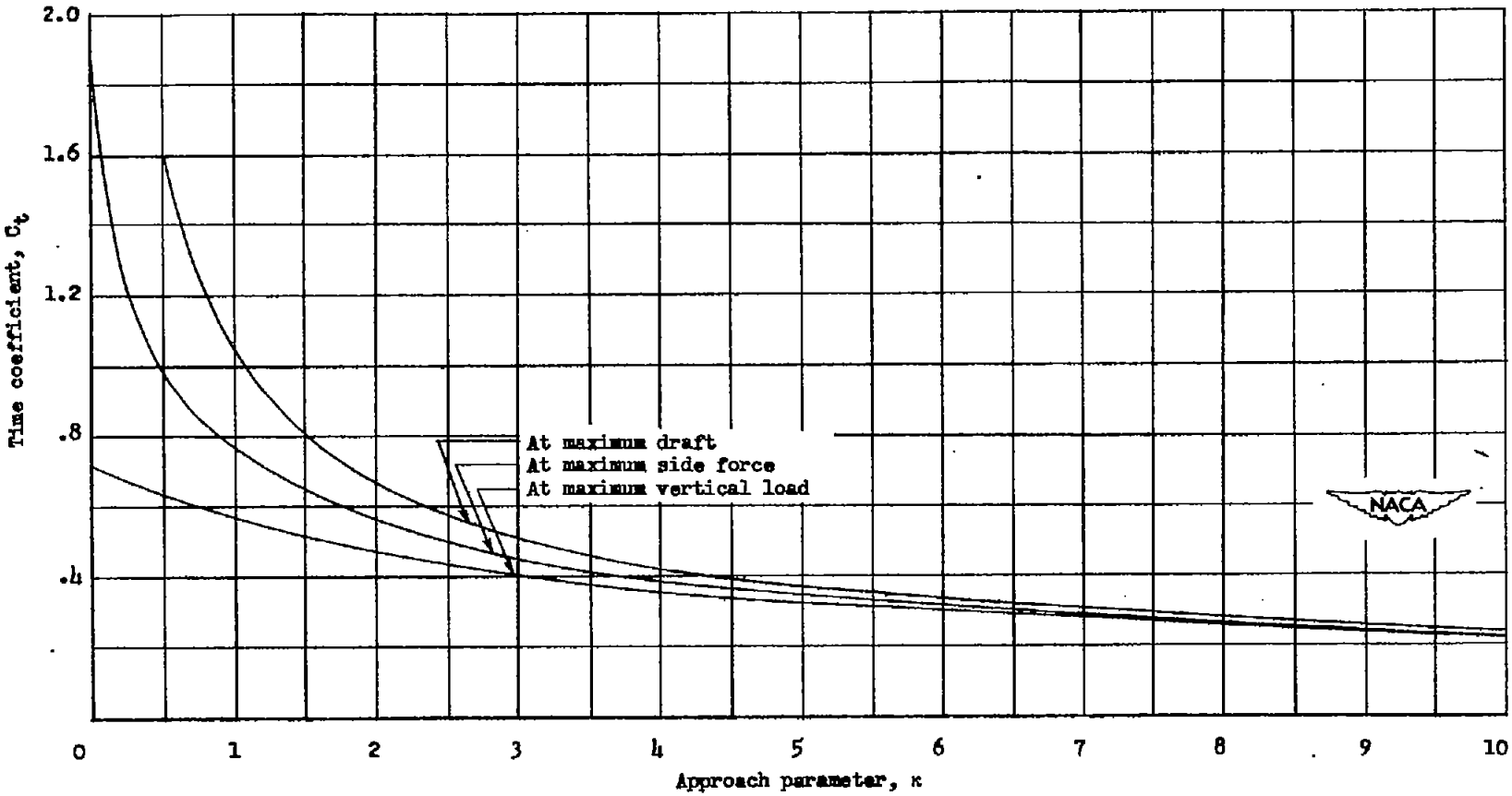

Figure 13.- Theoretical variation of the time coefficient with the approach parameter for a non-chine-immersed wedge.

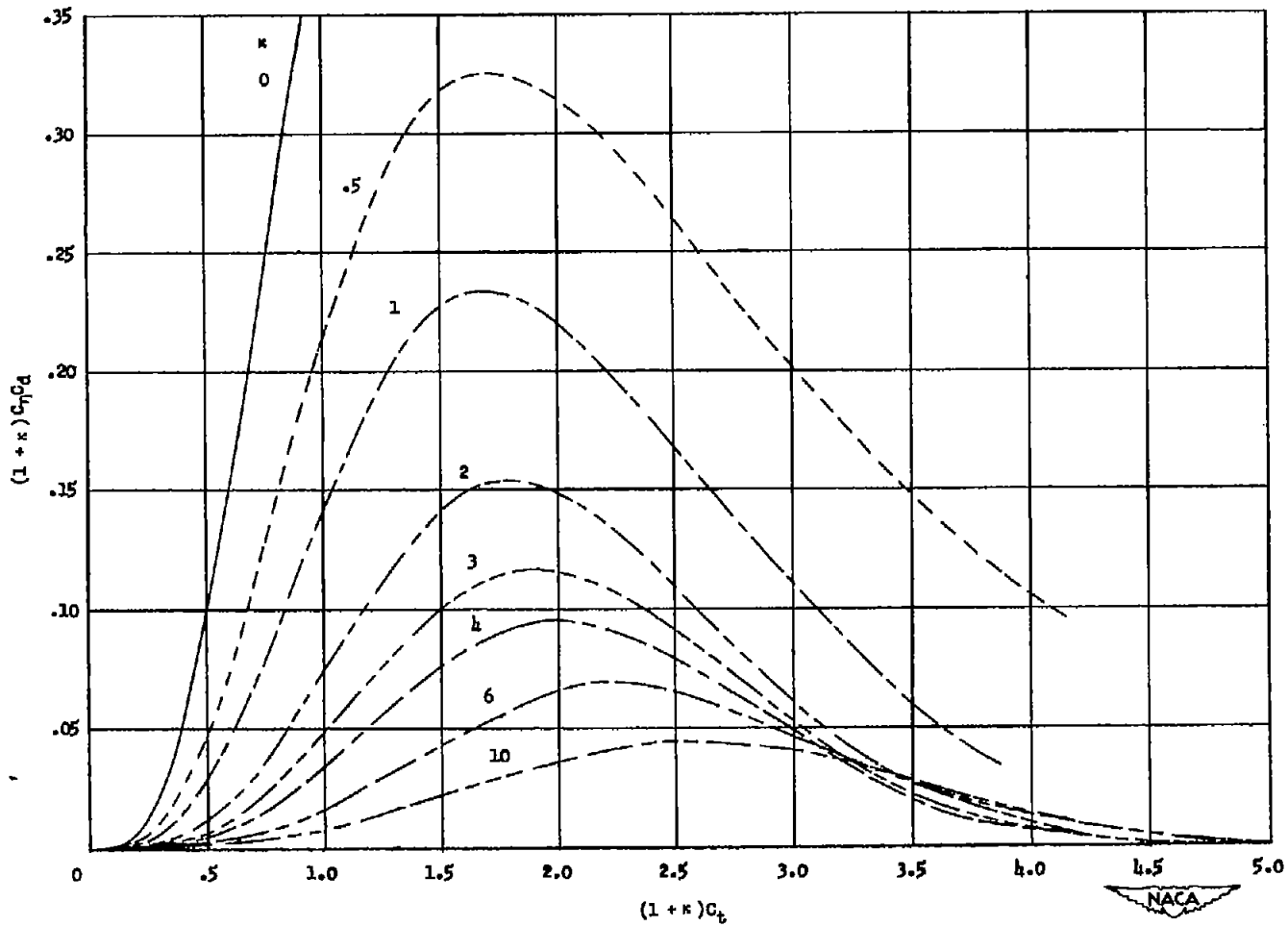

Figure 14.- Theoretical variation of the quantity $C_\eta C_d$ with the time coefficient for various values of approach parameter for a non-chine-immersed wedge. (Ordinates and abscissas have been multiplied by the factor $1 + \kappa$ to facilitate interpolation.)

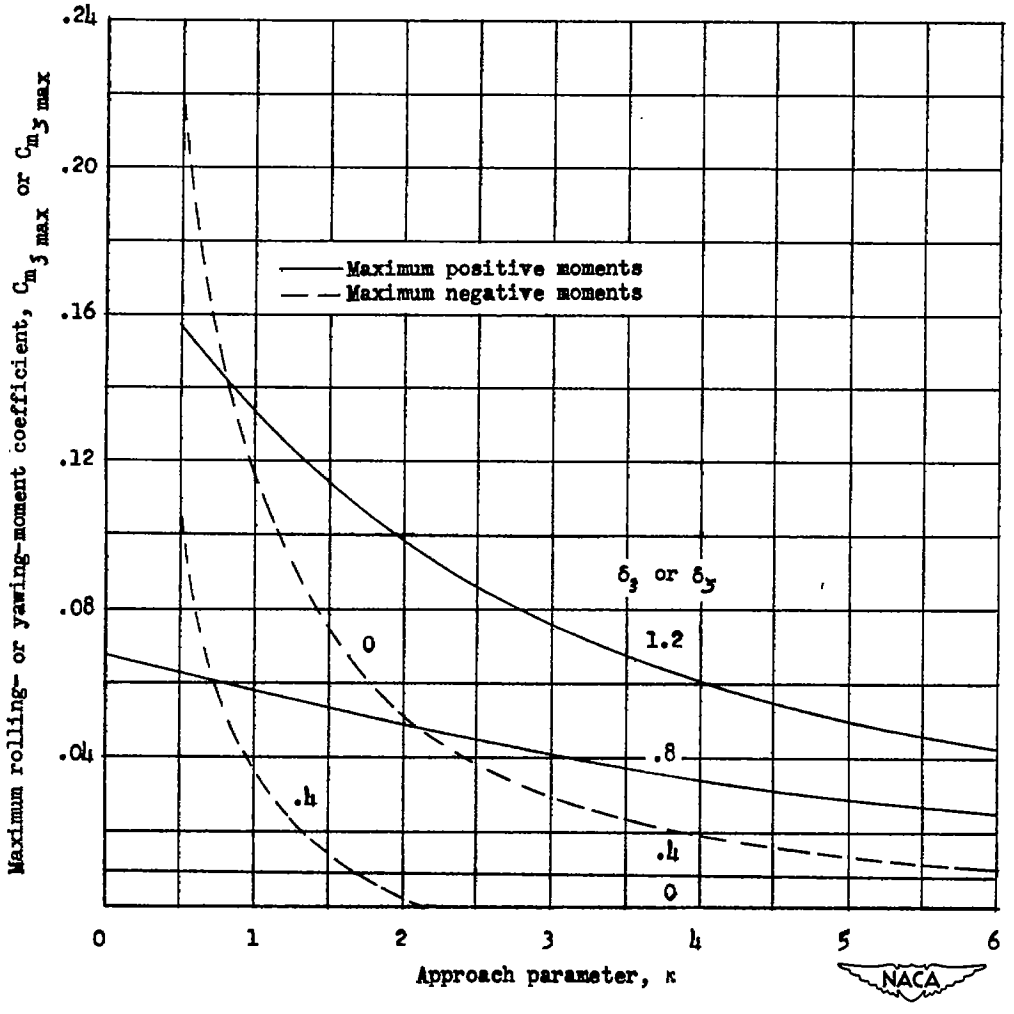

(a) Curves for small values of δ_ξ or δ_ζ.

Figure 15.- Theoretical variation of the maximum rolling- or yawing-moment coefficient with the approach parameter for a non-chine-immersed wedge.

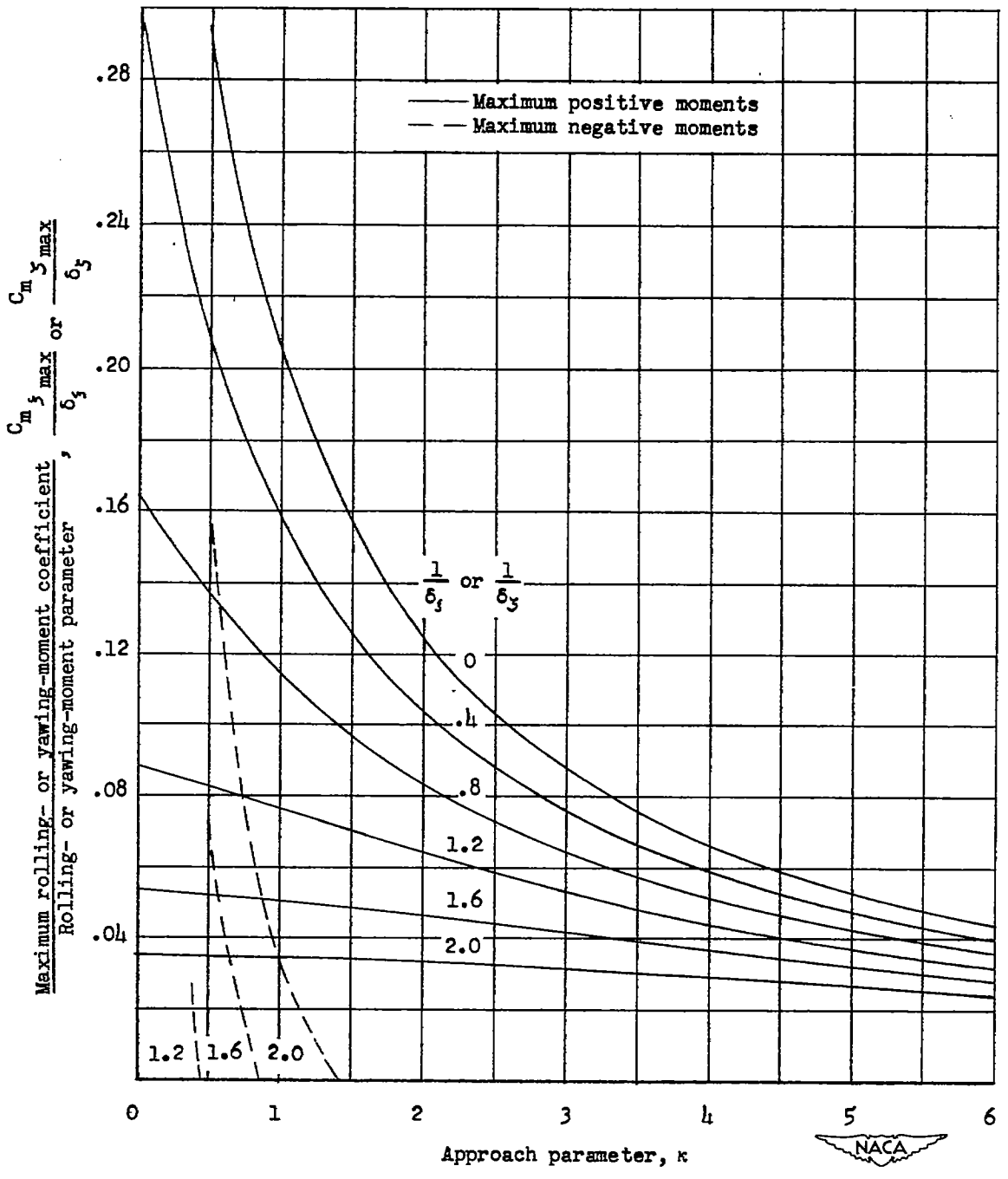

(b) Curves for large values of δ_ξ or δ_ζ.

Figure 15.- Concluded.

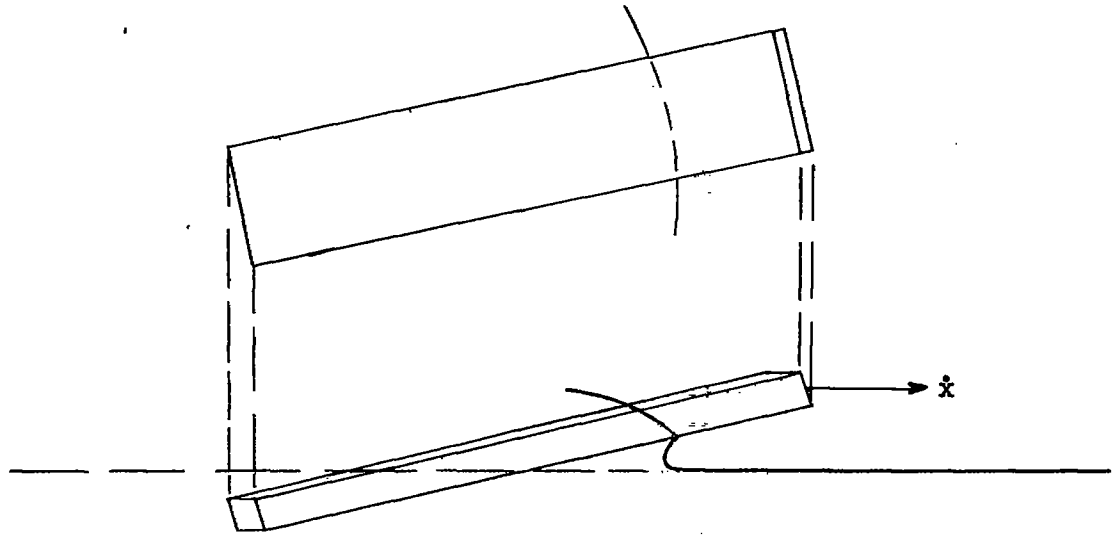

(a) Rectangular flat plate viewed perpendicular to the plane of motion.

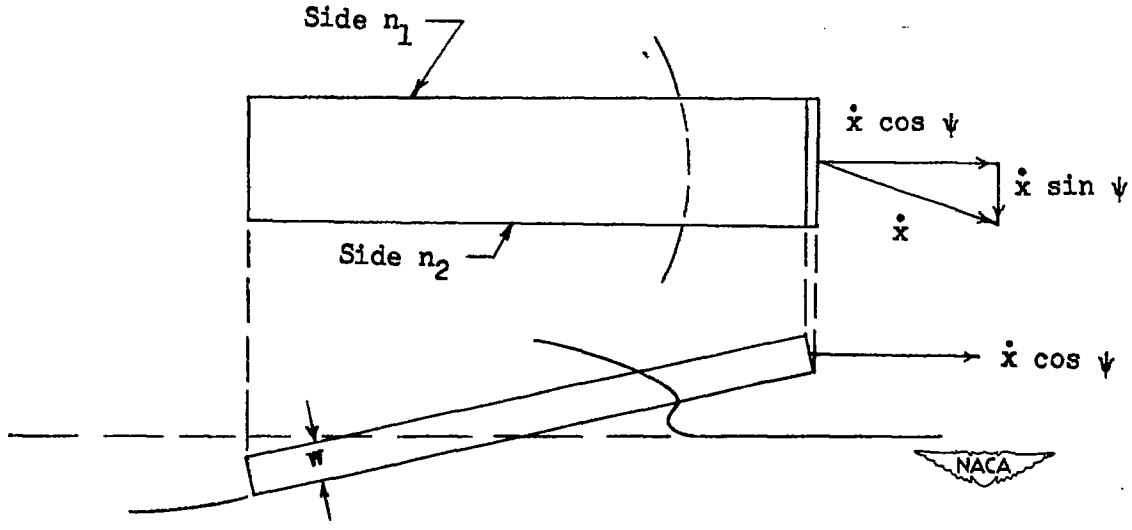

(b) Rectangular flat plate viewed perpendicular to the plane of symmetry of the plate.

Figure 16.- The yawed planing of a rectangular flat plate.

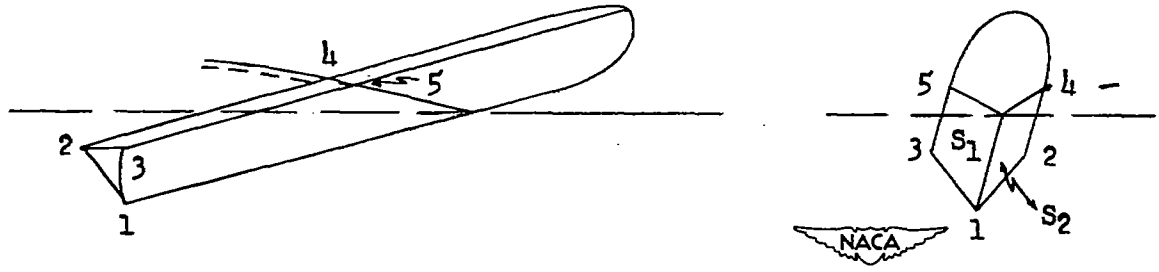

Figure 17.- Yawed wedge during steady planing.

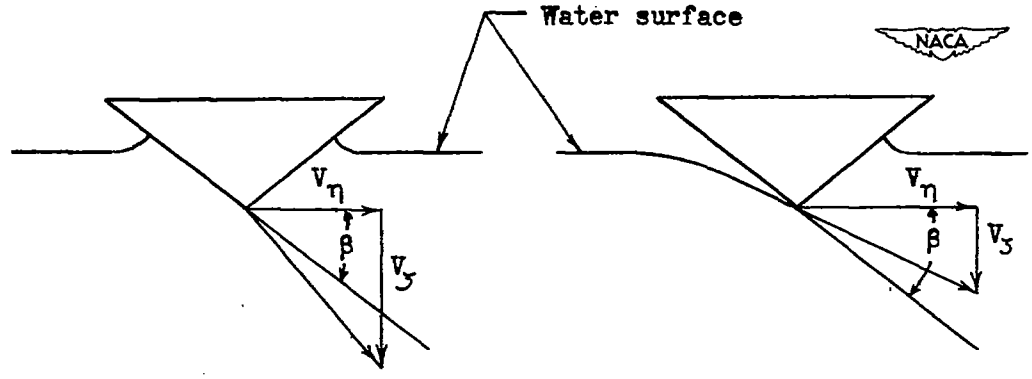

Figure 18.- Transverse sections of a non-chine-immersed wedge for values of $\frac{V_\eta}{V_\zeta} \tan \beta \lesseqgtr 1$.

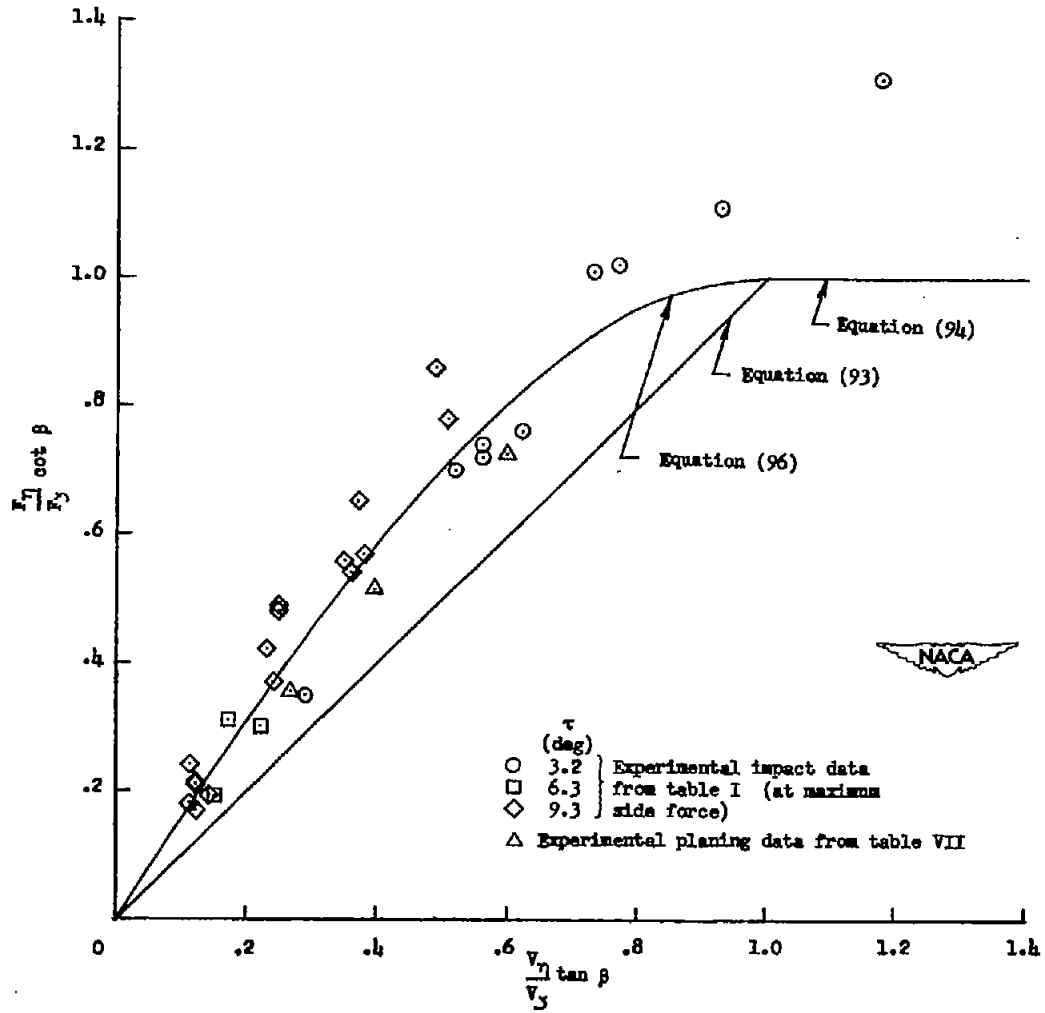

Figure 19.- Variation of $\frac{F_\eta}{F_\zeta}$ cot β with $\frac{V_\eta}{V_\zeta}$ tan β for a straight-sided wedge.

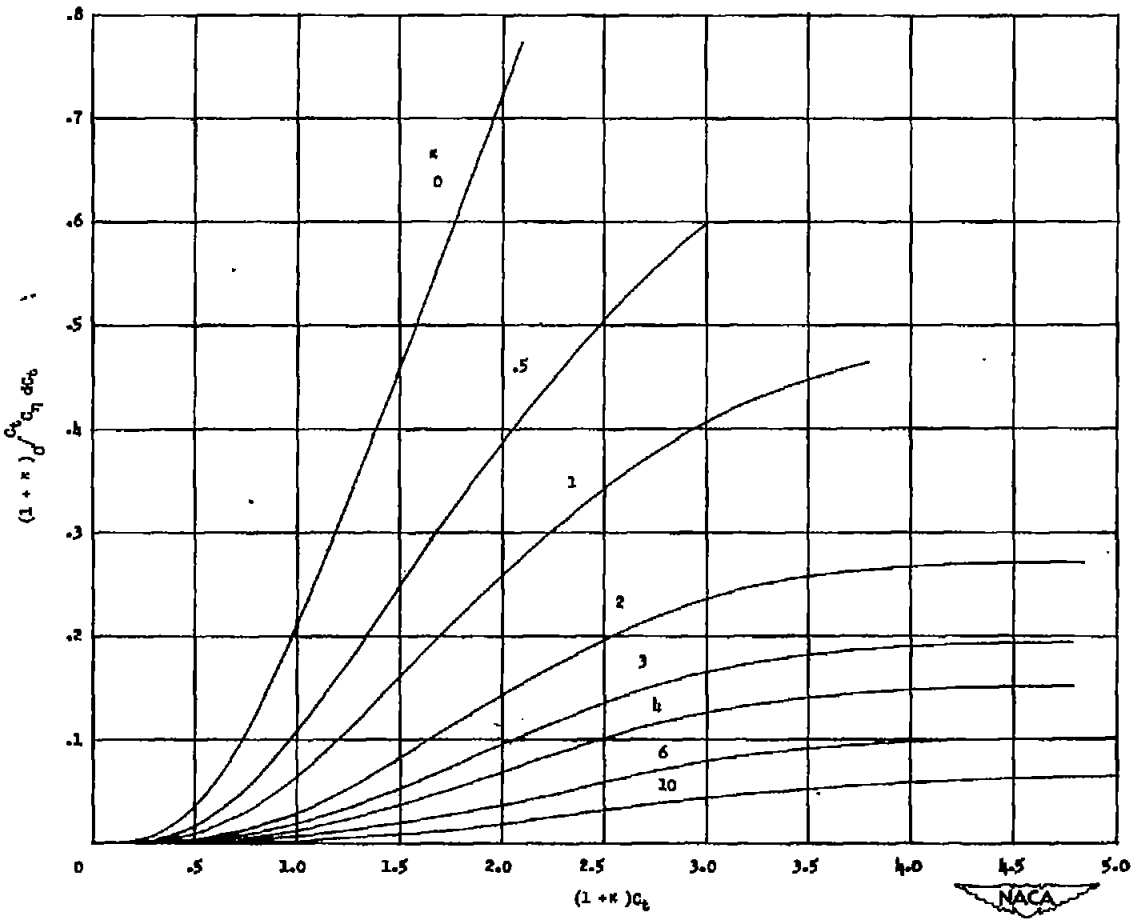

Figure 20.- Theoretical variation of the quantity $(1 + \kappa) \int_0^{Ct} C_\eta \, dCt$ with the time coefficient for various values of approach parameter for a non-chine-immersed wedge. (The abscissa has been multiplied by $1 + \kappa$ to permit use of this curve with figs. 11 and 14.)

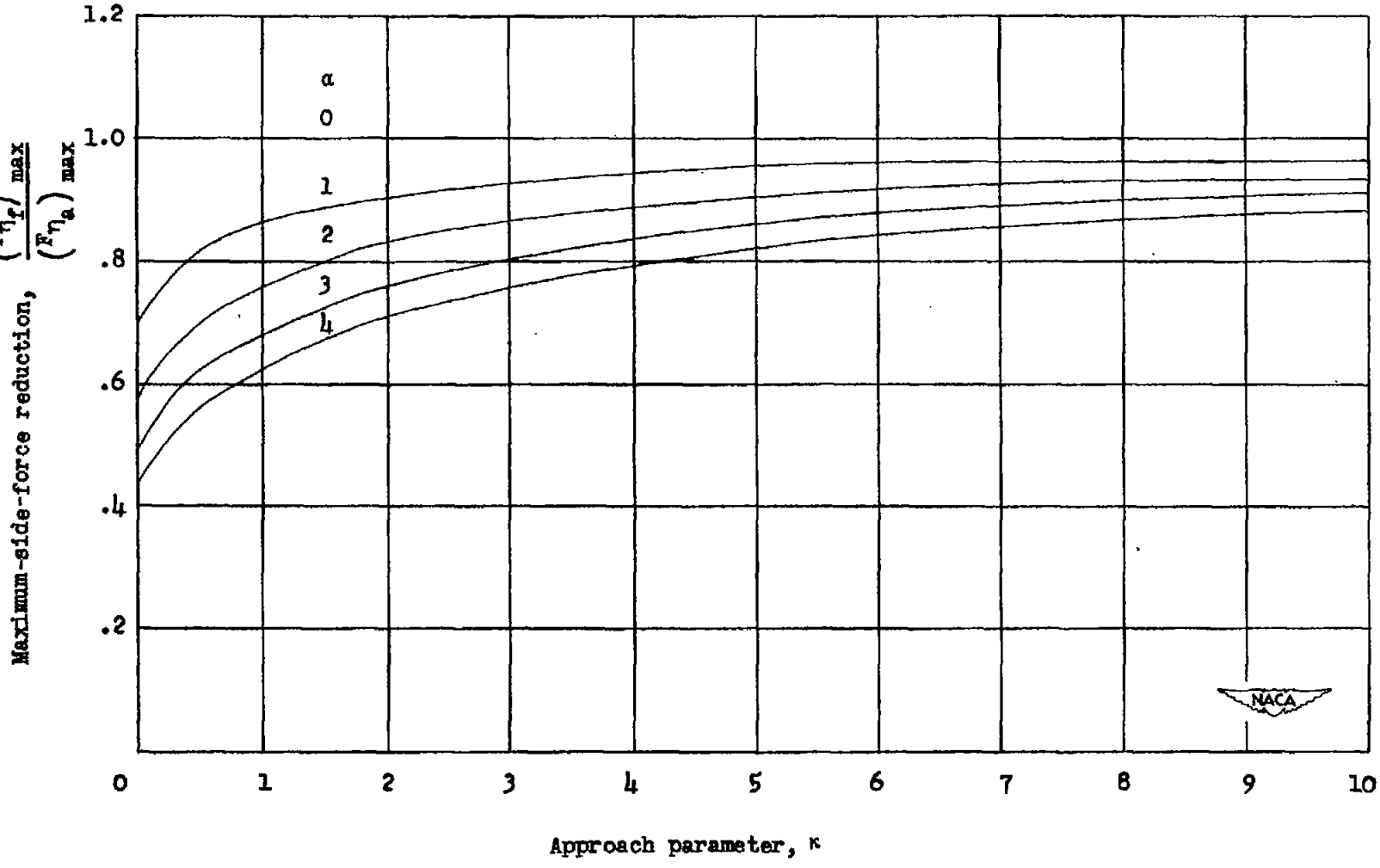

Figure 21.- Theoretical reduction in side force due to changing from restricted to free side motion for a non-chine-immersed wedge.

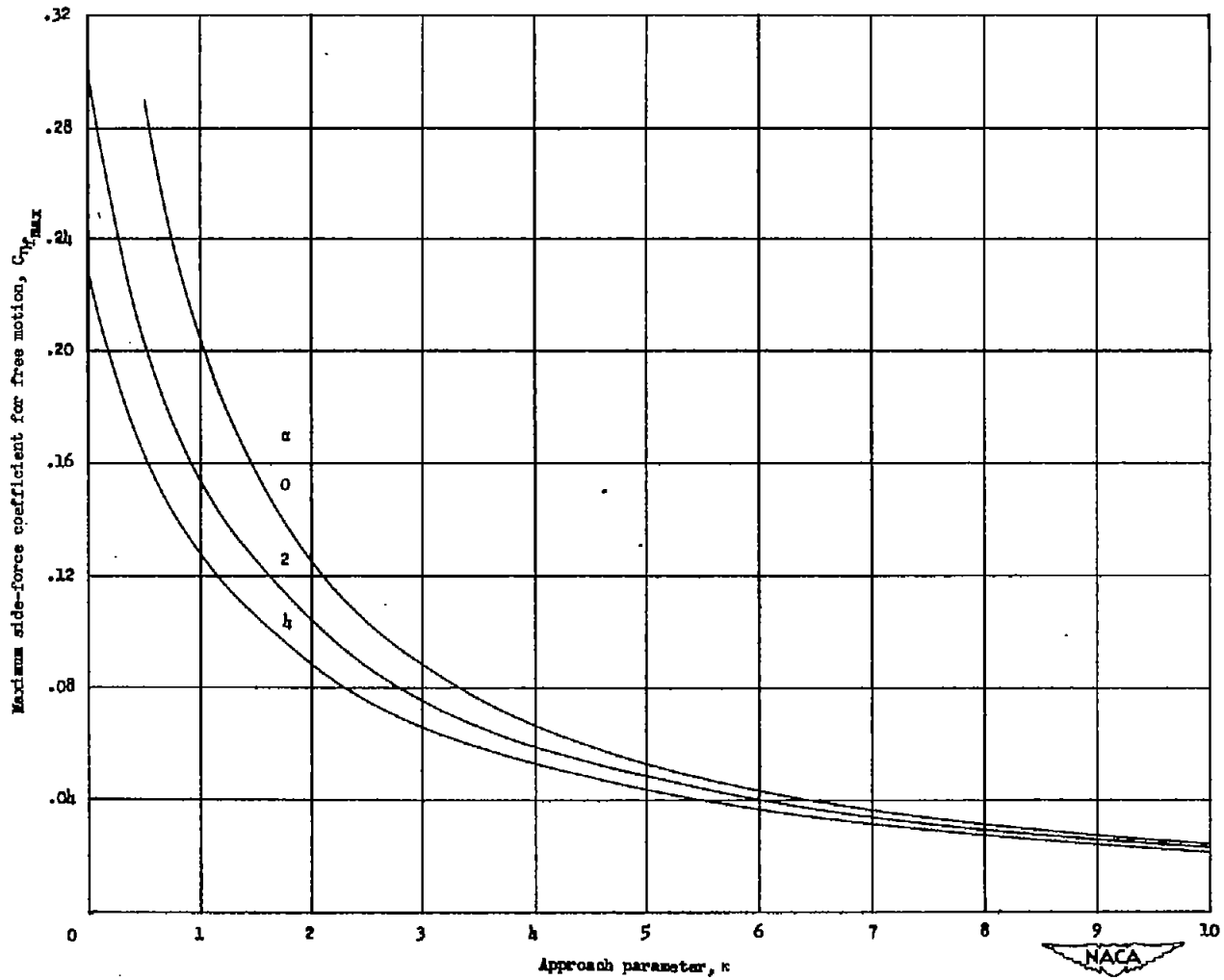

Figure 22.- Theoretical variation of the maximum side-force coefficient for free motion with the approach parameter for a non-chine-immersed wedge.

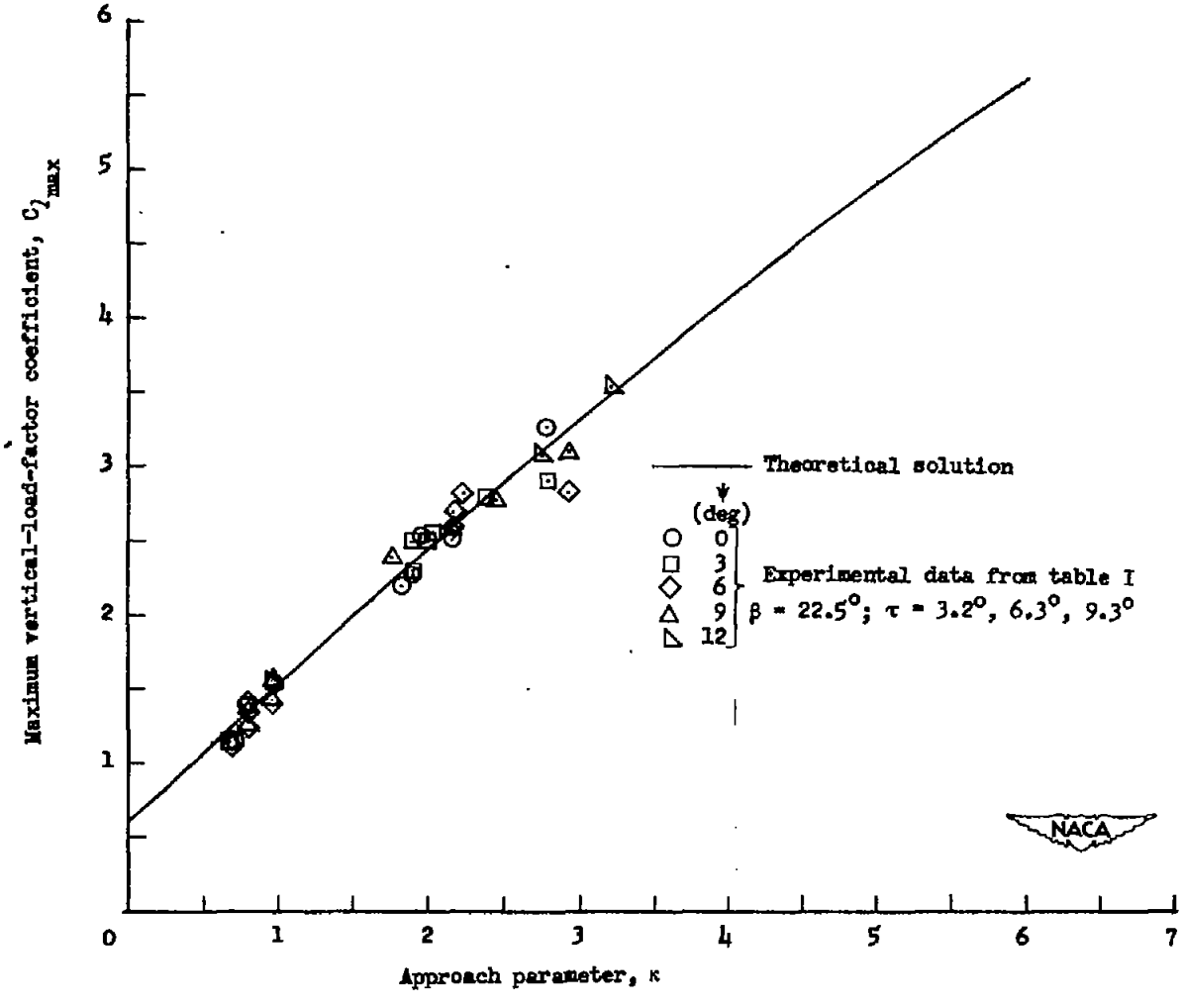

Figure 23.- Comparison between theoretical and experimental variations of the maximum vertical-load-factor coefficient with the approach parameter.

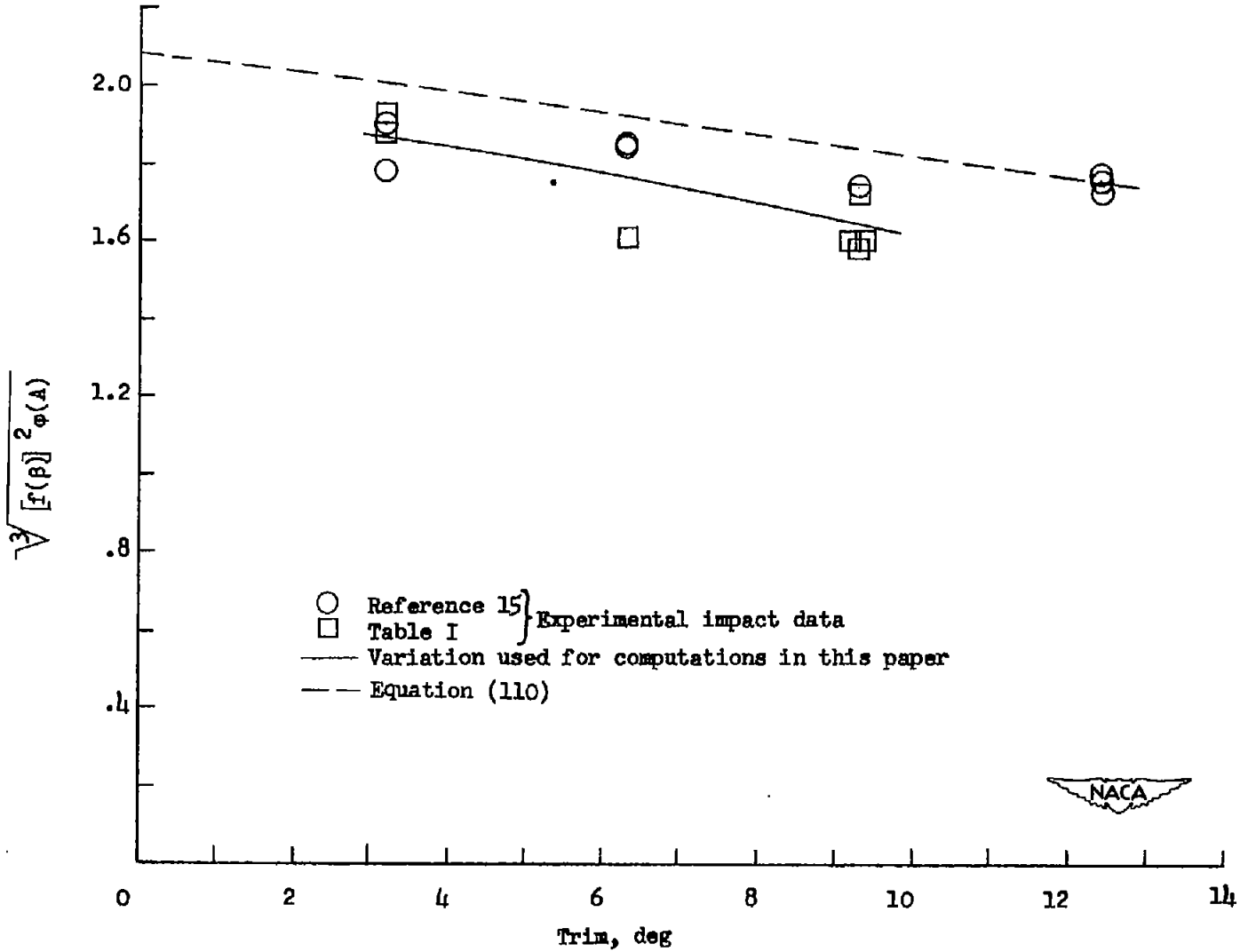

Figure 24.- Experimental variation of the dead-rise–aspect-ratio function with trim for an angle of dead rise of 22.5°.

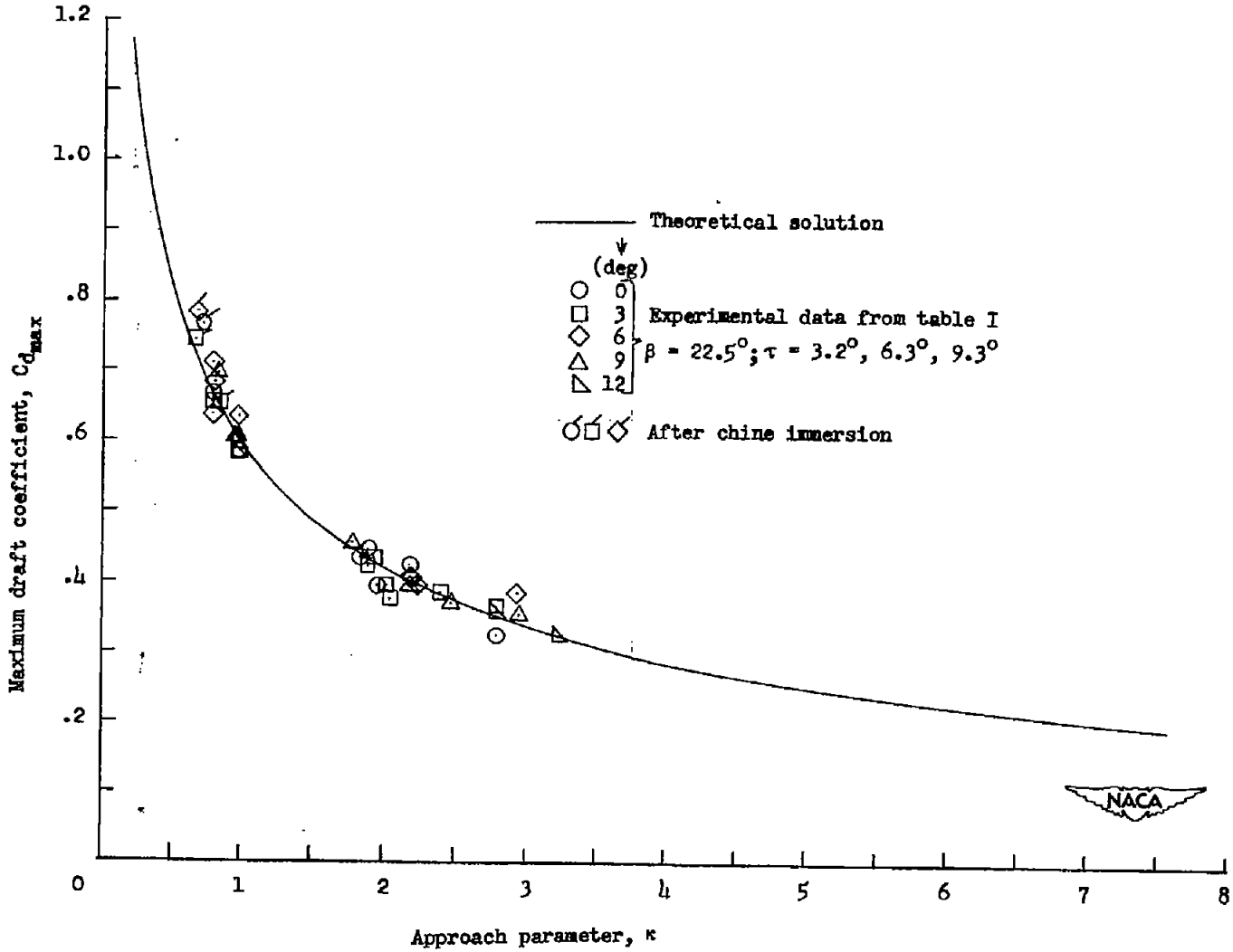

Figure 25.- Comparison between theoretical and experimental variations of the maximum draft coefficient with the approach parameter.

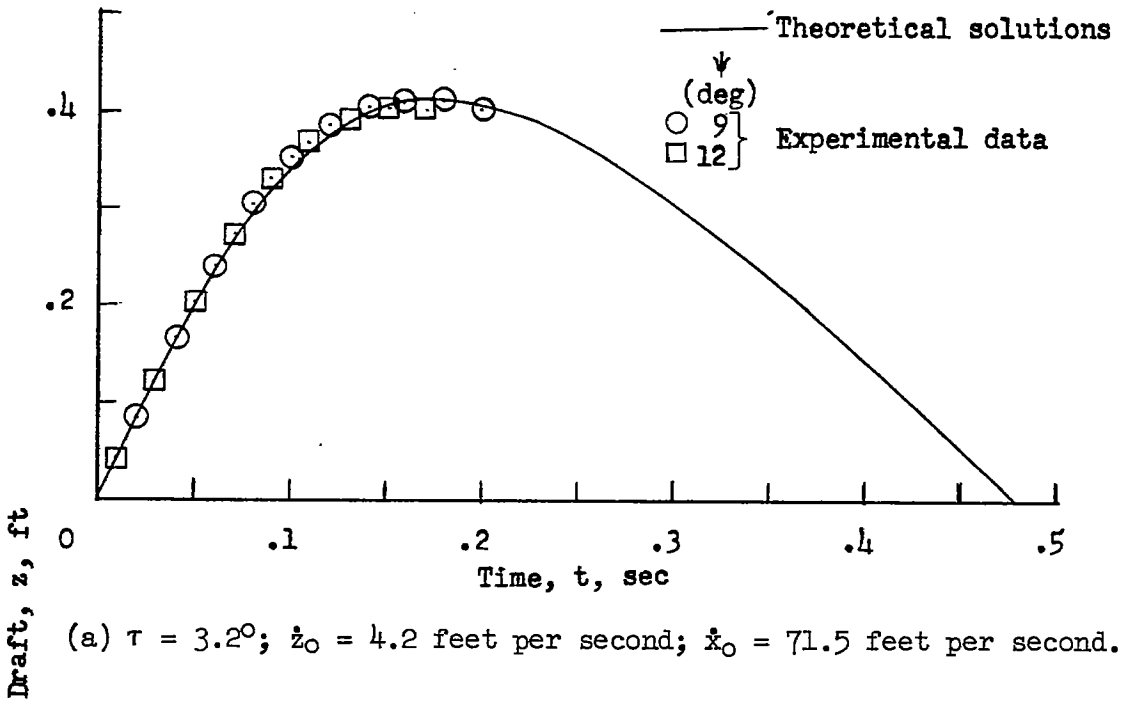

(a) $\tau = 3.2^{\circ}$; $\dot{z}_o = 4.2$ feet per second; $\dot{x}_o = 71.5$ feet per second.

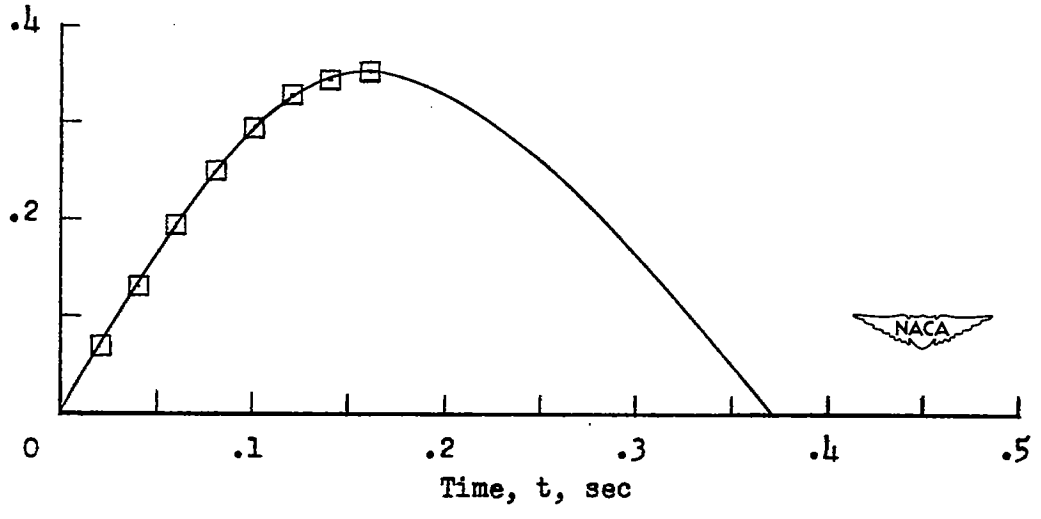

(b) $\tau = 9.3^{\circ}$; $\dot{z}_o = 3.3$ feet per second; $\dot{x}_o = 67.1$ feet per second.

Figure 26.- Comparison between theoretical and experimental draft time histories. $\beta = 22.5^{\circ}$; W = 1177 pounds.

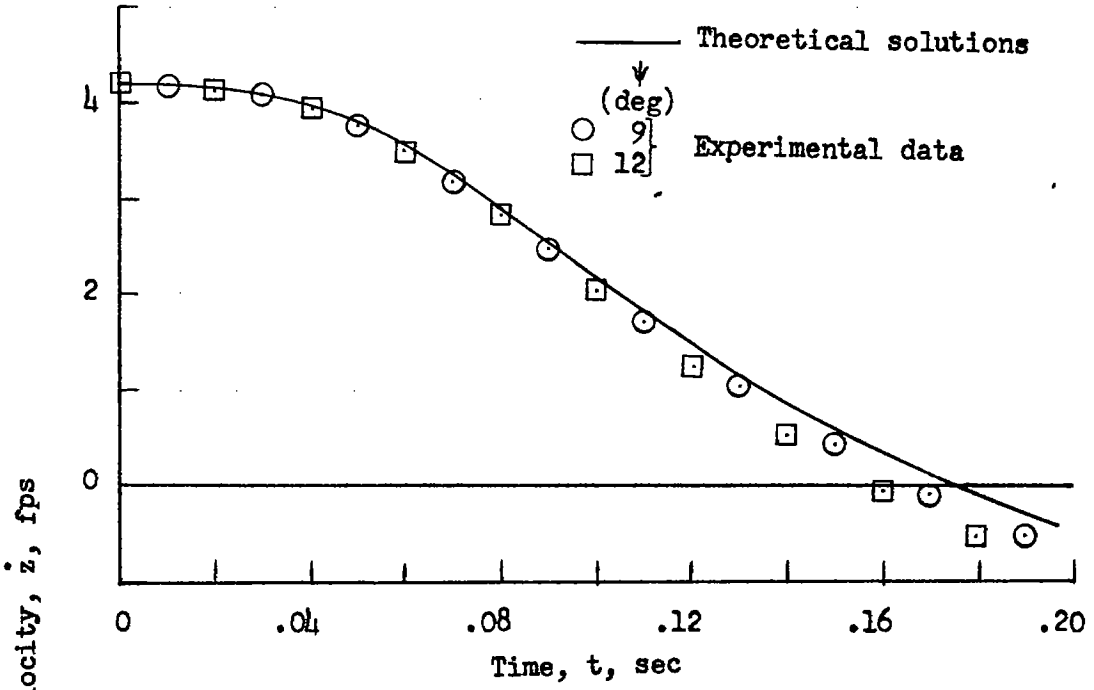

(a) $\tau = 3.2^{\circ}$; $\dot{z}_o = 4.2$ feet per second; $\dot{x}_o = 71.5$ feet per second.

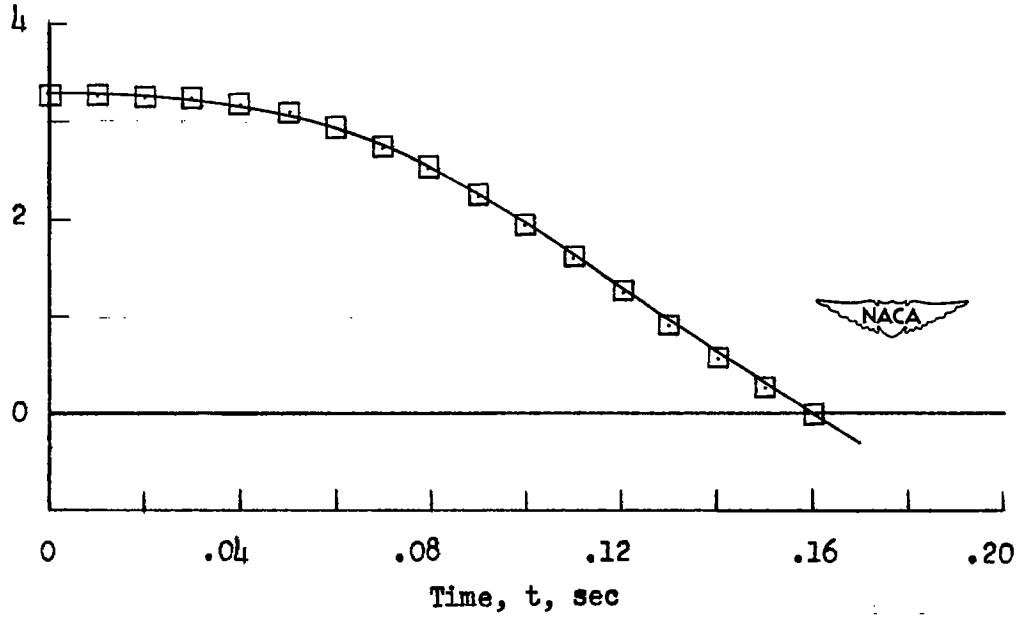

(b) $\tau = 9.3^{\circ}$; $\dot{z}_o = 3.3$ feet per second; $\dot{x}_o = 67.1$ feet per second.

Figure 27.- Comparison between theoretical and experimental vertical-velocity time histories. $\beta = 22.5^{\circ}$; W = 1177 pounds.

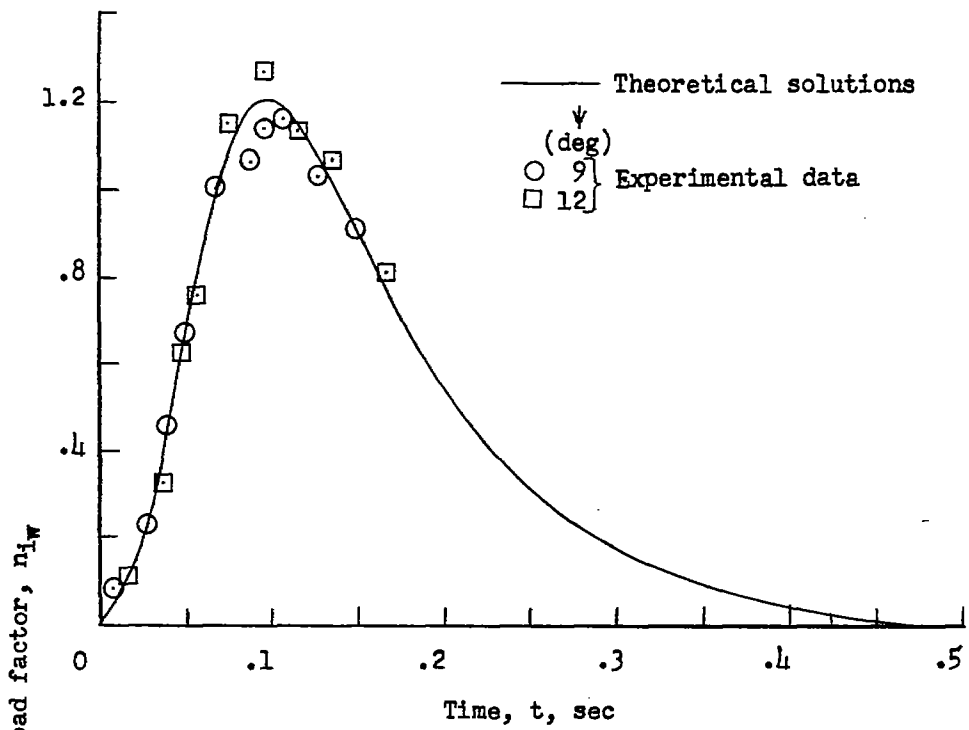

(a) $\tau = 3.2^\circ$; $\dot{z}_o = 4.2$ feet per second; $\dot{x}_o = 71.5$ feet per second.

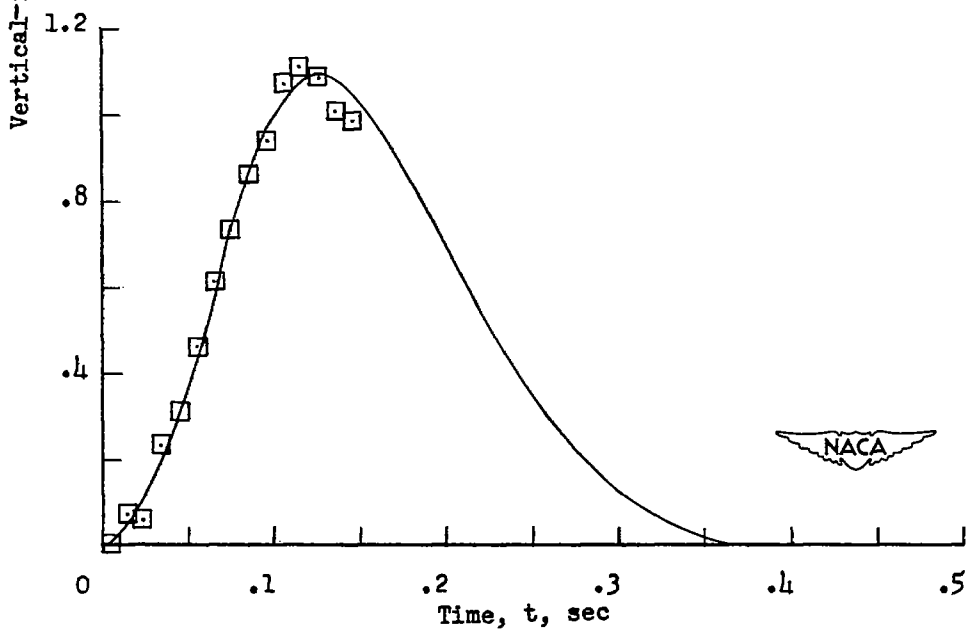

(b) $\tau = 9.3^\circ$; $\dot{z}_o = 3.3$ feet per second; $\dot{x}_o = 67.1$ feet per second.

Figure 28.- Comparison between theoretical and experimental vertical-load time histories. $\beta = 22.5^\circ$; $W = 1177$ pounds.

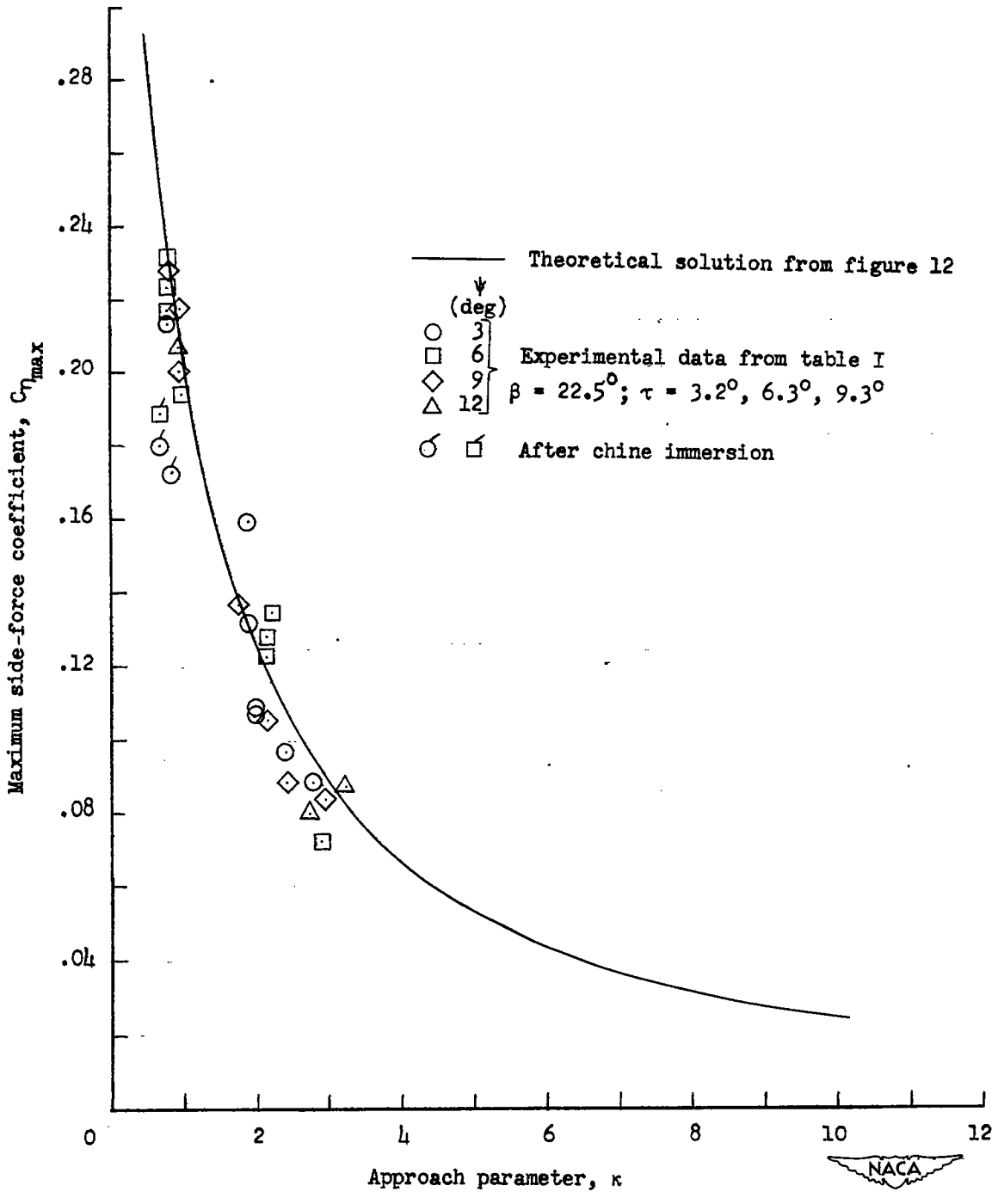

Figure 29.- Comparison of theoretical and experimental variations of maximum side-force coefficient with approach parameter.

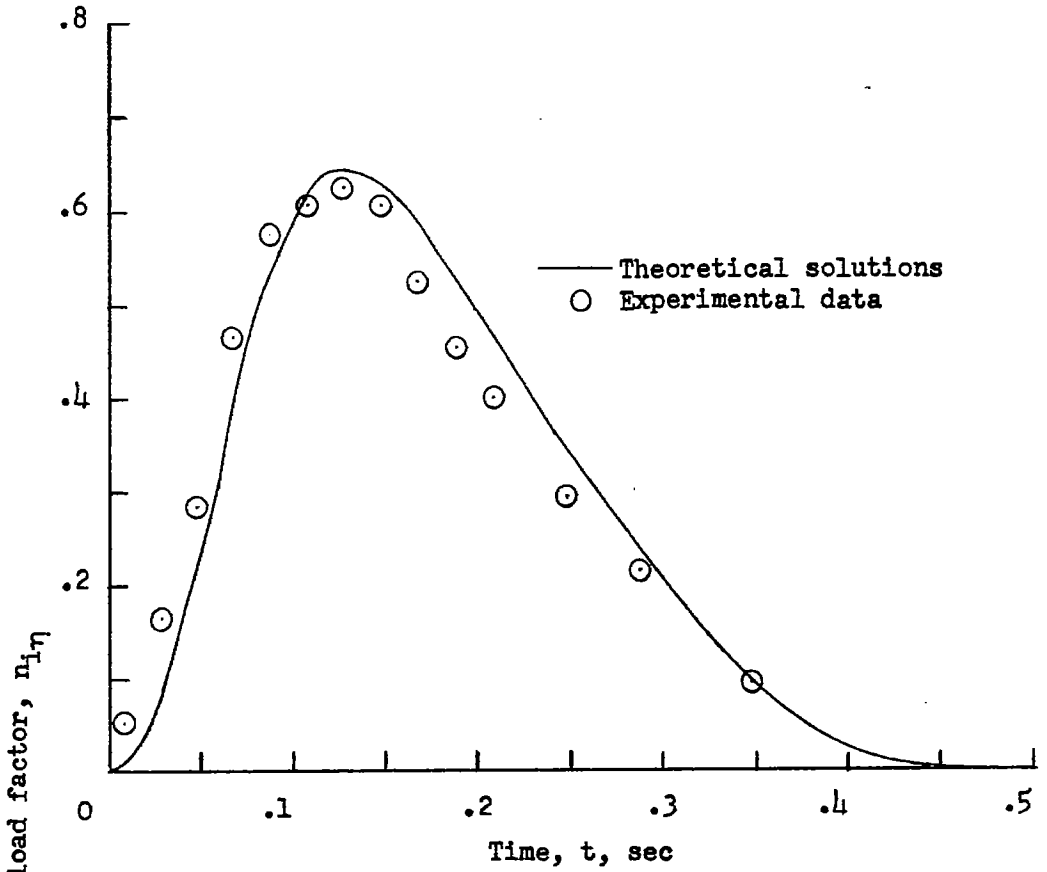

(a) $\tau = 3.2^\circ$; $\dot{z}_o = 4.2$ feet per second; $\dot{x}_o = 71.5$ feet per second.

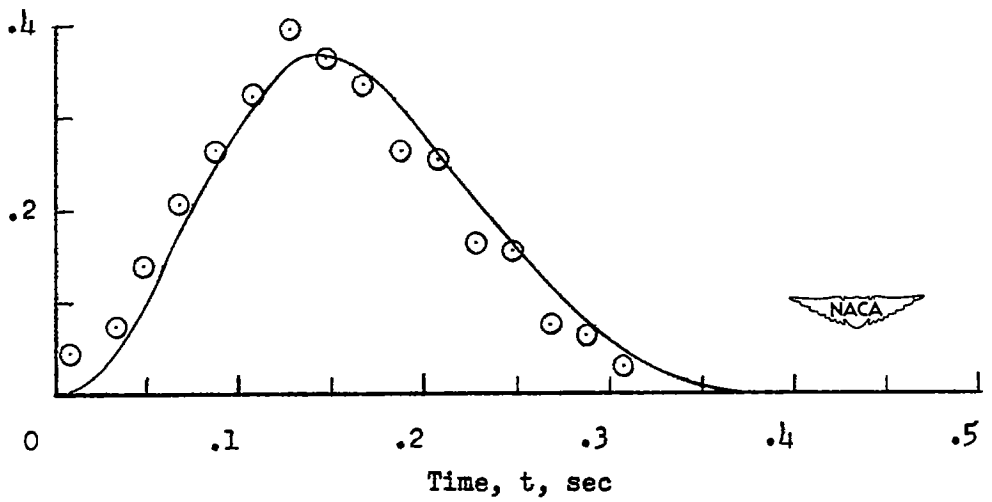

(b) $\tau = 9.3^\circ$; $\dot{z}_o = 3.3$ feet per second; $\dot{x}_o = 67.1$ feet per second.

Figure 30.- Comparison between theoretical and experimental side-load time histories. $\beta = 22.5^\circ$; $\Psi = 12^\circ$; $W = 1177$ pounds.

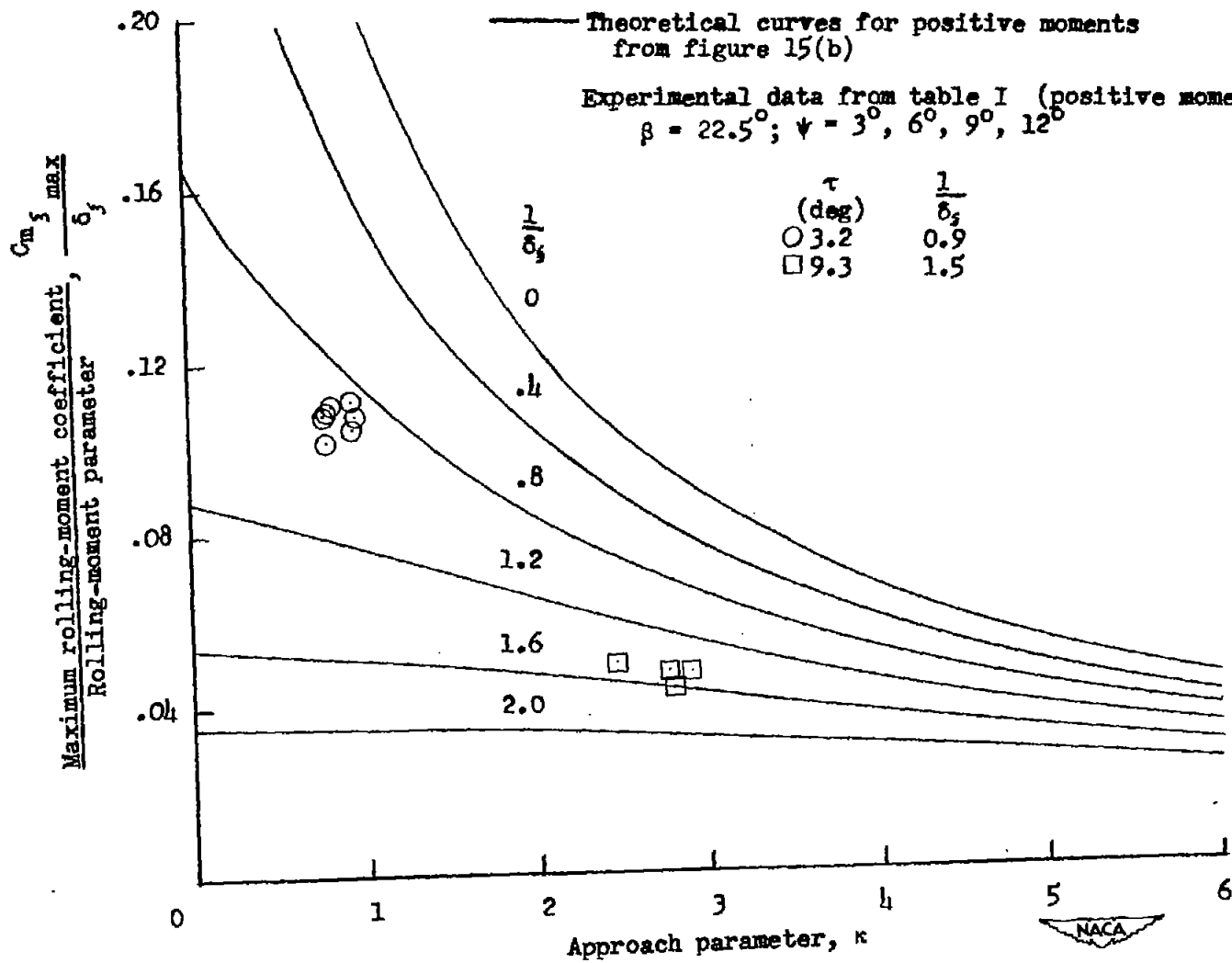

Figure 31.- Comparison of theoretical and experimental maximum rolling-moment coefficients for a non-chine-immersed wedge.

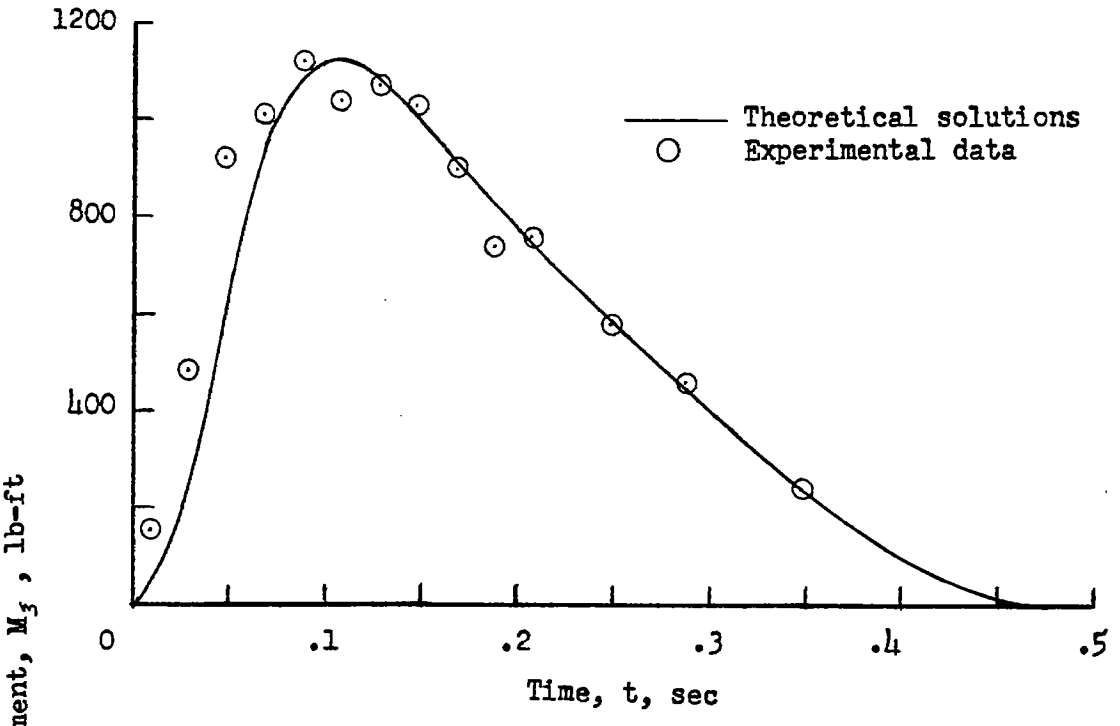

(a) $\tau = 3.2^\circ$; $\dot{z}_o = 4.2$ feet per second; $\dot{x}_o = 71.5$ feet per second.

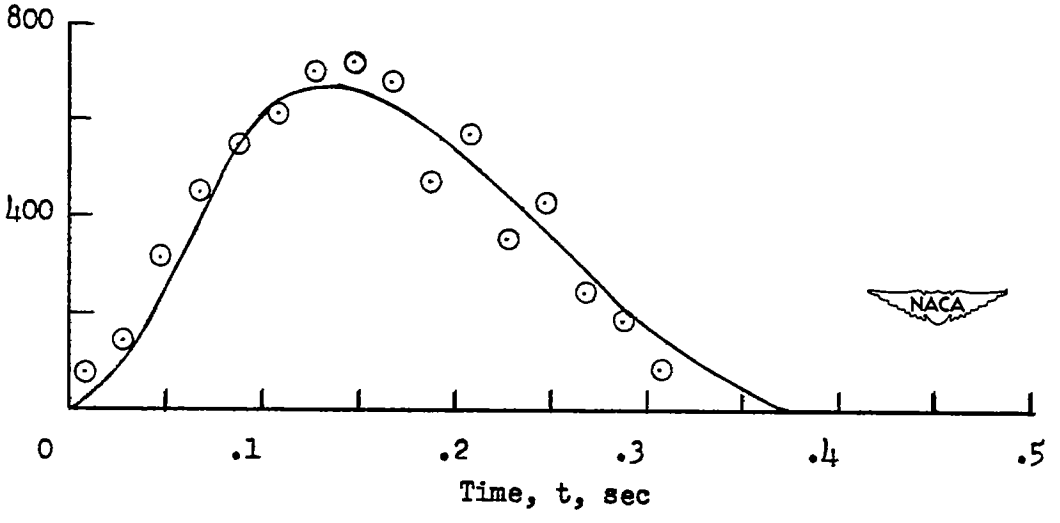

(b) $\tau = 9.3^\circ$; $\dot{z}_o = 3.3$ feet per second; $\dot{x}_o = 67.1$ feet per second.

Figure 32.- Comparison between theoretical and experimental rolling-moment time histories. $\beta = 22.5^\circ$; $\Psi = 12^\circ$; $a_\xi = 2.96$ feet; $W = 1177$ pounds.

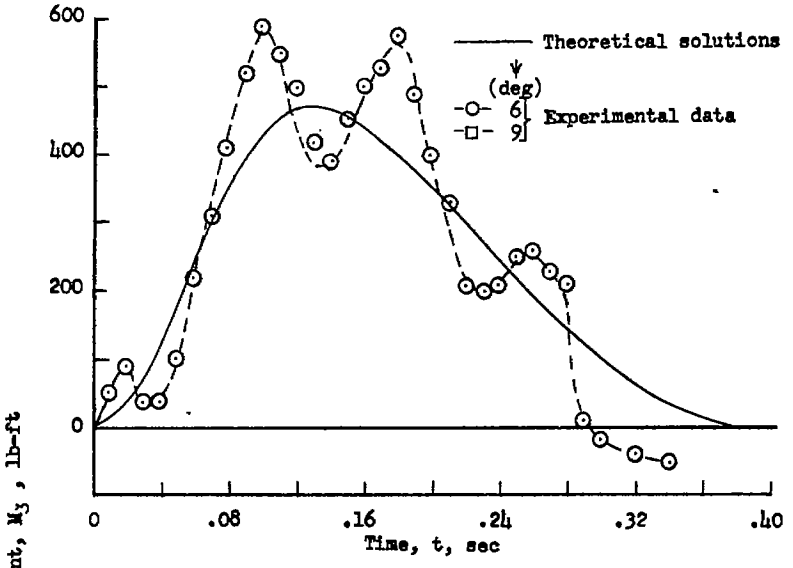

(a) $\tau = 9.3^{\circ}$; $\dot{z}_o = 4.2$ feet per second; $\dot{x}_o = 57.8$ feet per second.

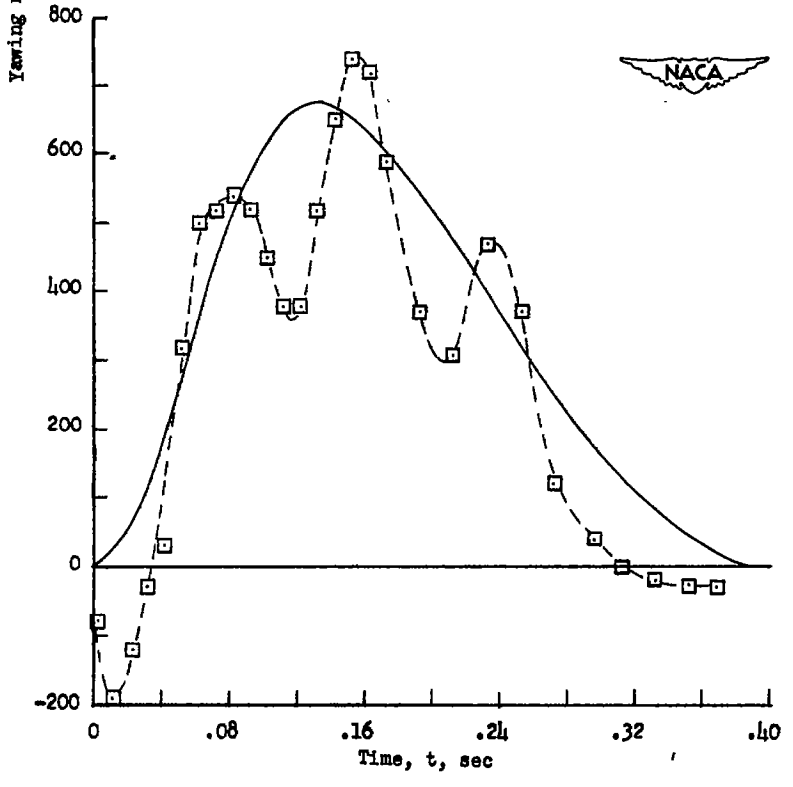

(b) $\tau = 9.3^{\circ}$; $\dot{z}_o = 4.1$ feet per second; $\dot{x}_o = 56.6$ feet per second.

Figure 33.- Comparison between theoretical and experimental yawing-moment time histories. $\beta = 22.5^{\circ}$; $a_\zeta = 2.87$ feet; W = 1177 pounds.

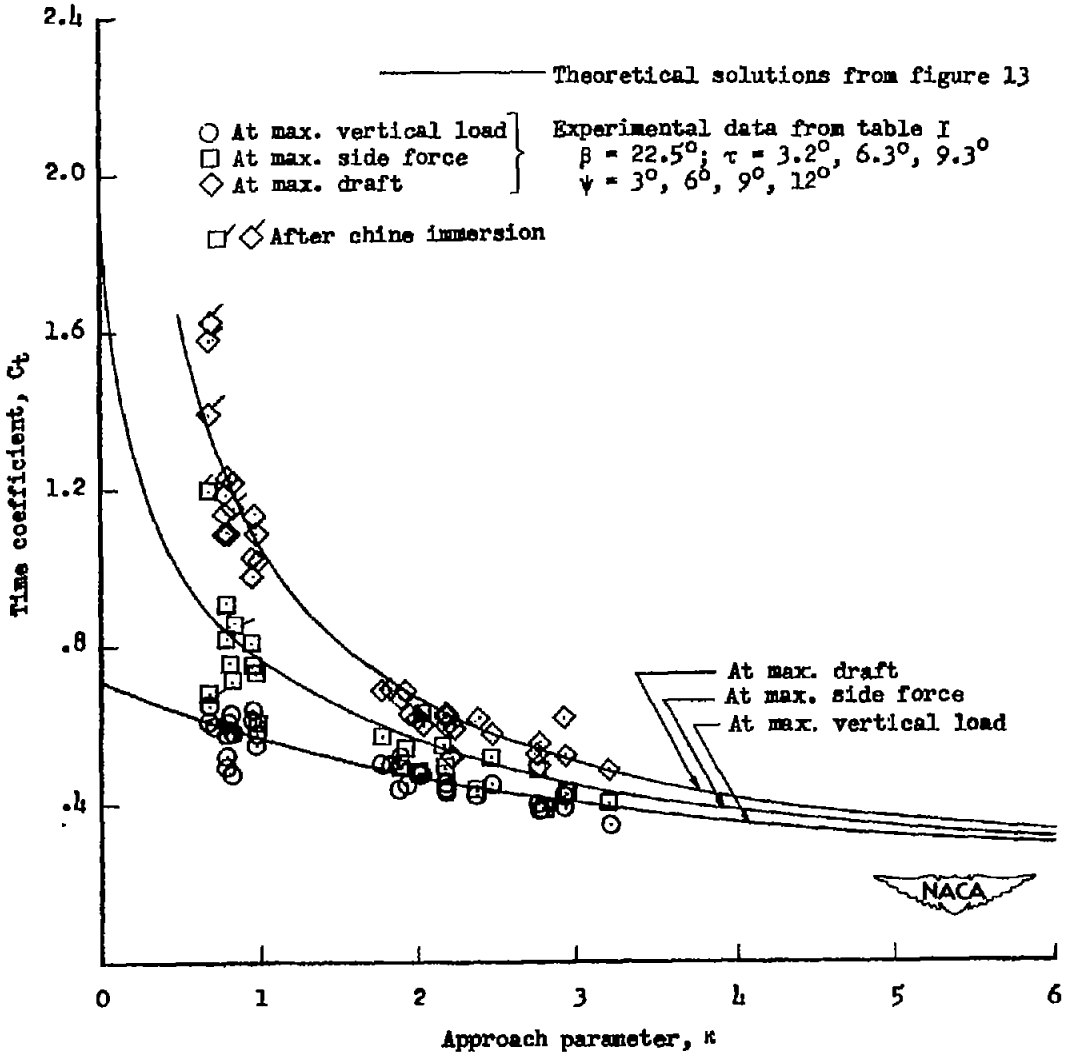

Figure 34.- Comparison of theoretical and experimental time coefficients for a non-chine-immersed wedge.

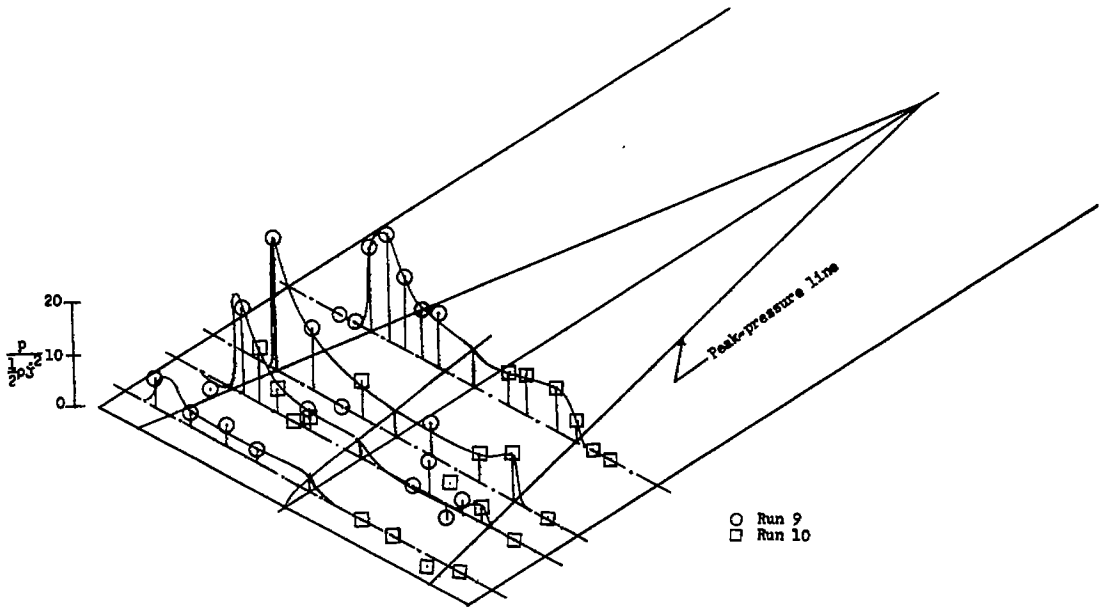

Experimental pressure distributions

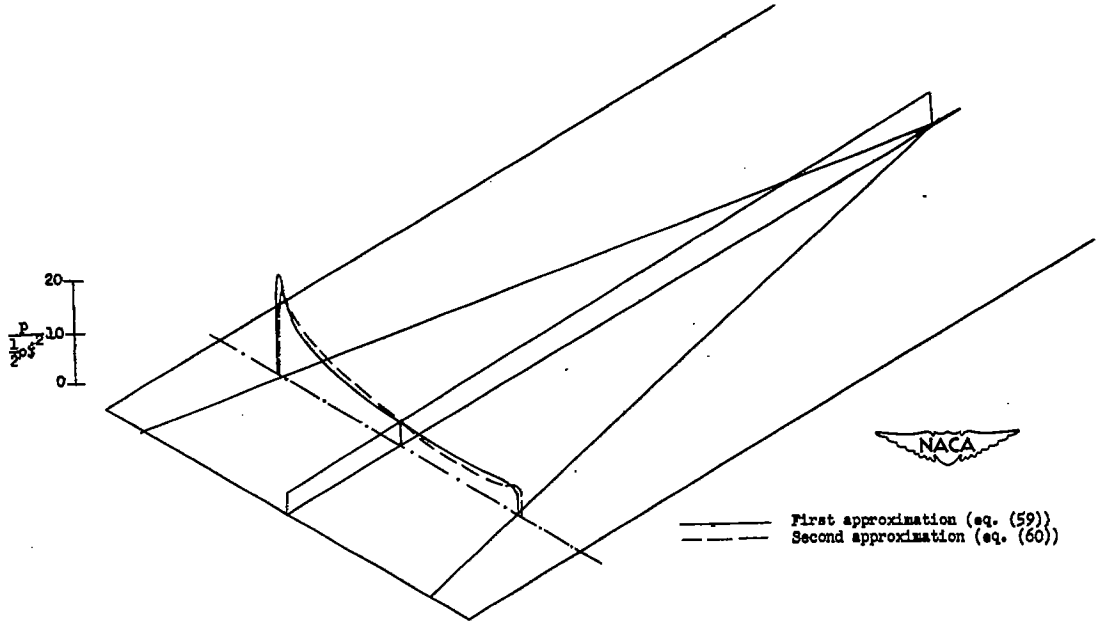

Theoretical pressure distributions

(a) $\tau = 3.2°$; $\psi = 6°$; $\frac{V_\eta}{V_\zeta} \approx 1.1$.

Figure 35.- Theoretical and experimental pressure distributions on a yawed prismatic float having an angle of dead rise of 22.5°.

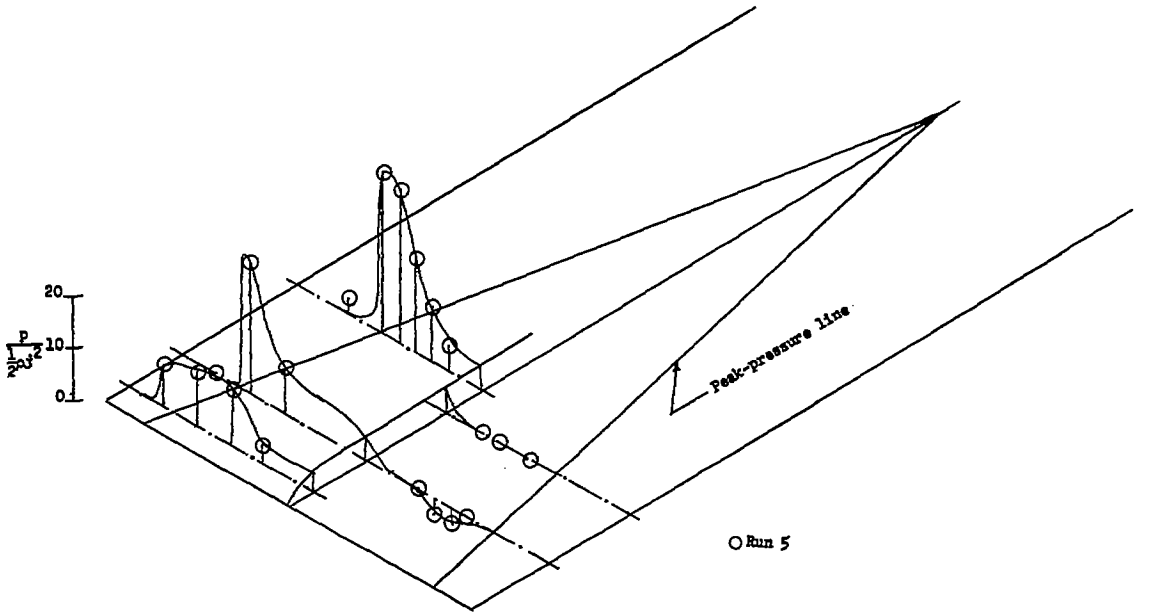

Experimental pressure distributions

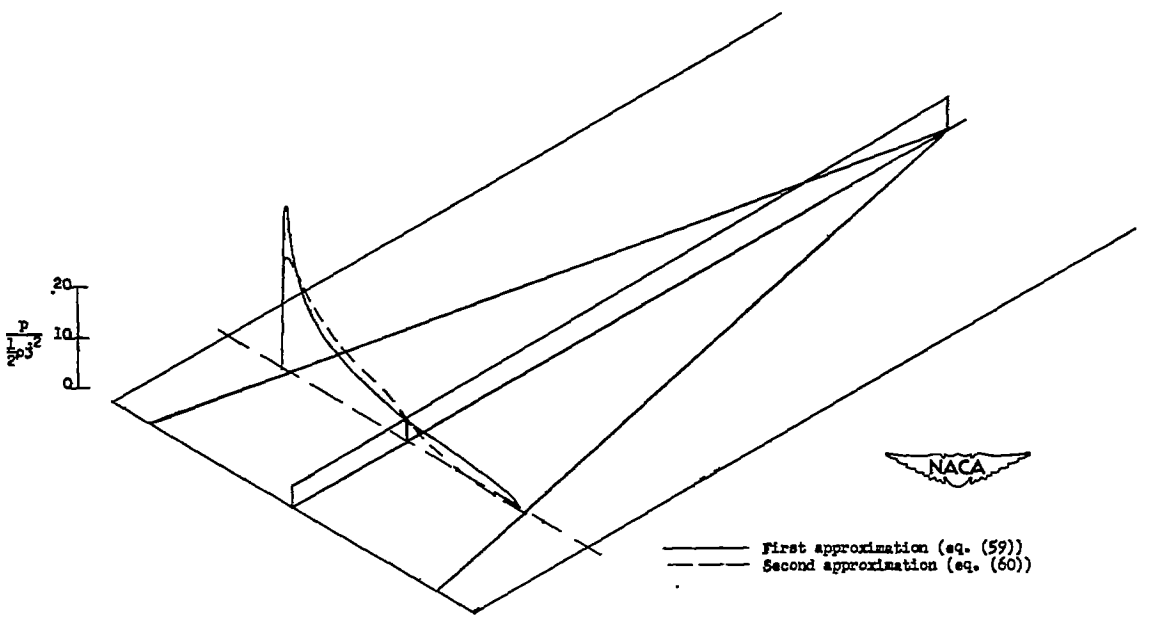

Theoretical pressure distributions

(b) $\tau = 3.2^{\circ}$; $\psi = 12^{\circ}$; $\frac{V_\eta}{V_\zeta} \approx 2.4$.

Figure 35.- Continued.

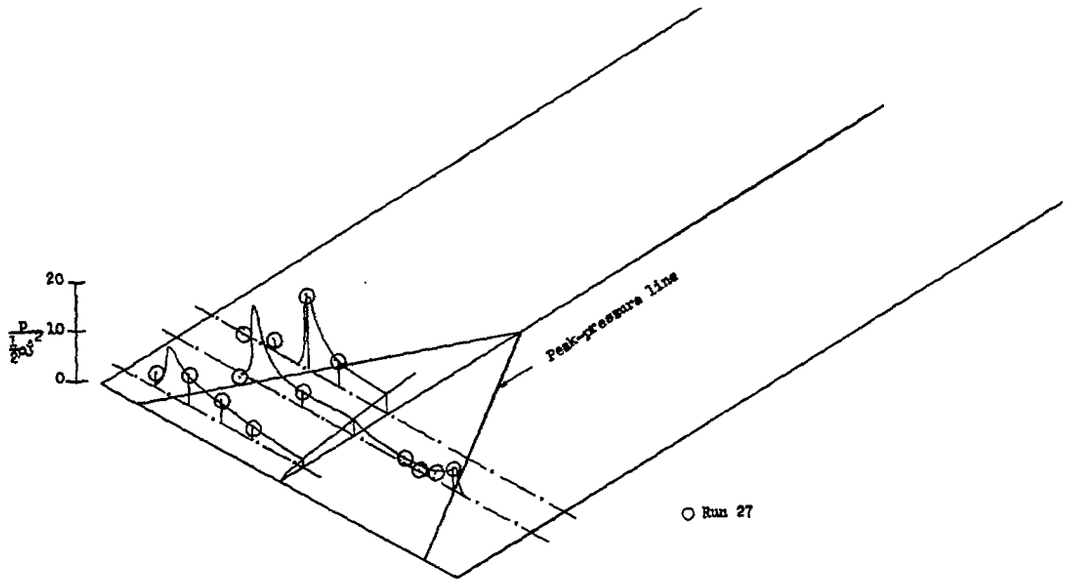

Experimental pressure distributions

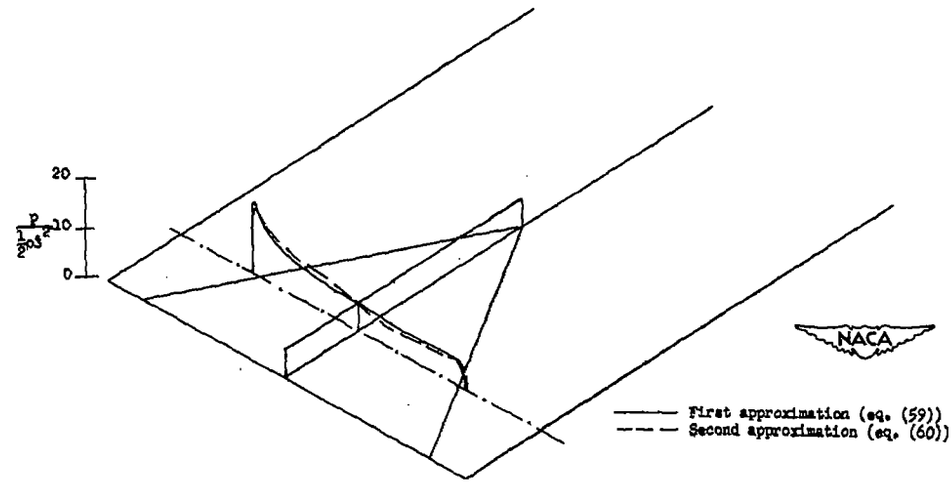

Theoretical pressure distributions

(c) $\tau = 9.3^\circ$; $\psi = 9^\circ$; $\frac{V_\eta}{V_\zeta} \approx 0.9$.

Figure 35.- Concluded.

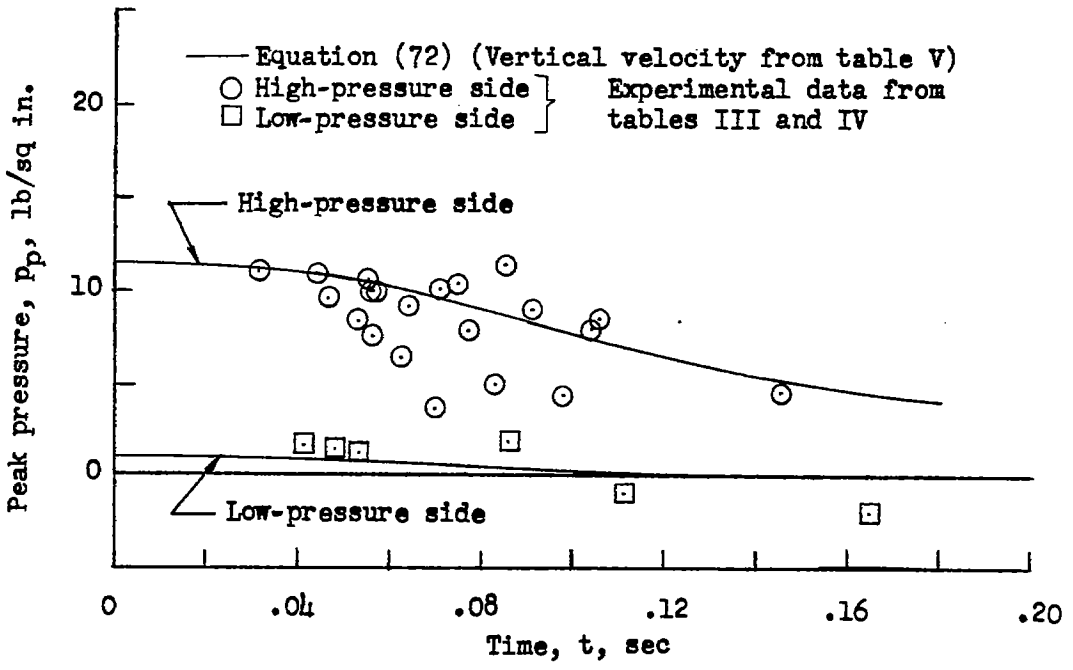

(a) Run 5: $\tau = 3.2^\circ$; $\psi = 12^\circ$; $\dot{x}_o = 71.5$ feet per second; $\dot{z}_o = 4.2$ feet per second.

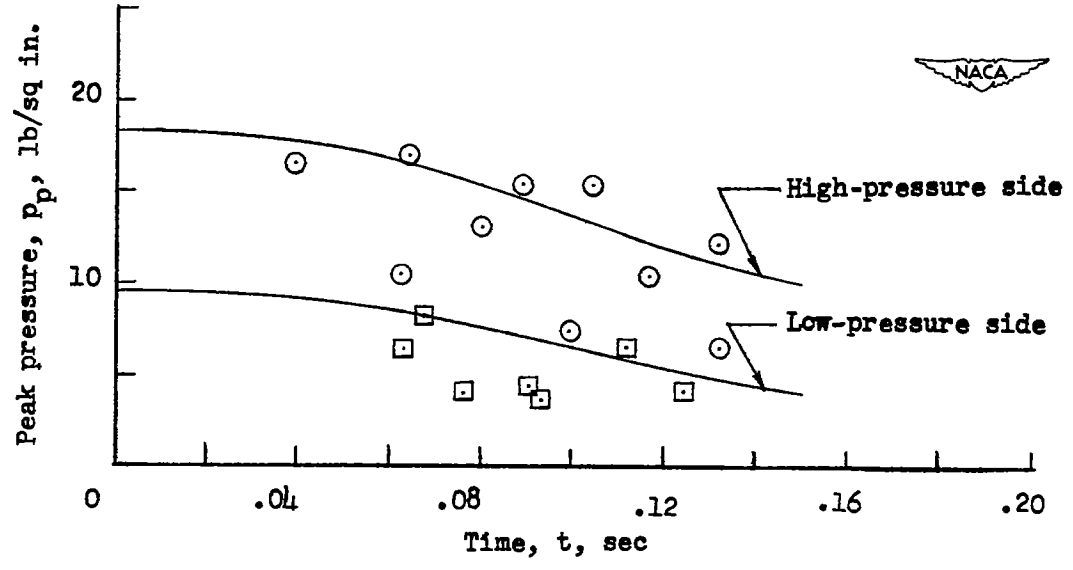

(b) Run 27: $\tau = 9.3^\circ$; $\psi = 9^\circ$; $\dot{x}_o = 67.2$ feet per second; $\dot{z}_o = 4.3$ feet per second.

Figure 36.- Comparisons of computed and experimental peak pressures. $\beta = 22.5^\circ$.

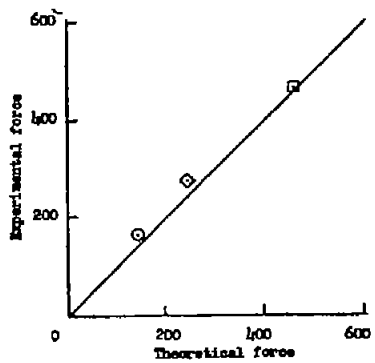

(a) Side force, F_η, pounds.

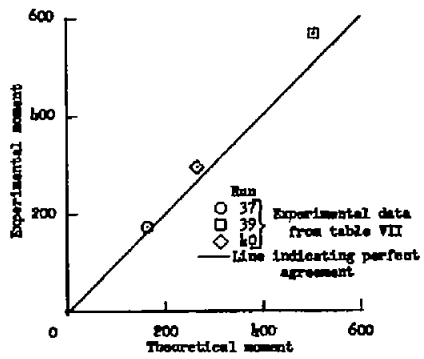

(b) Rolling moment, M_ξ, pound-feet.

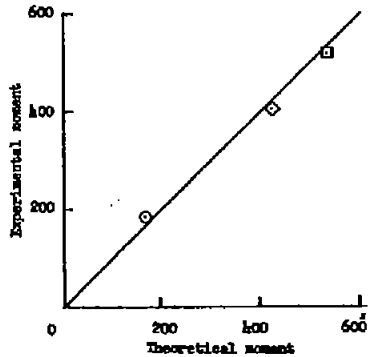

(c) Yawing moment, M_ζ, pound-feet.

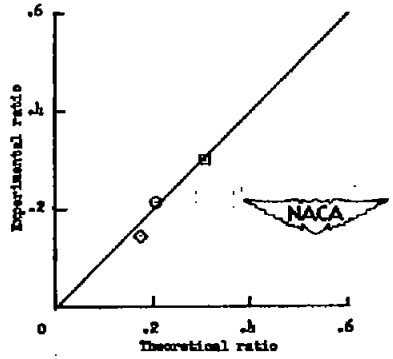

(d) Ratio of side to normal force, F_η/F_ζ.

Figure 37.- Comparison of experimental and theoretical forces and moments during yawed planing. $\beta = 22.5^\circ$.

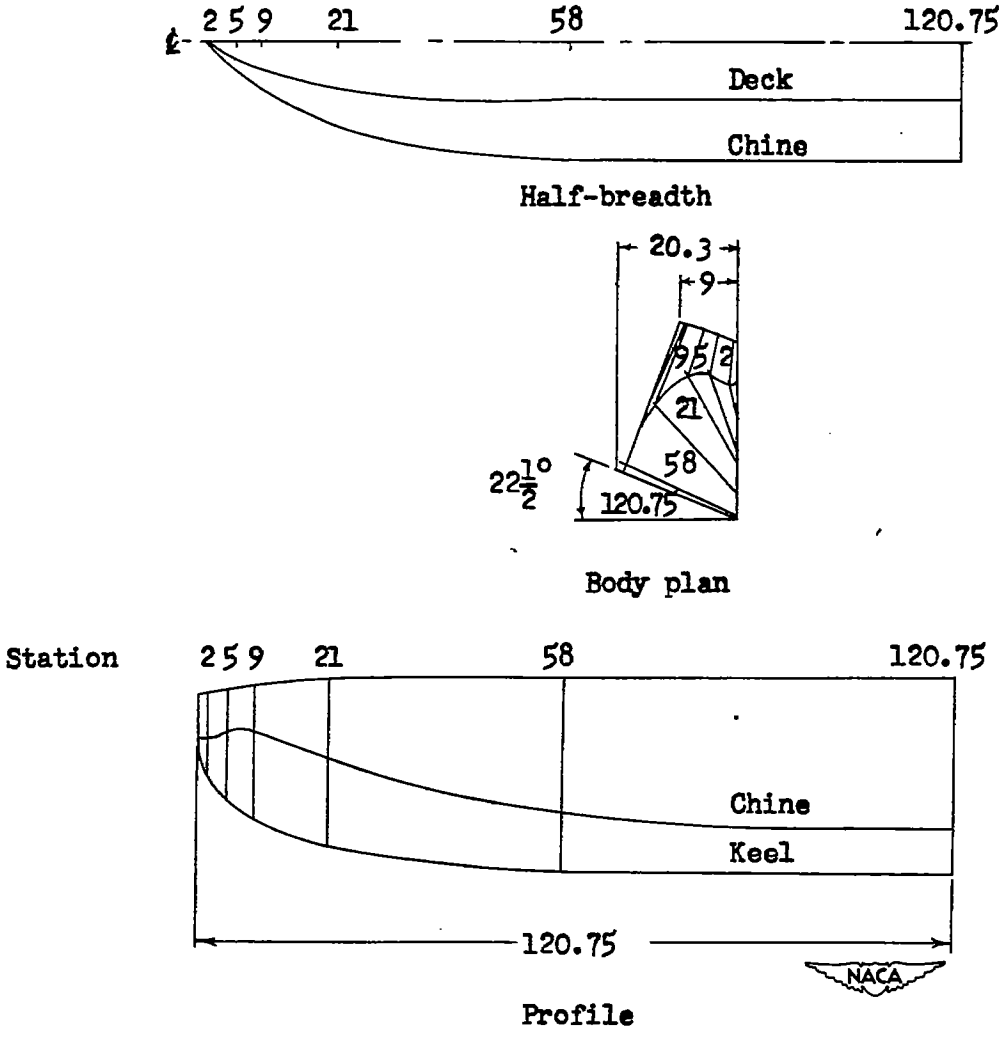

Figure 38.- Hull lines of float having a 22.5° angle of dead rise. All dimensions are in inches.

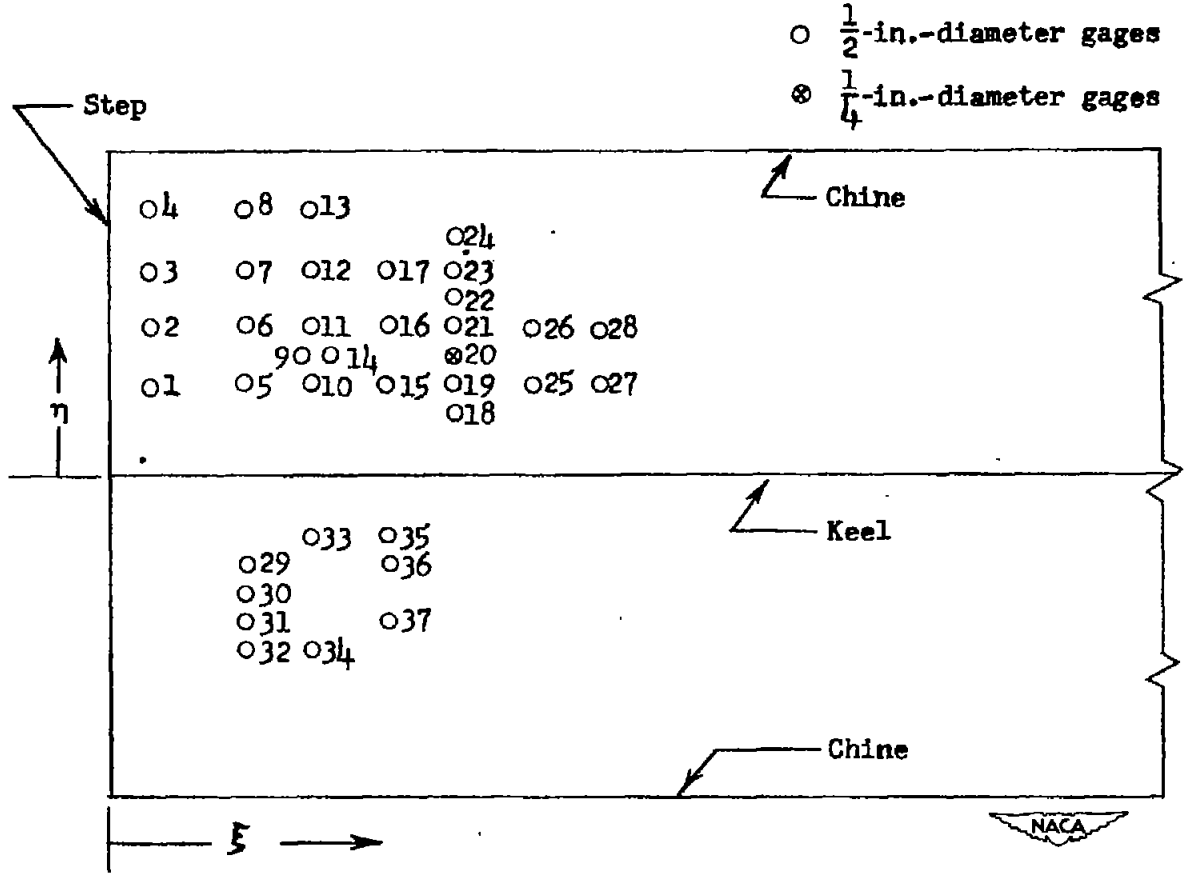

Figure 39.- Location of pressure gages in float bottom.

NACA-Langley - 11-14-53 - 1000